Appendix A.9:

Vangelis Ln and Fernbrook Pl – CPT 49582

Table 1: Site Description for Vangelis Ln and Fernbrook Pl (CPT 49582).

Attribute	Yes/No			Description/Date	Symbol in Figure 1
	10-m Buffer	20-m Buffer	50-m Buffer		
Near a body of surface water or other free face features?	No	No	No	The center of the site is 90 m away from one creek (~2.0 m high, N-S free face), 170 m away from another creek (~2.5 m high, NW-SE free face), and 1960 m away from the Avon River (~2.5 m high, SW-NE free face).	NA
Lateral spreading observed during the CES?	No	No	No	Absence of ground cracks indicates no lateral spreading, as observed by the mapping team.[1]	NA
Nearby buildings or structures?	No	Yes	Yes	Building coverage of the 20-m and 50-m buffers is 1% and 23%, respectively. Buildings are spread throughout all quadrants.	White Fill + Brown Outline
Sloping land?	No	No	No	Flat land, residential area with free field in the E portion of the 50-m buffer.	NA
Step changes in the ground surface?	No	No	Yes	Elevated playground is in the SW quadrant of the 50-m buffer and occupies 2% of the area.	Playground: White Fill + Yellow Outline
Retaining walls?	No	No	No	NA	NA
Vegetation?	Yes	Yes	Yes	Trees and bushes cover 3% of the 10-m buffer, 20% of the 20-m buffer, and 26% of the 50-m buffer. They are in the E half of the 10-m buffer and throughout all quadrants of the 20-m and 50-m buffers.	White Fill + Green Outline
Anthropogenic changes to the site between the LiDAR surveys?	No	Possibly Yes	No	Garage building in the SE quadrant of the 50-m buffer was built between Mar 2009 and Jun 2009. Preparation of soil for grass planting in the free field might have taken place between Mar 2009 and Jun 2009.	Building Addition in 2009: Orange Crossline
Other important factors?	Yes	Yes	Yes	Low-motor-vehicle-volume, two-way roadway occupies 70%, 33%, and 9% of the 10-m, 20-m, and 50-m buffers, respectively. It affects all quadrants of the three buffers and spreads mainly through the NE quadrant of the 50-m buffer. Access road covers 1%, 4%, and 3% of the 10-m, 20-m, and 50-m buffers, respectively, and is in their SW quadrants.	Road: White Fill + Gray Outline

Note: Buffer is the area within a circle of a specified radius with CPT investigations done at its center (172.650158°, -43.501489°).

[1] Canterbury Geotechnical Database. (2012). "Observed Ground Crack Locations", Map Layer CGD0400 - 23 July 2012, retrieved July 09, 2018 from https://canterburygeotechnicaldatabase.projectorbit.com/

Figure 1: Site plan with areas where LiDAR survey data is considered.

Note 1: Two patches (outlined in red) in free field were initially selected for settlement assessment as areas free of vegetation and structures. Further analyses revealed that Patch A is closer to a CPT than Patch B and has borehole investigations done in its proximity. Hence, Patch A was selected for detailed settlement assessment while Patch B was discarded in detailed settlement assessment. In addition, since significant amounts of ejecta were observed on roads in the CES, Road was considered for settlement assessment. Roads as hard, relatively flat surfaces provide many ground-classified points. Therefore, it is useful to compare settlement estimates on roads with settlement estimates for the patch.

Table 2: LiDAR flight error adjustments, global adjustments for the difference between average LiDAR point elevations and benchmark survey elevations, and vertical tectonic movement adjustments.

	Adjustments (mm)		
Earthquake Event(s)	LiDAR Flight Error	Global Offset[2]	Tectonic Vertical Movement
Sep-10	-100	-3	0
Feb-11	100	16	-64
Jun-11	0	38	-30
Dec-11	-100	-65	-4
CES	-100	-14	-98
Any LiDAR survey affected by ejecta?			No

Note: The negative sign indicates the subtraction from the ground surface subsidence, while the positive sign indicates the addition to the ground surface subsidence.

Table 3a: LiDAR Measurement Error for Patch A.

Surveys	Buffer	Area Averaged Difference Indicating Repeat Measurement Error (mm)	$\sigma^*_{\text{individual LiDAR points}}$ (mm)	%Reduction in σ due to Area Averaging of LiDAR Points
Post Feb 2011: Mar 2011 and May 2011	10-m	NA	59	[58,63]
	20-m	37		
	50-m	34		
Post Dec 2011: Feb 2012 and Oct 2015	10-m	NA	70	[57,61]
	20-m	40		
	50-m	43		

*Standard deviation.

[2] Russell, J., & van Ballegooy, S. (2015). *Canterbury Earthquake Sequence: Increased liquefaction vulnerability assessment methodology*. New Zealand: Tonkin & Taylor Ltd.

Table 3b: LiDAR Measurement Error for Road.

Surveys	Buffer	Area Averaged Difference Indicating Repeat Measurement Error (mm)	$\sigma^*_{individual\ LiDAR\ points}$ (mm)	%Reduction in σ due to Area Averaging of LiDAR Points
Post Feb 2011: Mar 2011 and May 2011	10-m	19	59	[27,32]
	20-m	16		
	50-m	14		
Post Dec 2011: Feb 2012 and Oct 2015	10-m	23	70	[33,39]
	20-m	27		
	50-m	26		

*Standard deviation.

Table 4a: Ground surface subsidence adjustments due to LiDAR measurement error for Patch A.

Earthquake Event(s)	$\sigma_{pre\text{-}EQ\ LiDAR\ survey}$ (mm)	$\sigma_{post\text{-}EQ\ LiDAR\ survey}$ (mm)	σ_{total} (mm)	Area Average Adjusted σ (mm) **
Sep-10	158	56	134	±84
Feb-11	56	59	59	±37
Jun-11	59	61	62	±39
Dec-11	61	70	87	±54
CES	158	70	124	±78

**Based on the highest %Reduction in Table 3a.

Table 4b: Ground surface subsidence adjustments due to LiDAR measurement error for Road.

Earthquake Event(s)	$\sigma_{pre\text{-}EQ\ LiDAR\ survey}$ (mm)	$\sigma_{post\text{-}EQ\ LiDAR\ survey}$ (mm)	σ_{total} (mm)	Area Average Adjusted σ (mm) **
Sep-10	158	56	134	±52
Feb-11	56	59	59	±23
Jun-11	59	61	62	±24
Dec-11	61	70	87	±33
CES	158	70	124	±48

**Based on the highest %Reduction in Table 3b.

Table 5a: Raw liquefaction-related ground surface subsidence using original LiDAR points for Patch A.

	Average Ground Surface Subsidence (mm)		
Earthquake Event(s)	10-m Buffer	20-m Buffer	50-m Buffer
Sep-10	NA	150	136
Feb-11	NA	41	44
Jun-11	NA	4	5
Dec-11	NA	68	66
CES	NA	263	251

Table 5b: Raw liquefaction-related ground surface subsidence using original LiDAR points for Road.

	Average Ground Surface Subsidence (mm)		
Earthquake Event(s)	10-m Buffer	20-m Buffer	50-m Buffer
Sep-10	83	105	112
Feb-11	71	68	63
Jun-11	32	26	27
Dec-11	83	83	81
CES	269	283	283

Table 6a: Corrected liquefaction-related ground surface subsidence using original LiDAR points for Patch A with the calculated adjustments in Table 2.

	Average Calculated Ground Surface Subsidence (mm)		
Earthquake Event(s)	10-m Buffer	20-m Buffer	50-m Buffer
Sep-10	NA	47$\pm$75	33$\pm$75
Feb-11	NA	93$\pm$25	96$\pm$25
Jun-11	NA	12$\pm$50	13$\pm$50
Dec-11	NA	-101$\pm$50	-103$\pm$50
CES	NA	51$\pm$75	39$\pm$75

Notes: Plus/minus values are same as those in Table 4b, but rounded to the nearest 25; Positive overall values indicate ground surface subsidence, while negative overall values indicate ground surface uplift.

Table 6b: Corrected liquefaction-related ground surface subsidence using original LiDAR points for Road with the calculated adjustments in Table 2.

	Average Calculated Ground Surface Subsidence (mm)		
Earthquake Event(s)	10-m Buffer	20-m Buffer	50-m Buffer
Sep-10	-20±50	2±50	9±50
Feb-11	123±25	120±25	115±25
Jun-11	40±25	34±25	35±25
Dec-11	-86±25	-86±25	-88±25
CES	57±50	70±50	71±50

Notes: Plus/minus values are same as those in Table 4b, but rounded to the nearest 25; Positive overall values indicate ground surface subsidence, while negative overall values indicate ground surface uplift.

Table 7a: Corrected liquefaction-related ground surface subsidence for Patch A using LiDAR DEMs.

	Estimated Ground Surface Subsidence (mm)								
	10-m Buffer			20-m Buffer			50-m Buffer		
Earthquake Event(s)	16th %ile	50th %ile	84th %ile	16th %ile	50th %ile	84th %ile	16th %ile	50th %ile	84th %ile
Sep-10	NA	NA	NA	<50	<50	50	<50	<50	50
Feb-11	NA	NA	NA	150	150	150	150	150	150
Jun-11	NA	NA	NA	50	50	50	50	50	50
Dec-11	NA	NA	NA	<50	<50	<50	<50	<50	50
CES	NA	NA	NA	150	150	150	100	150	150

Note: These percentiles are not the exact statistical measures; they indicate the spatial variability of ground surface subsidence.

Table 7b: Corrected liquefaction-related ground surface subsidence for Road using LiDAR DEMs.

	Estimated Ground Surface Subsidence (mm)								
	10-m Buffer			20-m Buffer			50-m Buffer		
Earthquake Event(s)	16th %ile	50th %ile	84th %ile	16th %ile	50th %ile	84th %ile	16th %ile	50th %ile	84th %ile
Sep-10	<50	<50	<50	<50	<50	<50	<50	<50	<50
Feb-11	150	150	150	150	150	150	150	150	150
Jun-11	50	50	50	50	50	50	50	50	50
Dec-11	<50	<50	<50	<50	<50	<50	<50	<50	<50
CES	100	150	150	100	150	150	100	150	150

Note: These percentiles are not the exact statistical measures; they indicate the spatial variability of ground surface subsidence.

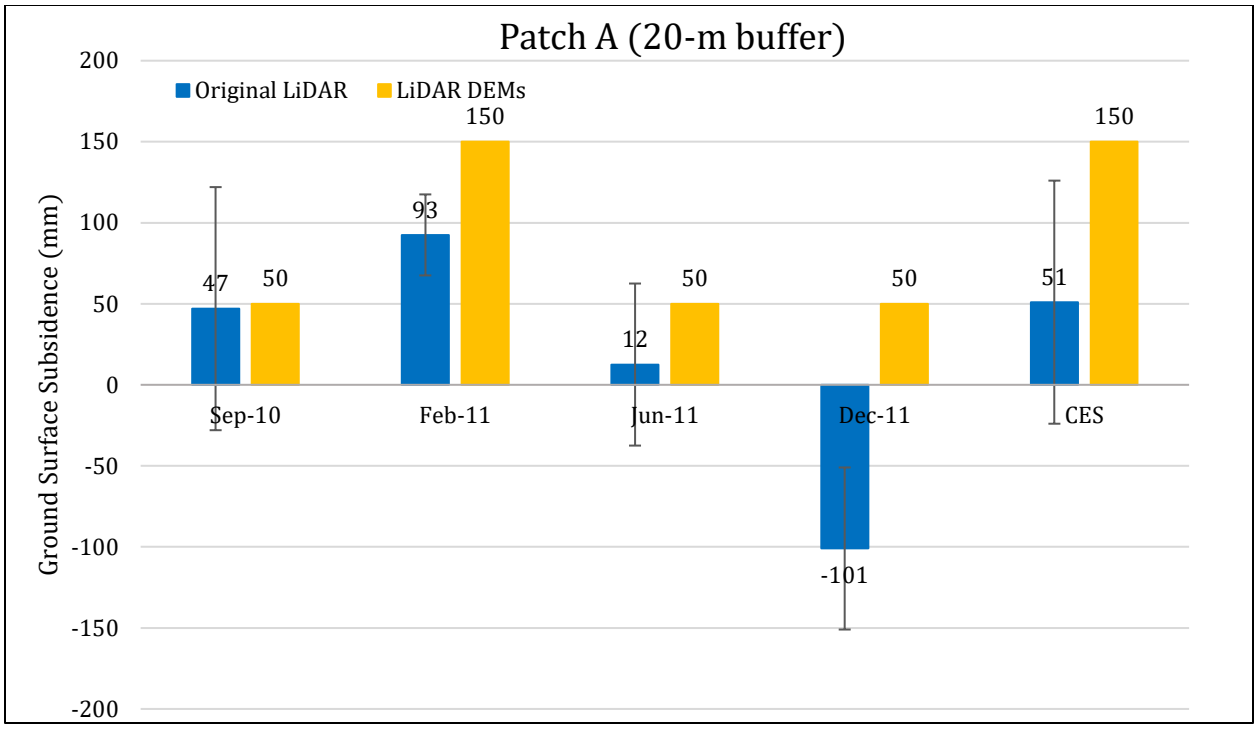

Figure 2: Comparison between ground surface subsidence determined from original LiDAR survey points and ground surface subsidence (50th %ile) estimated using LiDAR DEMs for Patch A for the 20-m buffer.

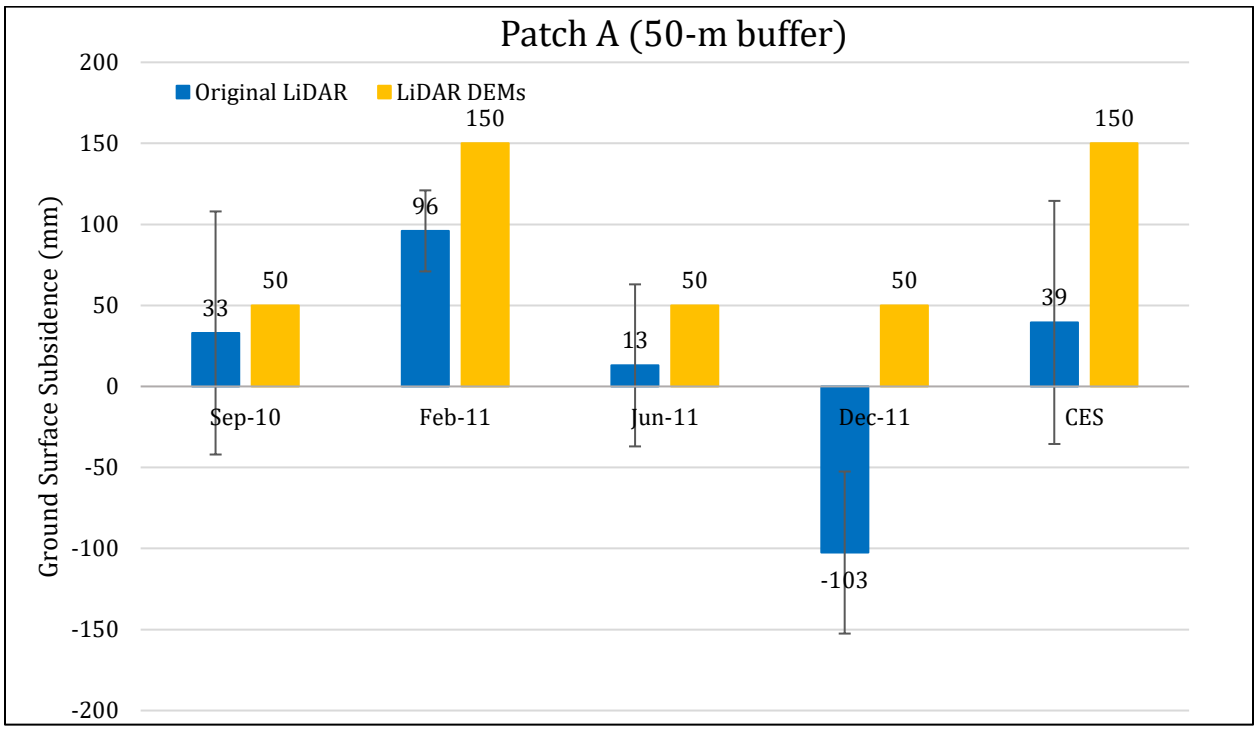

Figure 3: Comparison between ground surface subsidence determined from original LiDAR survey points and ground surface subsidence (50th %ile) estimated using LiDAR DEMs for Patch A for the 50-m buffer.

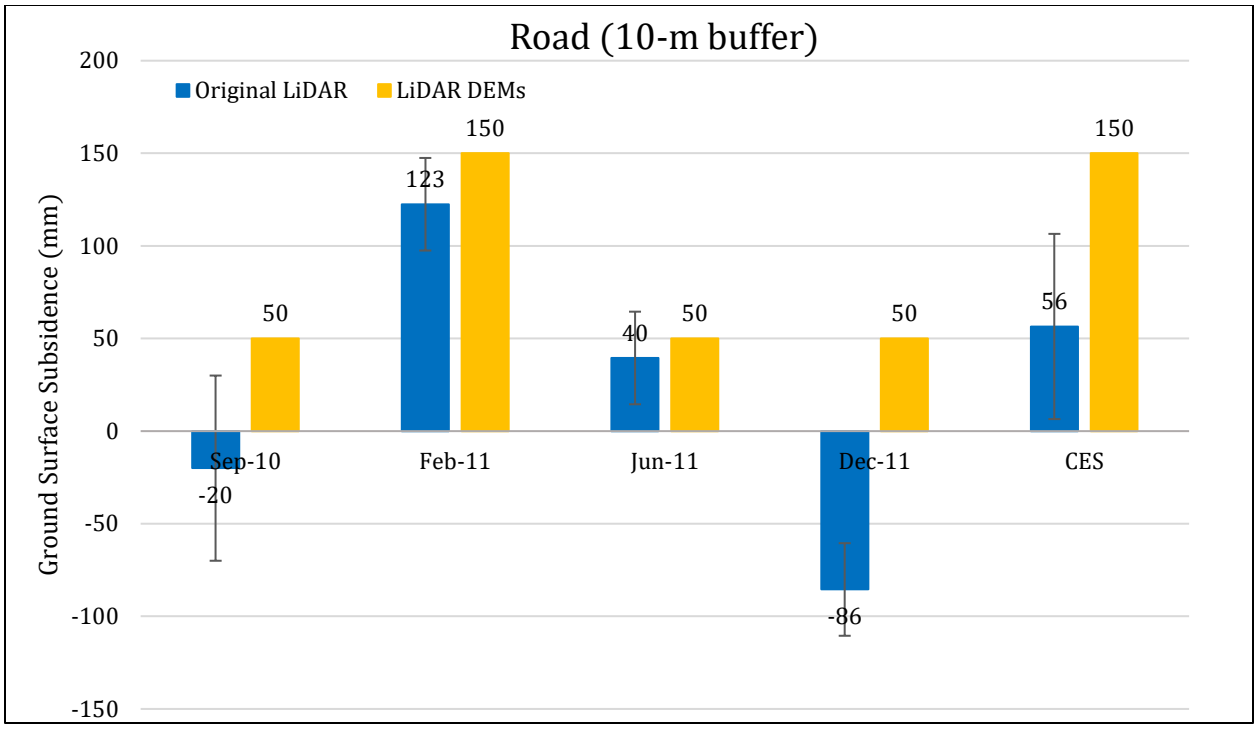

Figure 4: Comparison between ground surface subsidence determined from original LiDAR survey points and ground surface subsidence (50th %ile) estimated using LiDAR DEMs for Road for the 10-m buffer.

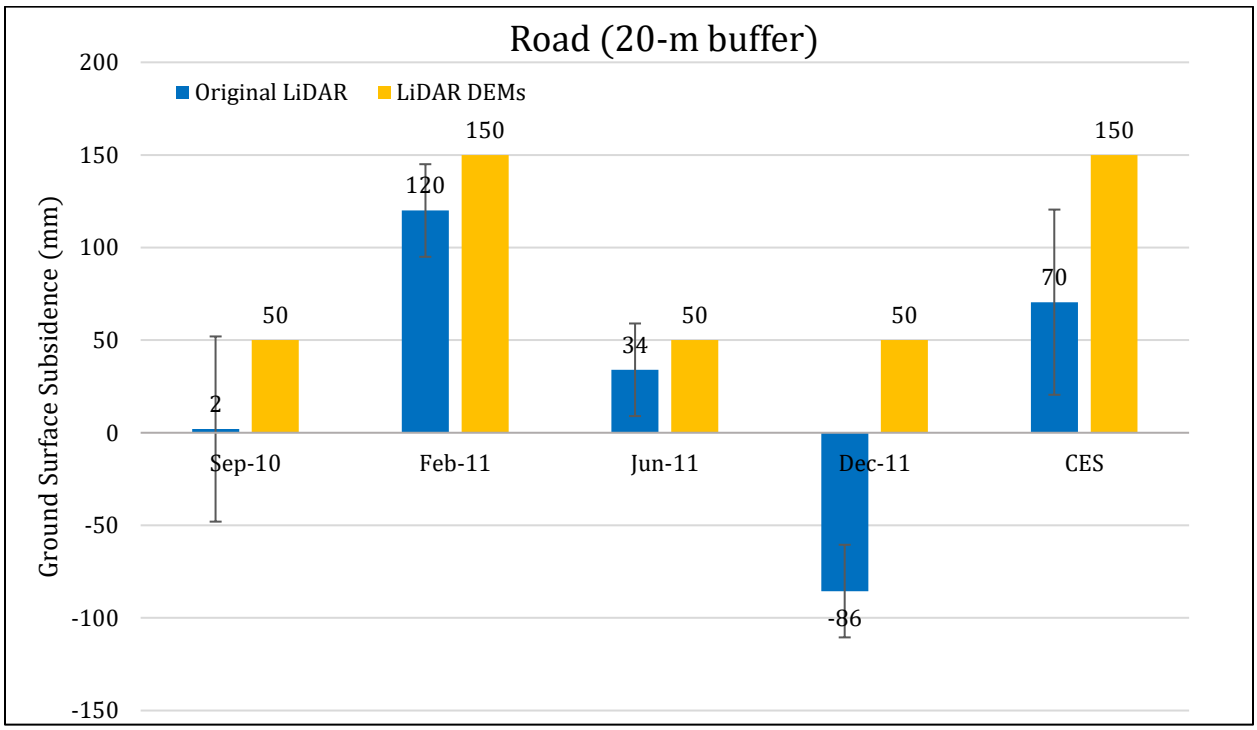

Figure 5: Comparison between ground surface subsidence determined from original LiDAR survey points and ground surface subsidence (50th %ile) estimated using LiDAR DEMs for Road for the 20-m buffer.

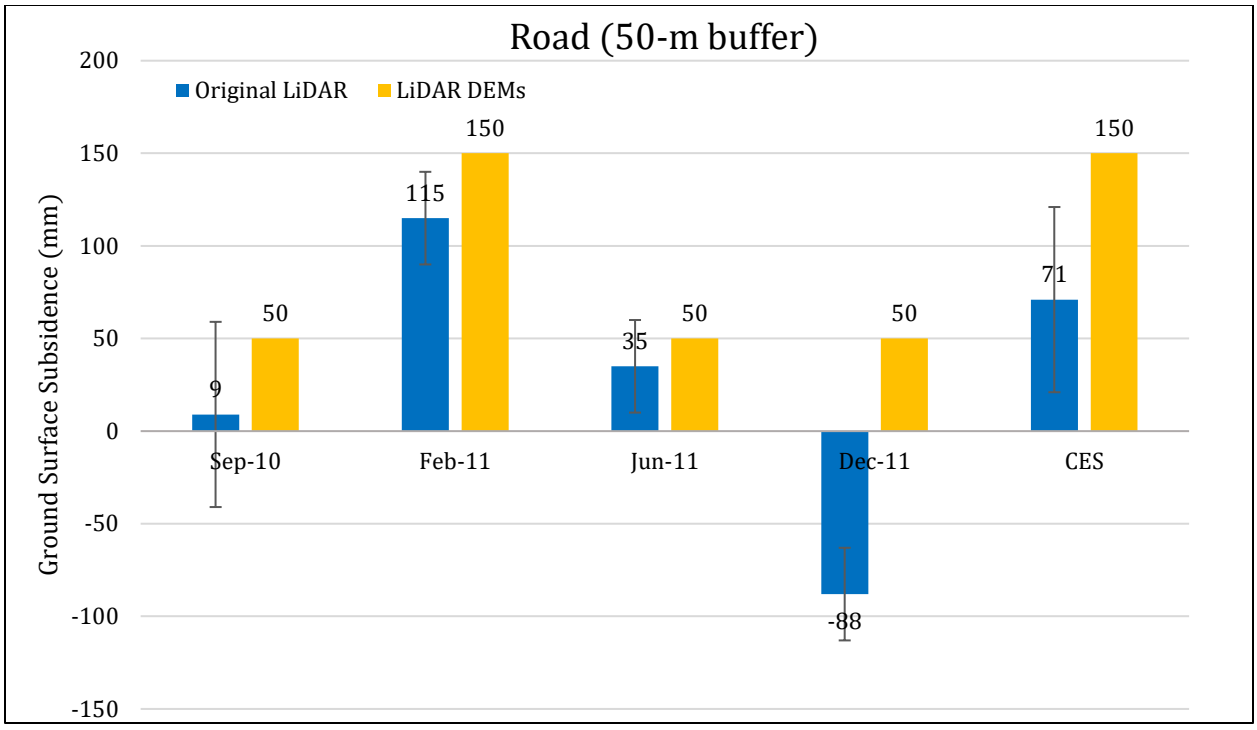

Figure 6: Comparison between ground surface subsidence determined from original LiDAR survey points and ground surface subsidence (50th %ile) estimated using LiDAR DEMs for Road for the 50-m buffer.

Note 2: The ground surface subsidence values determined using the original LiDAR survey points are similar to the ground surface subsidence values estimated using the LiDAR DEMs for the Sep-10, Feb-11, and Jun-11 earthquakes, and the CES. The discrepancy between the two approaches is observed for the Dec-11 earthquake.

Table 8a: Ejecta-Induced settlement for the top 20 m of the soil profile for Patch A within the 20-m buffer for the 50th %ile PGA, P_L=50%, and C_{FC}=0.13 using BI-2014, ZRB-2002, and I_c cutoff of 2.6.

Earthquake Event(s)	M_W	PGA (g)	Depth to Groundwater (m)	S_T (mm)	S_{V1D} (mm)	$S_{E,L}$ (mm)
Sep-10	7.1	0.20	2.2	47±75	66±20	-19±77
Feb-11	6.2	0.33	2.2	93±25	141±50	-48±56
Jun-11	6.2	0.19	1.5	12±50	32±25	-20±56
Dec-11	6.1	0.24	1.5	-101±50	73±50	-174±71

Notes: S_T = Total settlement (Table 6); S_{V1D} = Average vertical settlement due to volumetric compression using Boulanger and Idriss (2014) (BI-2014), Zhang et al. (2002) (ZRB-2002) procedures and de Greef and Lengkeek (2018) thin-layer correction; $S_{E,L}$ = Ejecta-induced settlement as the difference between the LiDAR-based S_T and S_{V1D}.

Table 8b: Ejecta-Induced settlement for the top 20 m of the soil profile for Patch A within the 50-m buffer for the 50th %ile PGA, P_L=50%, and C_{FC}=0.13 using BI-2014, ZRB-2002, and I_c cutoff of 2.6.

Earthquake Event(s)	M_W	PGA (g)	Depth to Groundwater (m)	S_T (mm)	S_{V1D} (mm)	$S_{E,L}$ (mm)
Sep-10	7.1	0.20	2.2	33±75	66±20	-33±77
Feb-11	6.2	0.33	2.2	96±25	141±50	-45±56
Jun-11	6.2	0.19	1.5	13±50	32±25	-19±56
Dec-11	6.1	0.24	1.5	-103±50	73±50	-176±71

Notes: S_T = Total settlement (Table 6); S_{V1D} = Average vertical settlement due to volumetric compression using Boulanger and Idriss (2014) (BI-2014), Zhang et al. (2002) (ZRB-2002) procedures and de Greef and Lengkeek (2018) thin-layer correction; $S_{E,L}$ = Ejecta-induced settlement as the difference between the LiDAR-based S_T and S_{V1D}.

Table 8c: Ejecta-Induced settlement for the top 20 m of the soil profile for Road within the 10-m buffer for the 50th %ile PGA, P_L=50%, and C_{FC}=0.13 using BI-2014, ZRB-2002, and I_c cutoff of 2.6.

Earthquake Event(s)	M_W	PGA (g)	Depth to Groundwater (m)	S_T(mm)	S_{V1D} (mm)	$S_{E,L}$ (mm)
Sep-10	7.1	0.20	2.2	-20±50	66±20	-46±54
Feb-11	6.2	0.33	2.2	123±25	141±50	-18±56
Jun-11	6.2	0.19	1.5	40±25	32±25	8±35
Dec-11	6.1	0.24	1.5	-86±25	73±50	-159±56

Notes: S_T = Total settlement (Table 6); S_{V1D} = Average vertical settlement due to volumetric compression using Boulanger and Idriss (2014) (BI-2014), Zhang et al. (2002) (ZRB-2002) procedures and de Greef and Lengkeek (2018) thin-layer correction; $S_{E,L}$ = Ejecta-induced settlement as the difference between the LiDAR-based S_T and S_{V1D}.

Table 8d: Ejecta-Induced settlement for the top 20 m of the soil profile for Road within the 20-m buffer for the 50th %ile PGA, P_L=50%, and C_{FC}=0.13 using BI-2014, ZRB-2002, and I_c cutoff of 2.6.

Earthquake Event(s)	M_W	PGA (g)	Depth to Groundwater (m)	S_T(mm)	S_{V1D} (mm)	$S_{E,L}$ (mm)
Sep-10	7.1	0.20	2.2	2±50	66±20	-64±54
Feb-11	6.2	0.33	2.2	120±25	141±50	-21±56
Jun-11	6.2	0.19	1.5	34±25	32±25	2±35
Dec-11	6.1	0.24	1.5	-86±25	73±50	-159±56

Notes: S_T = Total settlement (Table 6); S_{V1D} = Average vertical settlement due to volumetric compression using Boulanger and Idriss (2014) (BI-2014), Zhang et al. (2002) (ZRB-2002) procedures and de Greef and Lengkeek (2018) thin-layer correction; $S_{E,L}$ = Ejecta-induced settlement as the difference between the LiDAR-based S_T and S_{V1D}.

Table 8e: Ejecta-Induced settlement for the top 20 m of the soil profile for Road within the 50-m buffer for the 50th %ile PGA, P_L=50%, and C_{FC}=0.13 using BI-2014, ZRB-2002, and I_c cutoff of 2.6.

Earthquake Event(s)	M_W	PGA (g)	Depth to Groundwater (m)	S_T(mm)	S_{V1D} (mm)	$S_{E,L}$ (mm)
Sep-10	7.1	0.20	2.2	9±50	66±20	-57±54
Feb-11	6.2	0.33	2.2	115±25	141±50	-26±56
Jun-11	6.2	0.19	1.5	35±25	32±25	3±35
Dec-11	6.1	0.24	1.5	-88±25	73±50	-161±56

Notes: S_T = Total settlement (Table 6); S_{V1D} = Average vertical settlement due to volumetric compression using Boulanger and Idriss (2014) (BI-2014), Zhang et al. (2002) (ZRB-2002) procedures and de Greef and Lengkeek (2018) thin-layer correction; $S_{E,L}$ = Ejecta-induced settlement as the difference between the LiDAR-based S_T and S_{V1D}.

Note 3: The uncertainty for volumetric settlement was derived based on the sensitivity of volumetric settlement to PGA, C_{FC}, and P_L for each earthquake event for VsVp 57203 *Shirley Intermediate School* and CC LIQ 1 – CPT 5586 – *Vivian St* sites. Taking the 50th percentile as the baseline case, the minimum and maximum values corresponding to the difference between the 25th percentile and the 50th percentile and the 75th percentile and the 50th percentile were determined. The arithmetic mean of the range of the minimum and maximum difference was evaluated for each patch at the two sites. The maximum arithmetic mean for each earthquake event was rounded to the nearest five and used as the uncertainty value. Accordingly, the 1-D volumetric settlement uncertainties of ±20, ±50, ±25, and ±50 mm for the Sep-10, Feb-11, Jun-11, and Dec-11 earthquake events, respectively, were used for all sites in this study.

Table 9a: Coverage area and height of ejecta estimates for Patch A (20- and 50-m buffers) using photographs.

Earthquake Event	$A_{E,thick}$ (m^2)	$H_{E,thick}$ (mm)	$A_{E,thin}$ (m^2)	$H_{E,thin}$ (mm)	$A_{T,20\text{-m buffer}}$/ $A_{T,50\text{-m buffer}}$ (m^2)
Sep-10	0	0	0	0	108/489
Feb-11	0	0	0	0	108/489
Jun-11	0	0	0	0	108/489
Dec-11	0	0	0	0	108/489

Notes: $A_{E,thick/thin}$ = Coverage area of thick/thin ejecta layers; $H_{E,thick/thin}$ = Lower-upper estimate of height of thick/thin ejecta layers; A_T = Total assessment area of a buffer being considered; Thin and thick layers correspond to light gray and dark gray colors of ejecta observed in aerial photographs.

Table 9b: Coverage area and height of ejecta estimates for Road within the 10-m buffer using photographs.

Earthquake Event	$H_{E,thin}$ (mm)	$A_{E,thin}$ (m^2)	$H_{E,thick}$ (mm)	$A_{E,thick}$ (m^2)	A_T (m^2)
Sep-10	0	0	0	0	227
Feb-11	0	0	10-30	86	191
Jun-11	0	0	0	0	227
Dec-11	5-10	7.3	0	0	225

Notes: $A_{E,thick/thin}$ = Coverage area of thick/thin ejecta layers; $H_{E,thick/thin}$ = Lower-upper estimate of height of thick/thin ejecta layers; A_T = Total assessment area of a buffer being considered; Thin and thick layers correspond to light gray and dark gray colors of ejecta observed in aerial photographs.

Table 9c: Coverage area and height of ejecta estimates for Road within the 20-m buffer using photographs.

EQ Event	$H_{E,thin}$ (mm)	$A_{E,thin}$ (m^2)	$H_{E,thick}$ (mm)	$A_{E,thick}$ (m^2)	$H_{E,cone}$ (mm)	$A_{E,cone}$ (m^2)	A_T (m^2)
Sep-10	0	0	0	0	0	0	401
Feb-11	5-10	7.0	10-30	161	100-200	4.4	353
Jun-11	0	0	0	0	0	0	401
Dec-11	5-10	7.3	0	0	0	0	375

Notes: $A_{E,thick/thin}$ = Coverage area of thick/thin ejecta layers; $H_{E,thick/thin}$ = Lower-upper estimate of height of thick/thin ejecta layers; Thin and thick layers correspond to light gray and dark gray colors of ejecta observed in aerial photographs; $A_{E,cone}$ = Coverage area of conically shaped ejecta layers; $H_{E,cone}$ = Lower-upper estimate of height of conically shaped ejecta layers; A_T= Total assessment area of a buffer being considered.

Table 9d: Coverage area and height of ejecta estimates for Road within the 50-m buffer (without the 20-m buffer) using photographs.

EQ Event	$H_{E,thin}$ (mm)	$A_{E,thin}$ (m^2)	$H_{E,thick}$ (mm)	$A_{E,thick}$ (m^2)	$H_{E,cone}$ (mm)	$A_{E,cone}$ (m^2)	$H_{E,prism/pyr}$ (mm)	$V_{E,prism/pyr}$ (m^2)	A_T (m^2)
Sep-10	0	0	0	0	0	0	0	0	679
Feb-11	5-10	27	10-30	193	100-200	4.4	12-49	0.156-0.313	595
Jun-11	0	0	0	0	0	0	0	0	679
Dec-11	5-10	7.3	0	0	0	0	0	0	632

Notes: $A_{E,thick/thin}$ = Coverage area of thick/thin ejecta layers; $H_{E,thick/thin}$ = Lower-upper estimate of height of thick/thin ejecta layers; Thin and thick layers correspond to light gray and dark gray colors of ejecta observed in aerial photographs; $A_{E,cone}$ = Coverage area of conically shaped ejecta layers; $H_{E,cone}$ = Lower-upper estimate of height of conically shaped ejecta layers; $H_{E,prism/pyr}$ = Lower-upper estimate of ejecta height near the curb based on 2-4% cross slope of normal crown; $V_{E,prism}$ = Lower-upper estimate of total volume of prismatic-shape ejecta; $V_{E,pyr}$ = Lower-upper estimate of total volume of pyramidal-shape ejecta; A_T= Total assessment area of a buffer being considered.

Note 4: The values in Table 9 correspond to the coverage area of ejecta outlined in aerial photographs (Figures 82 through 86) and the lower and upper estimates of ejecta height based on ground photographs (Figure 87) and EQC LDAT inspection reports for properties within the 50-m buffer (e.g., some properties settled 0-50 mm globally (minor damage), some properties settled 0-20 mm due to tilting (minor damage) and/or 0-10 mm due to twisting (minor damage), and land experienced cosmetic to significant undulation). The ejecta-induced settlement using photographs and engineering judgment, $S_{E,P}$, is estimated as

$$S_{E,P} = \frac{\sum_{i=1}^{a} A_{E,thick,i} * H_{E,thick,i} + \sum_{j=1}^{b} A_{E,thin,j} * H_{E,thin,j}}{A_T} + \frac{\frac{1}{3}\sum_{m=1}^{e} A_{E,cone,m} * H_{E,cone,m} + \frac{1}{2}\sum_{n=1}^{f} W_{E,prism,n} * H_{E,prism,n} * L_{E,prism,n}}{A_T} + \frac{\frac{1}{3}\sum_{p=1}^{g} W_{E,pyramid,p} * H_{E,pyramid} * L_{E,pyramid}}{A_T} = \frac{\sum_{i=1}^{a} V_{E,thick,i} + \sum_{j=1}^{b} V_{E,thin,j}}{A_T} + \frac{\sum_{m=1}^{e} V_{E,cone,m} + \sum_{n=1}^{f} V_{E,prism,n} + \sum_{p=1}^{g} V_{E,pyramid,p}}{A_T}$$

where

- $A_{E,thick,i}$ and $H_{E,thick,i}$ are the area and the height of a thick ejecta layer, respectively;
- $A_{E,thin,j}$ and $H_{E,thin,j}$ are the area and the height of a thin ejecta layer, respectively;
- $A_{E,cone,m}$ and $H_{E,cone,m}$ are the area and the height of a conically shaped ejecta, respectively;
- $W_{E,prism,n}$ and $L_{E,prism,n}$ are the width and the length of the coverage area of a prismatically shaped ejecta layer, respectively, and $H_{E,prism,n}$ is the height of a prism-like ejecta layer;
- $W_{E,pyr,p}$ and $L_{E,pyr,p}$ are the width and the length of the coverage area of a pyramid-like ejecta layer, respectively, and $H_{E,pyr,p}$ is the height of a pyramid-like ejecta layer;
- A_T is the total assessment area for a buffer being considered (Figure 1).

Table 10a: Ejecta-induced settlement estimates for Patches A based on photographs.

Earthquake Event	Patch A (10-m buffer)		Patch A (20-m buffer)		Patch A (50-m buffer)	
	$S_{E,P,lower}$ (mm)	$S_{E,P,upper}$ (mm)	$S_{E,P,lower}$ (mm)	$S_{E,P,upper}$ (mm)	$S_{E,P,lower}$ (mm)	$S_{E,P,upper}$ (mm)
Sep-10	NA	NA	0	0	0	0
Feb-11	NA	NA	0	0	0	0
Jun-11	NA	NA	0	0	0	0
Dec-11	NA	NA	0	0	0	0

Note: $S_{E,P,lower}$ and $S_{E,P,upper}$ correspond to lower and upper estimates of $S_{E,P}$, respectively.

Table 10b: Ejecta-induced settlement estimates for Road based on photographs.

Earthquake Event	Road (10-m buffer)		Road (20-m buffer)		Road (50-m buffer)	
	$S_{E,P,lower}$ (mm)	$S_{E,P,upper}$ (mm)	$S_{E,P,lower}$ (mm)	$S_{E,P,upper}$ (mm)	$S_{E,P,lower}$ (mm)	$S_{E,P,upper}$ (mm)
Sep-10	0	0	0	0	0	0
Feb-11	5	13	5	15	4	11
Jun-11	0	0	0	0	0	0
Dec-11	≈0	≈0	≈0	≈0	≈0	≈0

Note: $S_{E,P,lower}$ and $S_{E,P,upper}$ correspond to lower and upper estimates of $S_{E,P}$, respectively.

Table 11a: Best final estimates of ejecta-induced settlement for Patch A.

EQ Event	Patch A (10-m buffer)			Patch A (20-m buffer)			Patch A (50-m buffer)		
	$S_{E,L}$ (mm)	$S_{E,P}$ (mm)	$S_{E,final}$ (mm)	$S_{E,L}$ (mm)	$S_{E,P}$ (mm)	$S_{E,final}$ (mm)	$S_{E,L}$ (mm)	$S_{E,P}$ (mm)	$S_{E,final}$ (mm)
Sep-10	NA	NA	NA	-19±77	0	0	-33±77	0	0
Feb-11	NA	NA	NA	-48±56	0	0	-45±56	0	0
Jun-11	NA	NA	NA	-20±56	0	0	-19±56	0	0
Dec-11	NA	NA	NA	-174±71	0	0	-176±71	0	0

Notes: $S_{E,L}$ = Ejecta-induced settlement based on LiDAR data reported in Table 8; $S_{E,P}$ = Median ejecta-induced settlement for the range of values reported in Table 10; $S_{E,final}$ = Best final estimate of ejecta-induced settlement rounded to the nearest 5; Final plus/minus values are also rounded to the nearest 5.

Table 11b: Best final estimates of ejecta-induced settlement for Road.

EQ Event	Road (10-m buffer)			Road (20-m buffer)			Road (50-m buffer)		
	$S_{E,L}$ (mm)	$S_{E,P}$ (mm)	$S_{E,final}$ (mm)	$S_{E,L}$ (mm)	$S_{E,P}$ (mm)	$S_{E,final}$ (mm)	$S_{E,L}$ (mm)	$S_{E,P}$ (mm)	$S_{E,final}$ (mm)
Sep-10	-46±54	0	0	-64±54	0	0	-57±54	0	0
Feb-11	-18±56	9±4	10±5	-21±56	10±5	10±5	-26±56	7.5±3.5	10±5
Jun-11	8±35	0	0	2±35	0	0	3±35	0	0
Dec-11	-159±56	≈0	<5	-159±56	≈0	<5	-161±56	≈0	<5

Notes: $S_{E,L}$ = Ejecta-induced settlement based on LiDAR data reported in Table 8; $S_{E,P}$ = Median ejecta-induced settlement for the range of values reported in Table 10; $S_{E,final}$ = Best final estimate of ejecta-induced settlement rounded to the nearest 5; Final plus/minus values are also rounded to the nearest 5.

Note 5: $S_{E,final}$ for Patch A and Road for all earthquake events is based solely on $S_{E,P}$. The uncertainty associated with $S_{E,final}$ is also based on the uncertainty associated with $S_{E,P}$ only. The weights are based on the LiDAR error bands, LPI prediction error (Maurer et al. 2014[3]), and completeness of visual evidence (i.e., ground and aerial photographs and EQC LDAT property inspection reports for the site). The negative $S_{E,L}$ values are given a zero weight. The Vangelis Ln & Fernbrook Pl site is in the apparent zone of higher ground surface subsidence for the Sep-10 and Dec-11 EQs and in the apparent zone of

[3] Maurer, B. W., Green, R. A., Cubrinovski, M., & Bradley, B. A. (2014). Evaluation of the Liquefaction Potential Index for Assessing Liquefaction Hazard in Christchurch, New Zealand. *Journal of Geotechnical and Geoenvironmental Engineering*, 140(7), 04014032-1-11. doi:10.1061/(asce)gt.1943-5606.0001117

lower ground surface subsidence for the Feb-10 EQ. The site is also in the zone of moderate LPI overprediction of liquefaction severity for the Sep-10 and Feb-11 EQs. There are high-resolution aerial photographs as well as EQC LDAT property inspection reports for properties within the site with ground photographs.

Summary 1:

- **The best estimate of the ejecta-induced free-field ground settlement at the Vangelis Ln & Fernbrook Pl site for the SEP 2010, FEB 2011, JUN 2011, and DEC 2011 earthquake is 0 mm, 0 mm, 0 mm, and 0 mm, respectively.**
- **The best estimate of the ejecta-induced settlement of the road at the Vangelis Ln & Fernbrook Pl site for the SEP 2010, FEB 2011, JUN 2011, and DEC 2011 earthquake is 0 mm, 10±5 mm, 0 mm, and <5 mm, respectively.**

Note 6: The site was initially labeled as CC LIQ 7, as can be seen in some of the following figures.

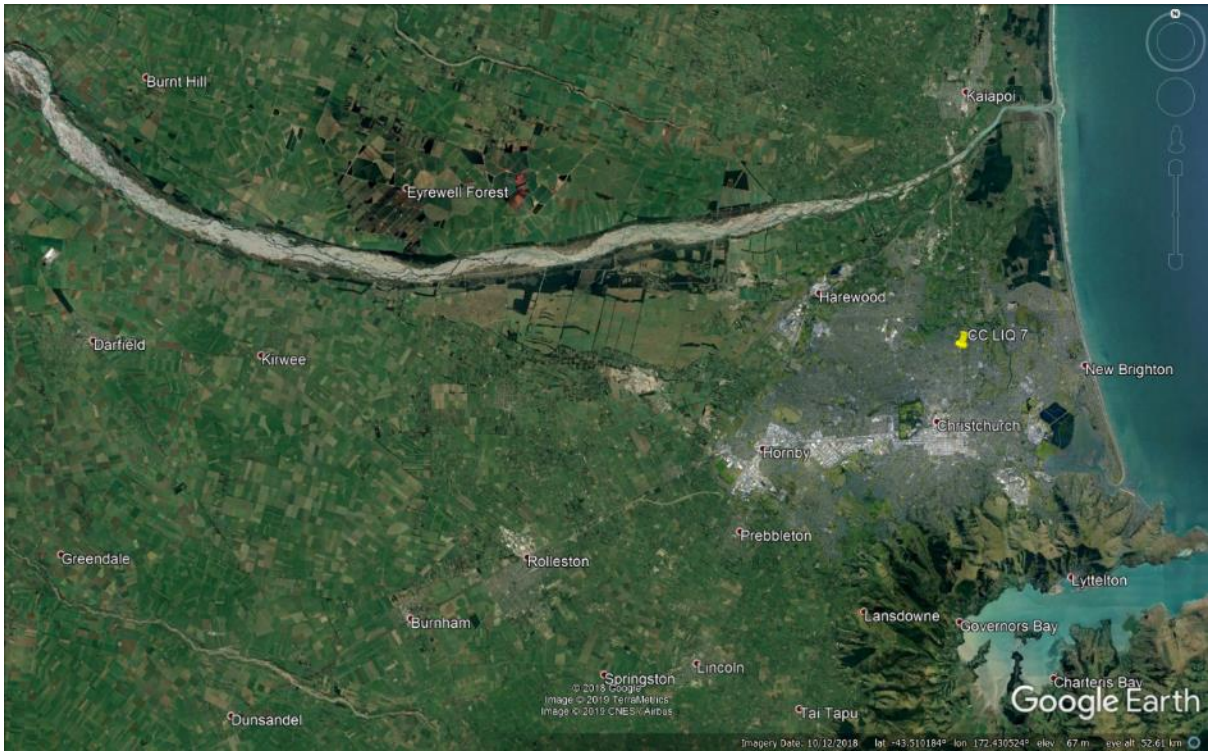

Figure 7: Location of the site.

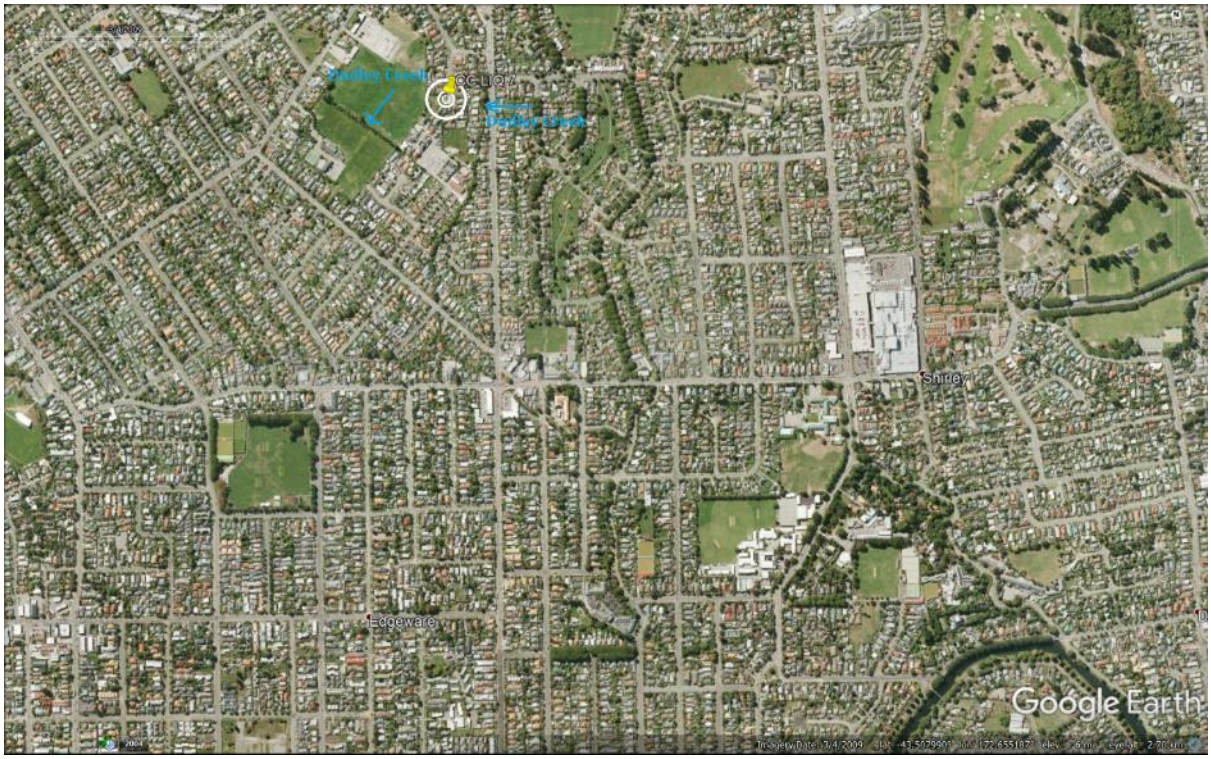

Figure 8: Position of the site relative to nearby buildings, vegetation, and free-face features.

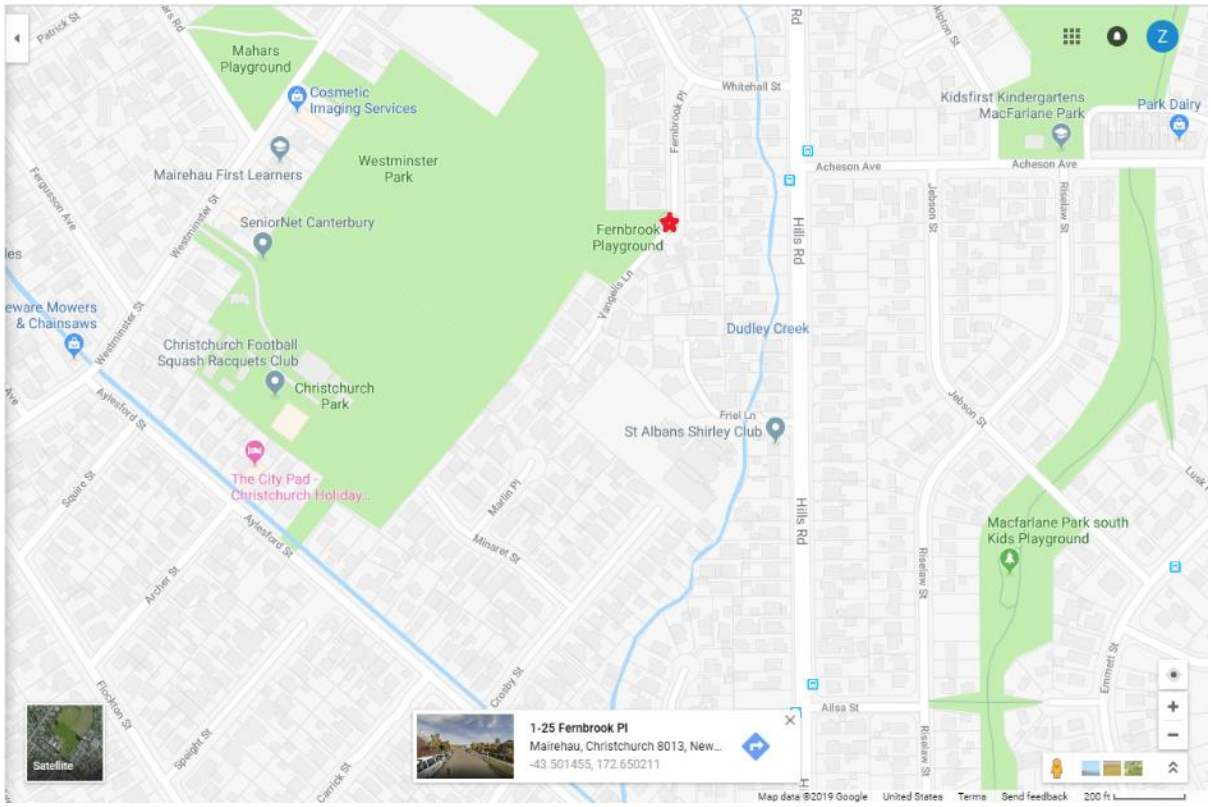

Figure 9: Position of the site relative to two branches of Dudley Creek.

Figure 10: Street view of the site showing flat land.

Figure 11: Satellite image of the site taken in Dec 2004.

Figure 12: Satellite image of the site taken in Mar 2009.

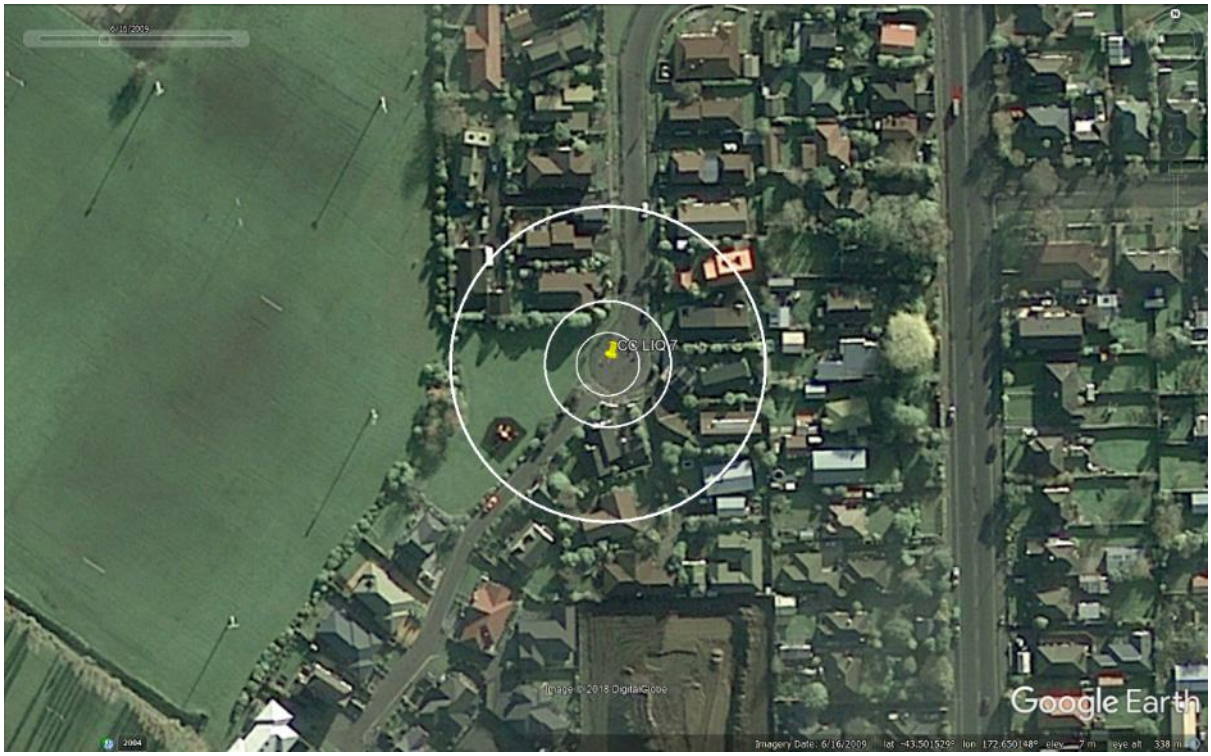

Figure 13: Satellite image of the site taken in Jun 2009.

Figure 14: Satellite image of the site taken in Apr 2012.

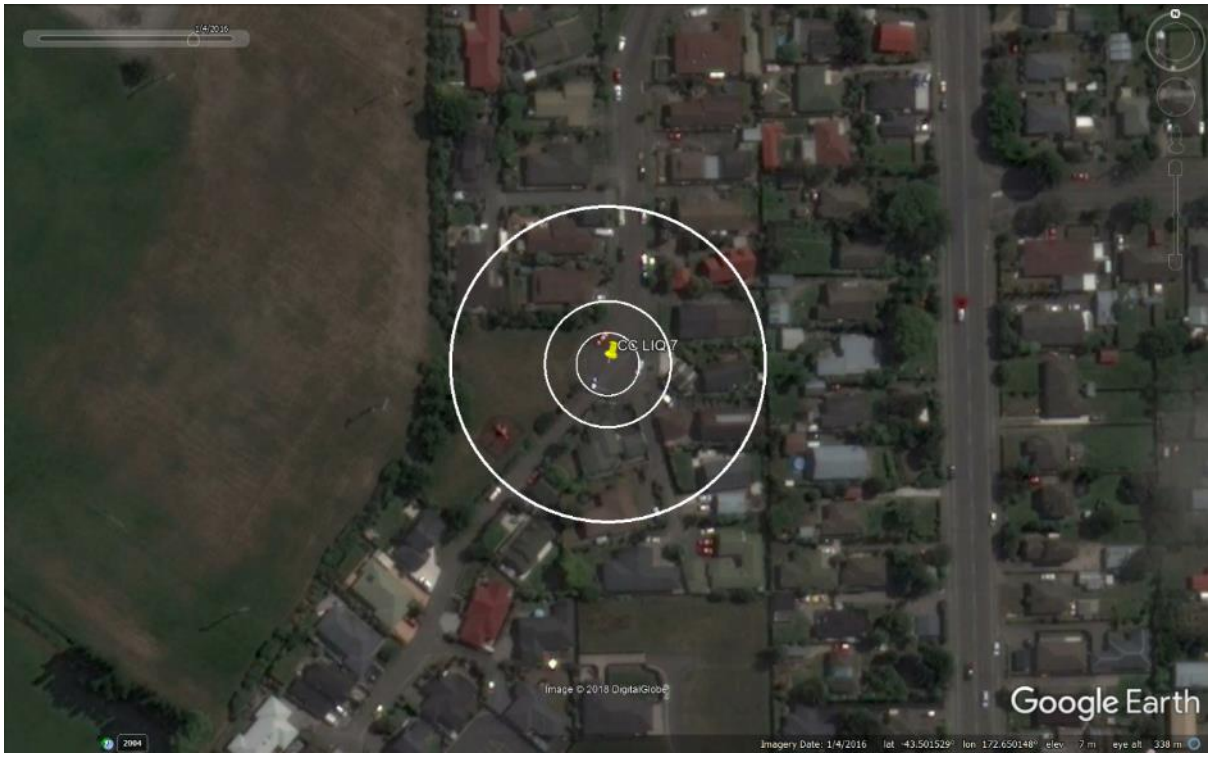

Figure 15: Satellite image of the site taken in Jan 2016.

Figure 16: Aerial photograph of the site taken on Sep 4, 2010.

Figure 17: Aerial photograph of the site taken on Feb 24, 2011.

Figure 18: Aerial photograph of the site taken on June 14-15, 2011.

Figure 19: Aerial photograph of the site taken on June 16, 2011.

Figure 20: Aerial photograph of the site taken on Dec 24, 2012.

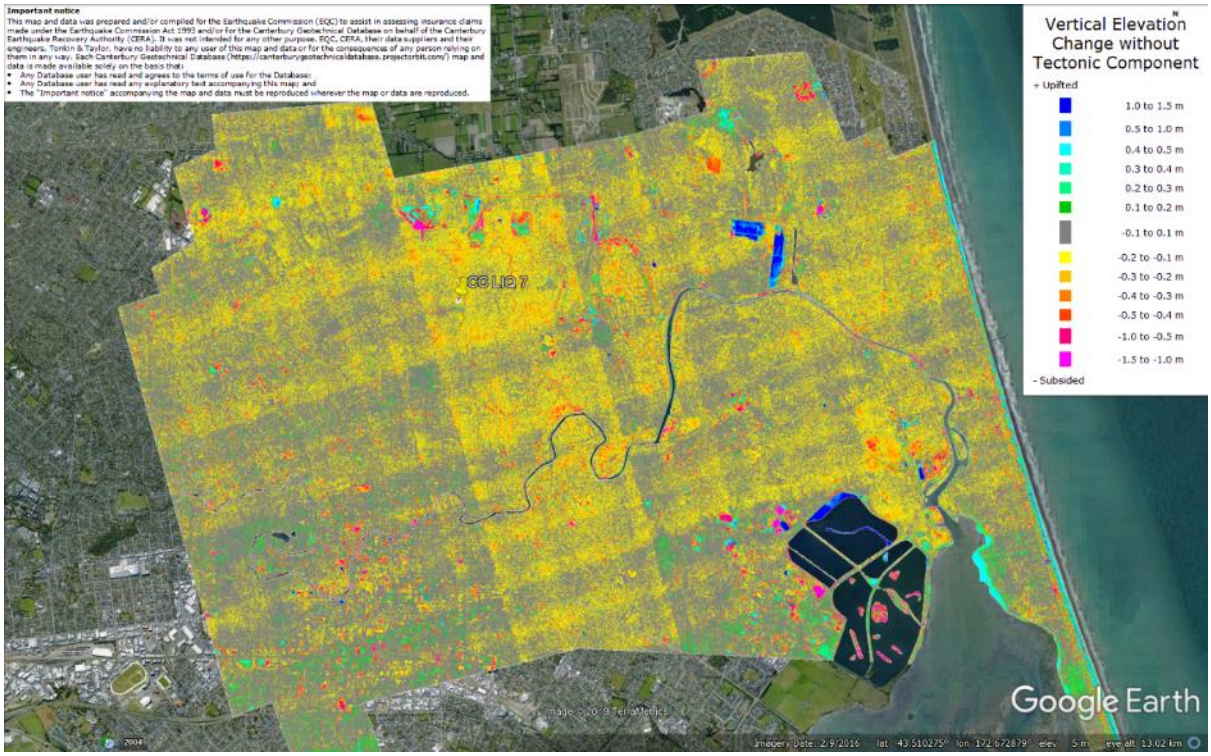

Figure 21: Vertical Ground Movements (Surface – Tectonic) for Sep 2010 Earthquake – the site is in the apparent zone of overestimated ground surface subsidence.

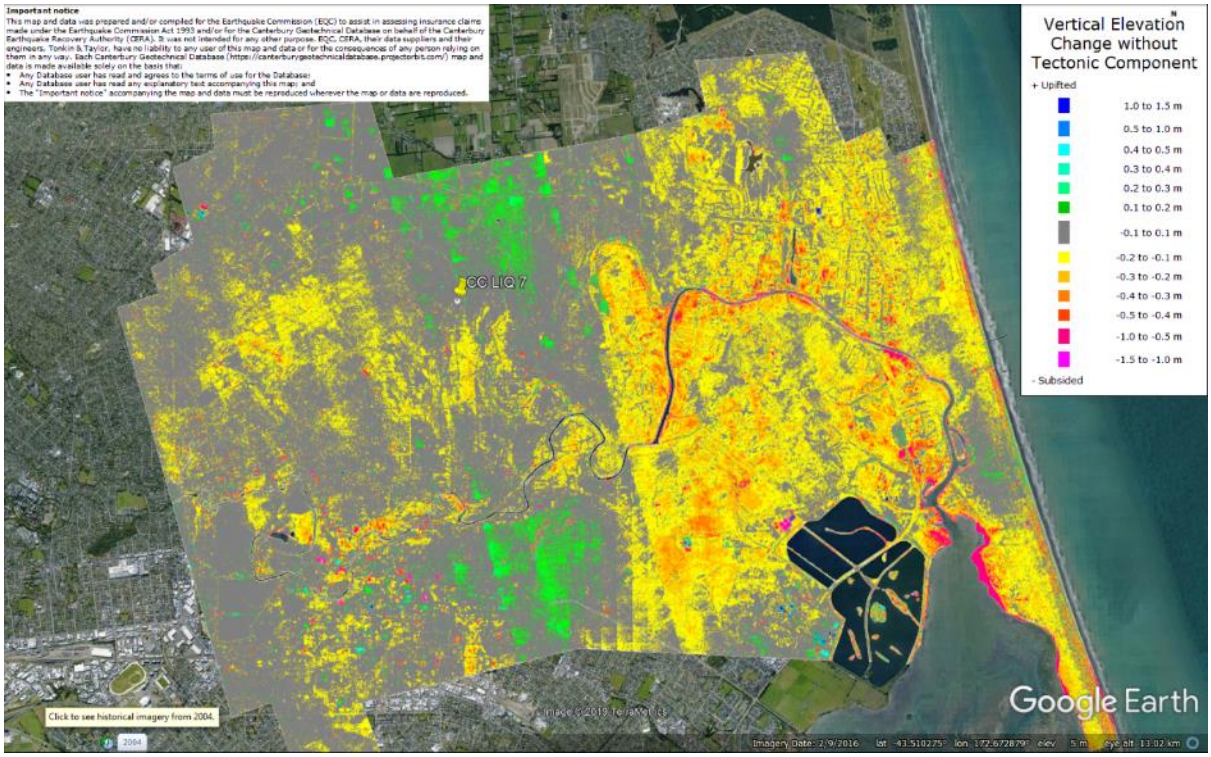

Figure 22: Vertical Ground Movements (Surface – Tectonic) for Feb 2011 Earthquake – the site is in the apparent zone of underestimated ground surface subsidence.

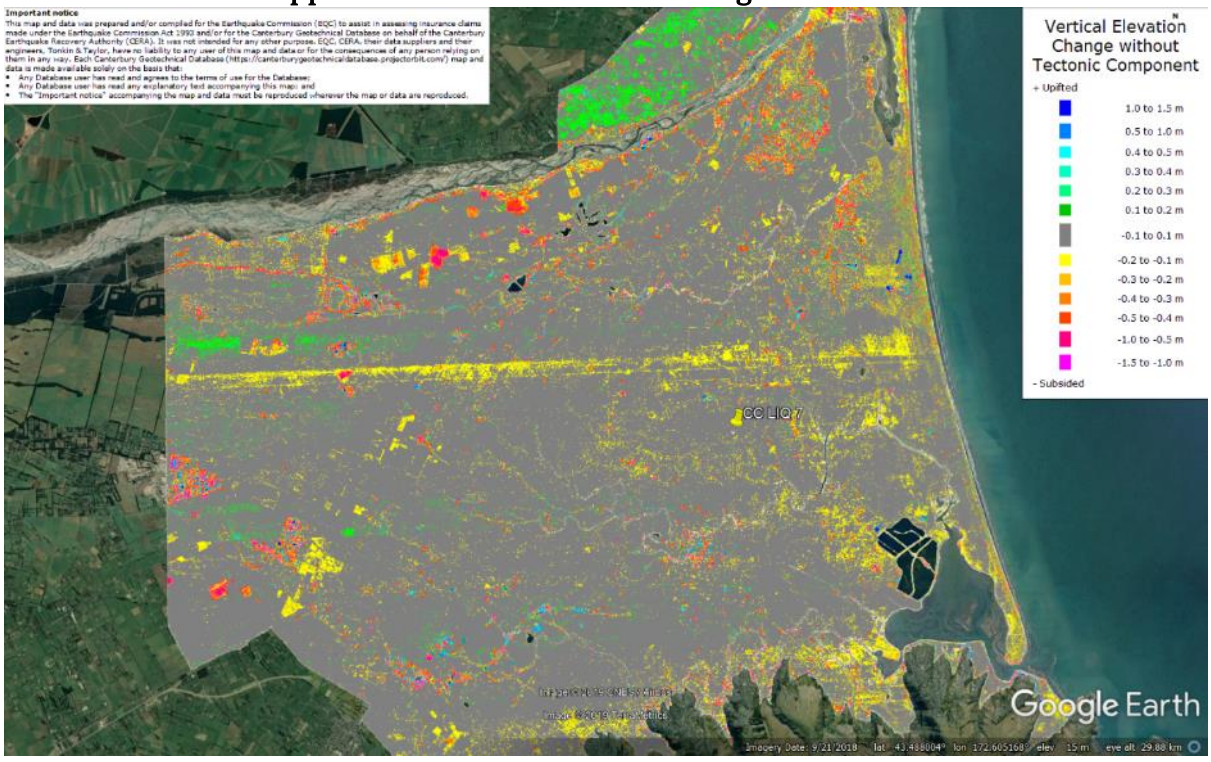

Figure 23: Vertical Ground Movements (Surface – Tectonic) for June 2011 Earthquake – the site is not in the apparent zone of overestimated or underestimated ground surface subsidence.

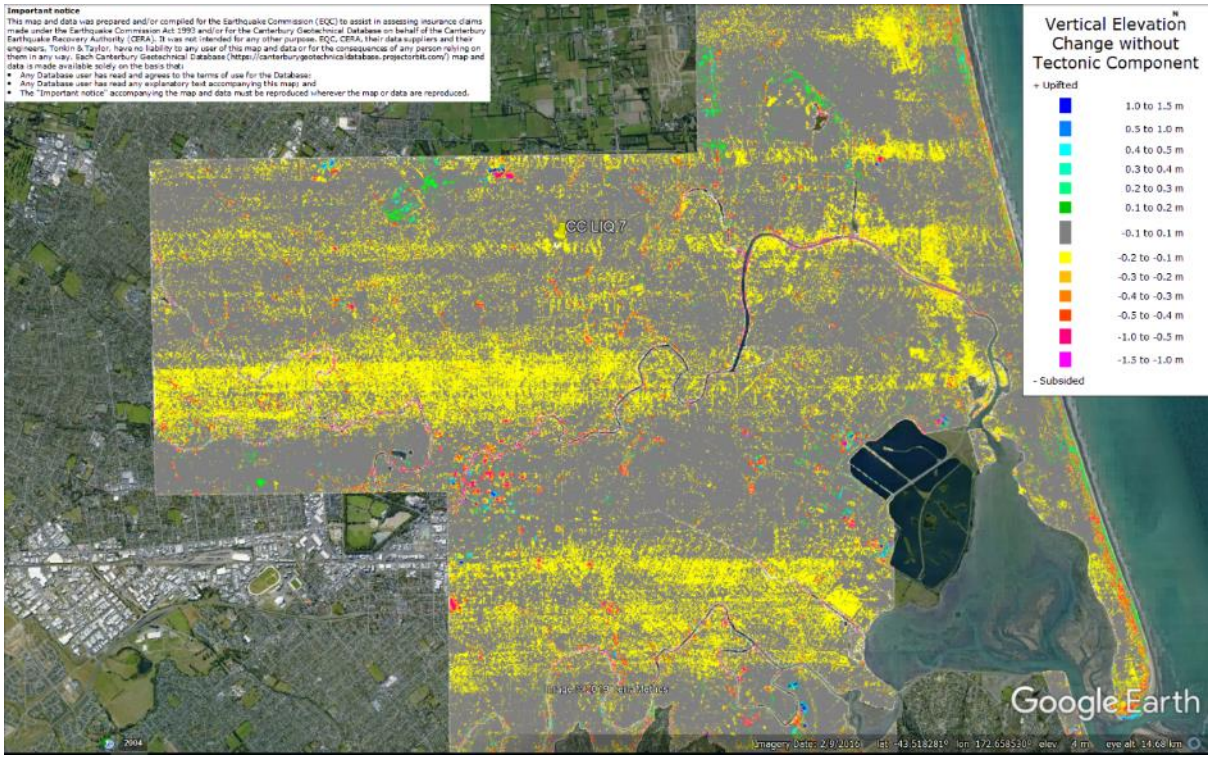

Figure 24: Vertical Ground Movements (Surface – Tectonic) for Dec 2011 Earthquake – the site is in the apparent zone of overestimated ground surface subsidence (i.e., Feb 2012 LiDAR flight error).

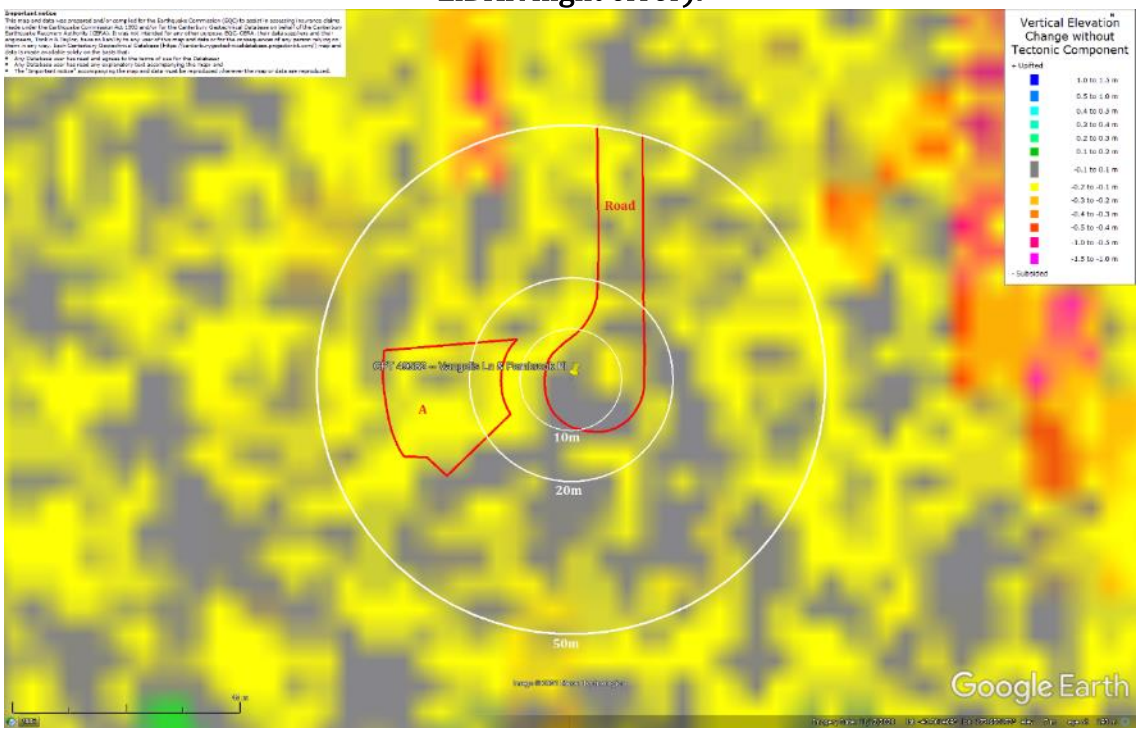

Figure 25: Ground surface subsidence without tectonic component for Sep 2010 Earthquake according to the LiDAR DEM.

Figure 26: Ground surface subsidence without tectonic component for Feb 2011 Earthquake according to the LiDAR DEM.

Figure 27: Ground surface subsidence without tectonic component for Jun 2011 Earthquake according to the LiDAR DEM.

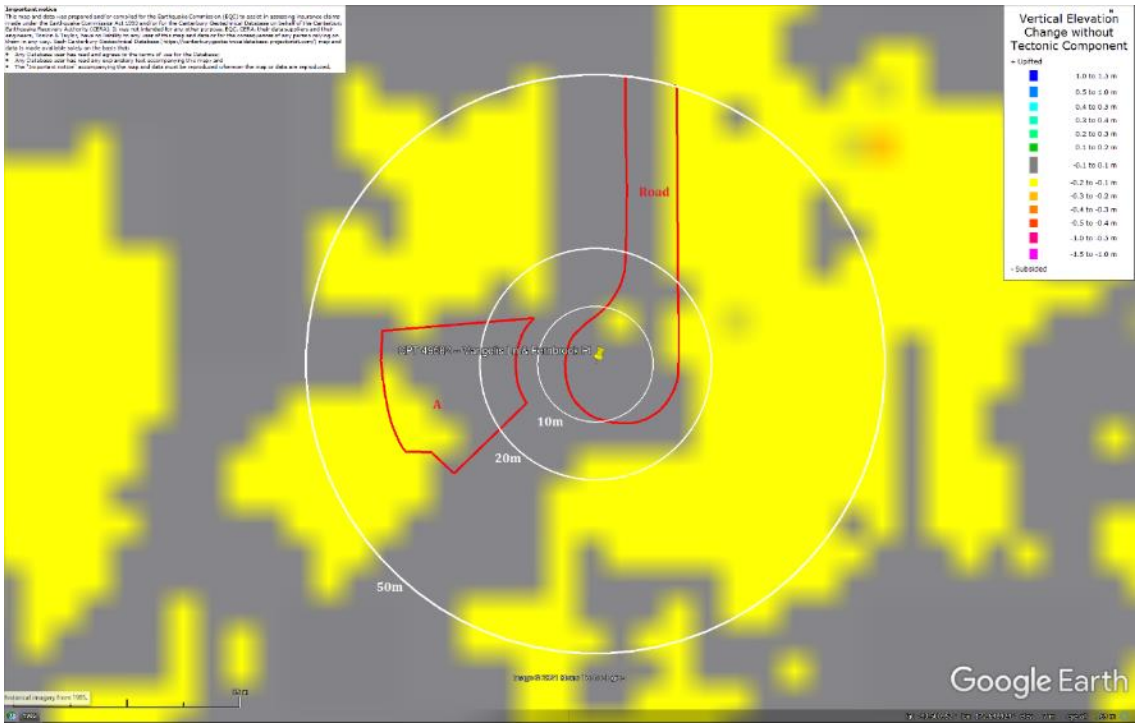

Figure 28: Ground surface subsidence without tectonic component for Dec 2011 Earthquake according to the LiDAR DEM.

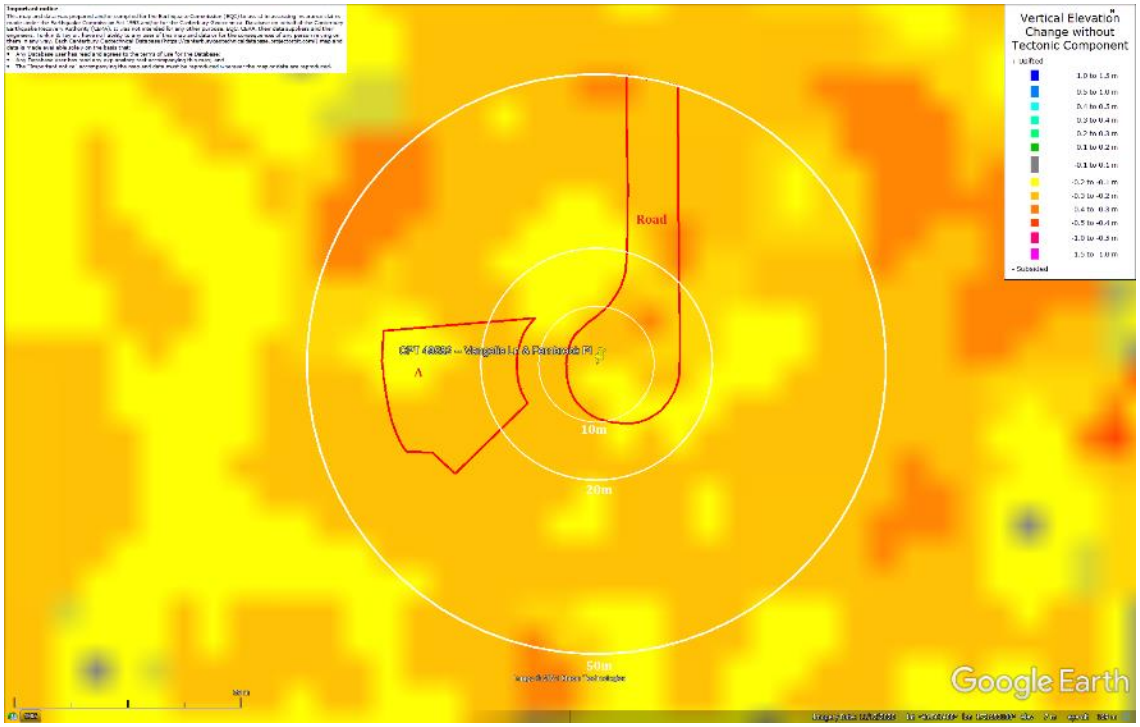

Figure 29: Ground surface subsidence without tectonic component for Canterbury Earthquake Sequence according to the LiDAR DEM.

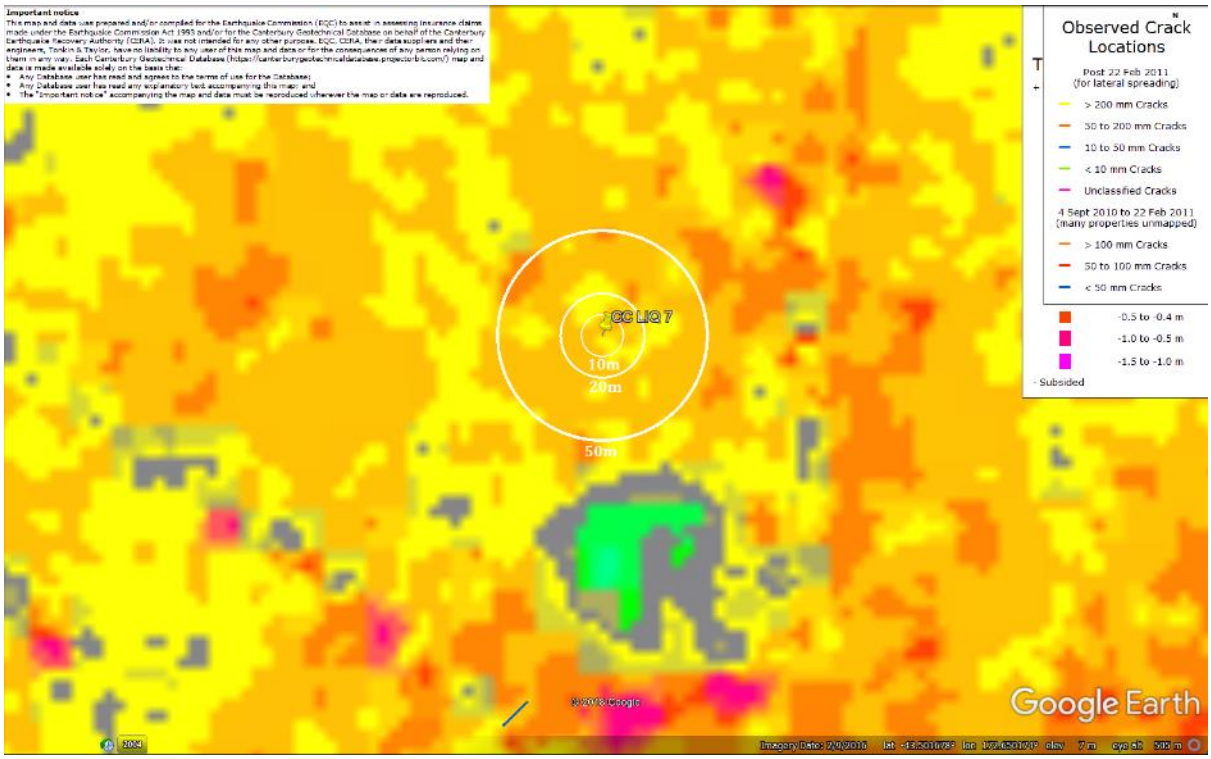

Figure 30: Absence of ground cracks indicates no lateral spreading for Canterbury Earthquake Sequence.

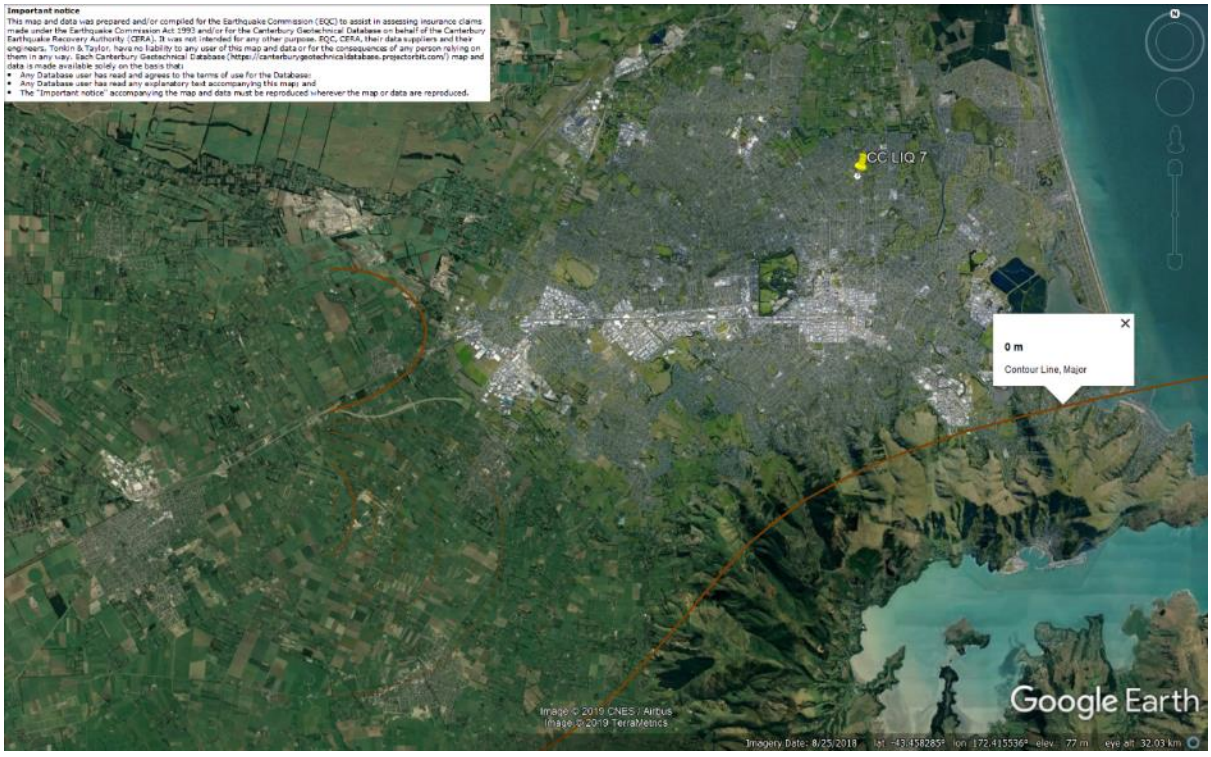

Figure 31: Vertical tectonic movements for Sep 2010 Earthquake.

Figure 32: Vertical tectonic movements for Feb 2011 Earthquake.

Figure 33: Vertical tectonic movements for June 2011 Earthquake.

Figure 34: Vertical tectonic movements for Dec 2011 Earthquake.

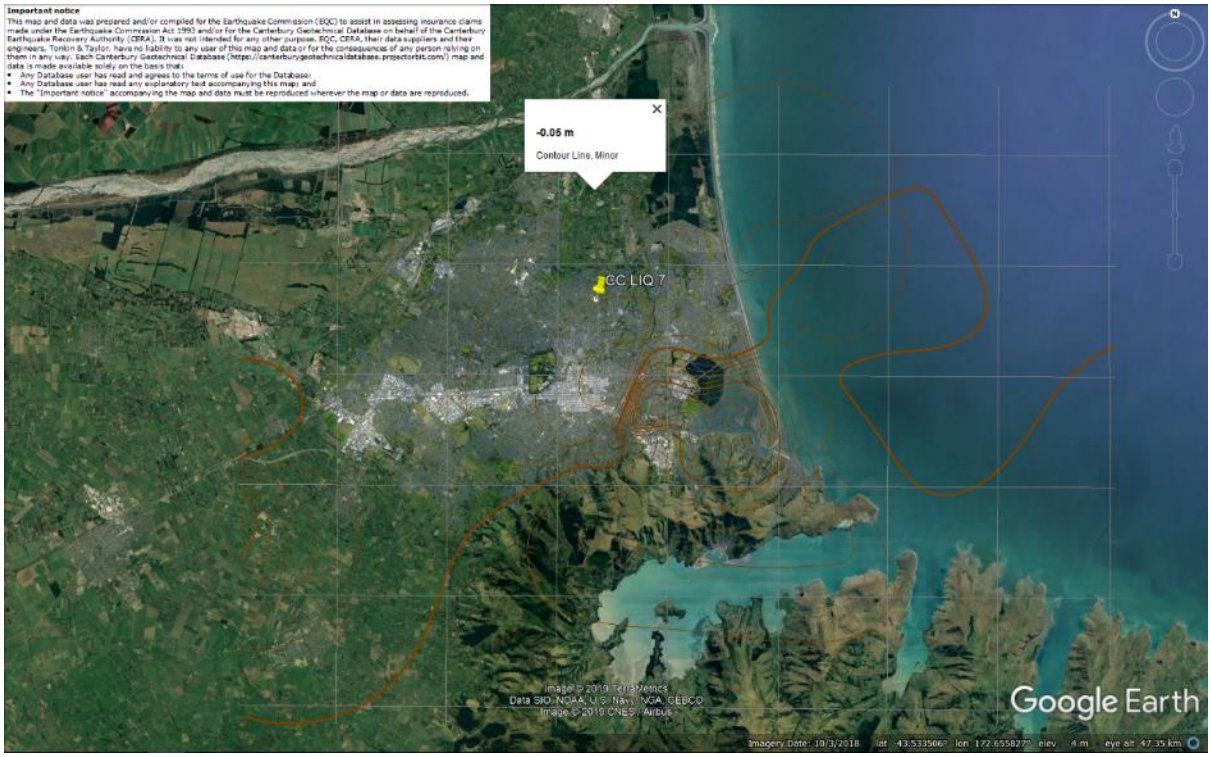

Figure 35: Vertical tectonic movements for Canterbury Earthquake Sequence.

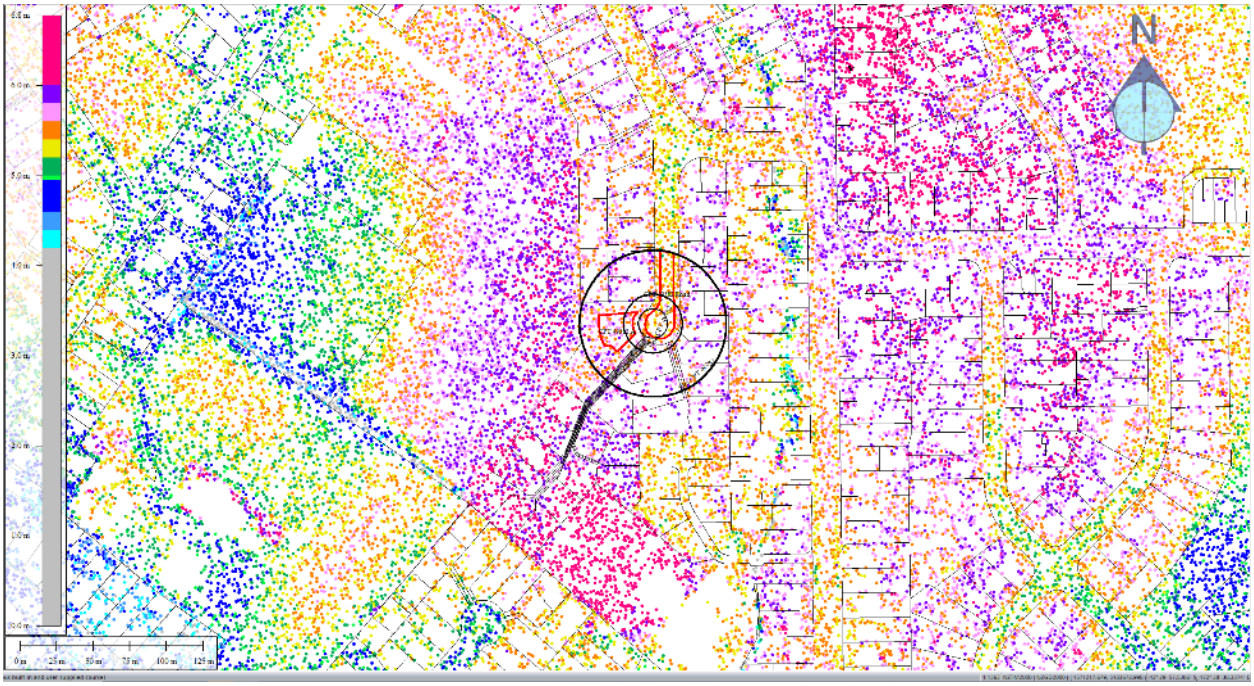

Figure 36: Jul 2003 LiDAR survey.

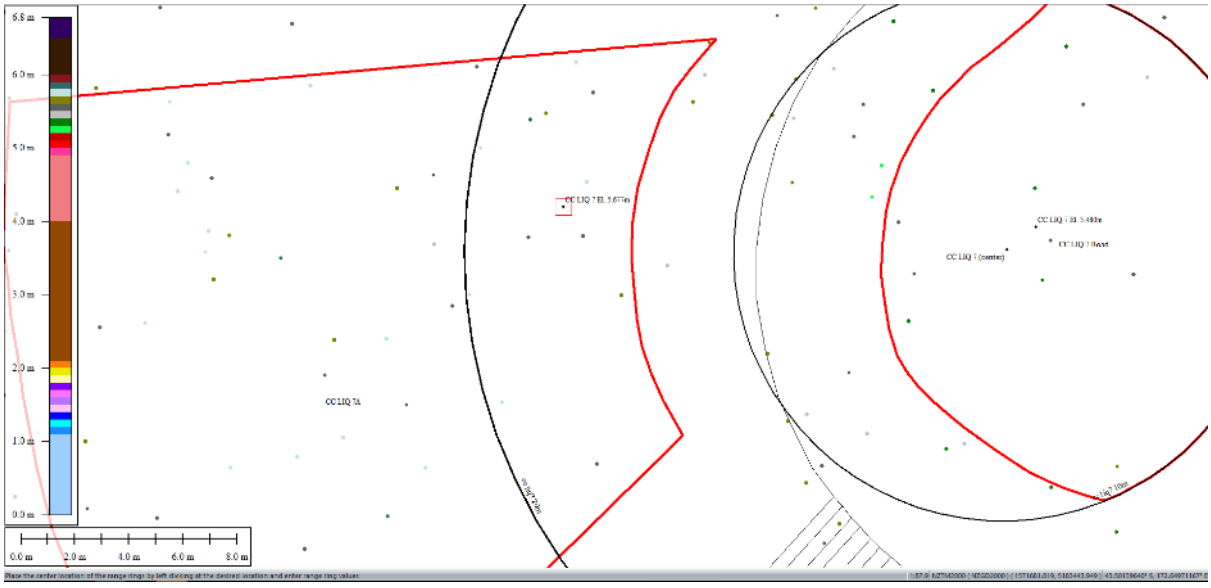

Figure 37: Ground surface elevation averaged over 20-m buffer for Patch A for Jul 2003 LiDAR survey.

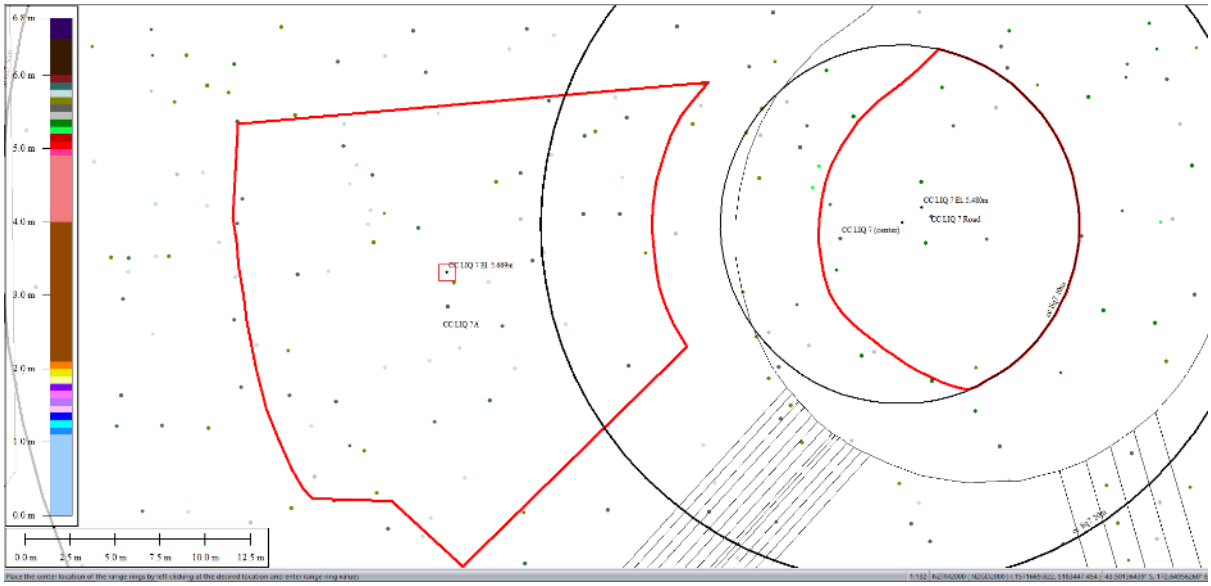

Figure 38: Ground surface elevation averaged over 50-m buffer for Patch A for Jul 2003 LiDAR survey.

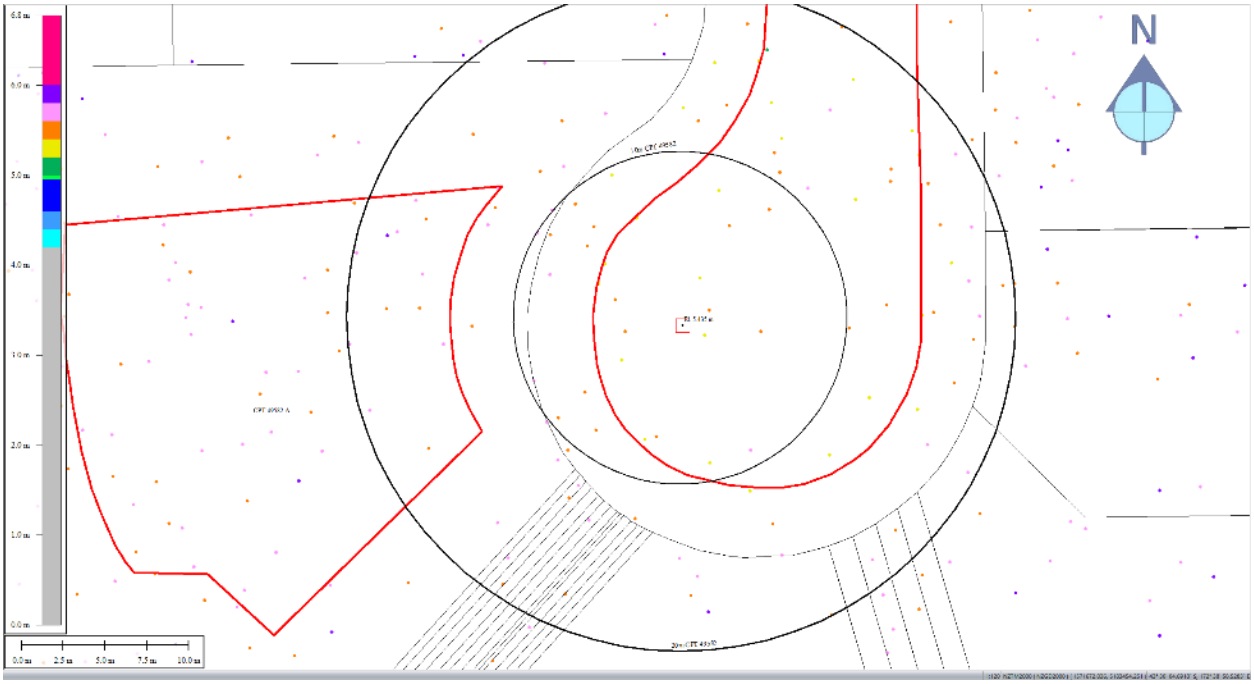

Figure 39: Ground surface elevation averaged over 10-m buffer for Road for Jul 2003 LiDAR survey.

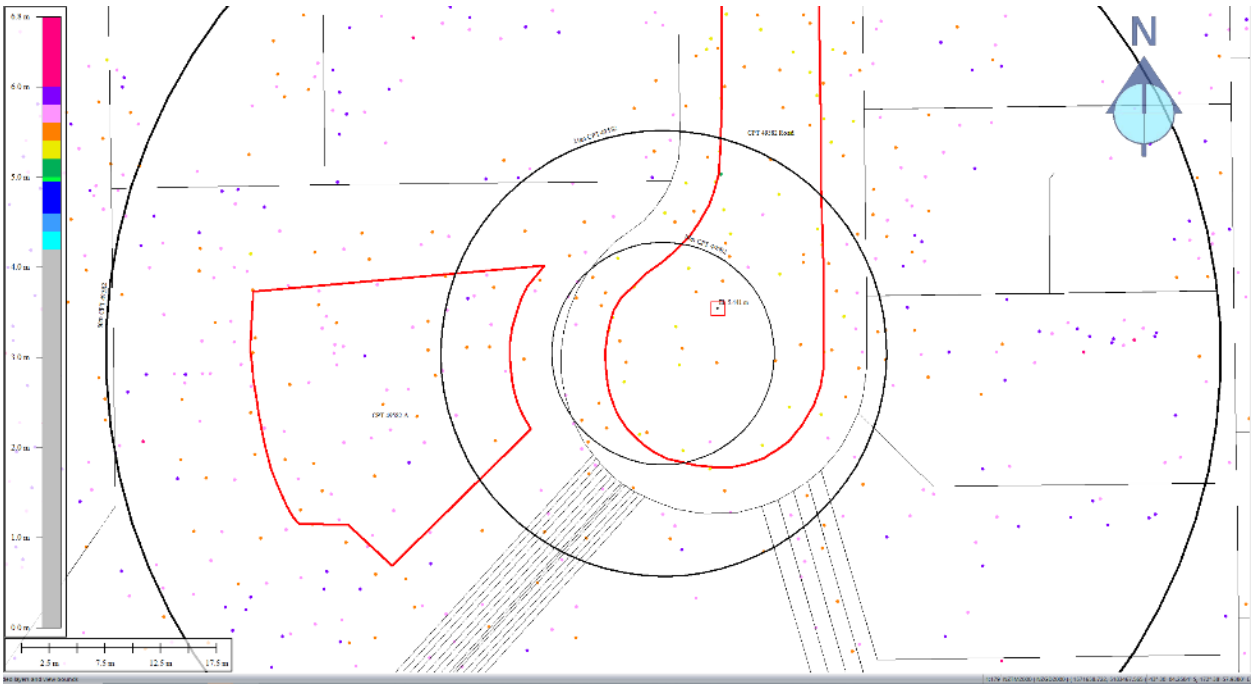

Figure 40: Ground surface elevation averaged over 20-m buffer for Road for Jul 2003 LiDAR survey.

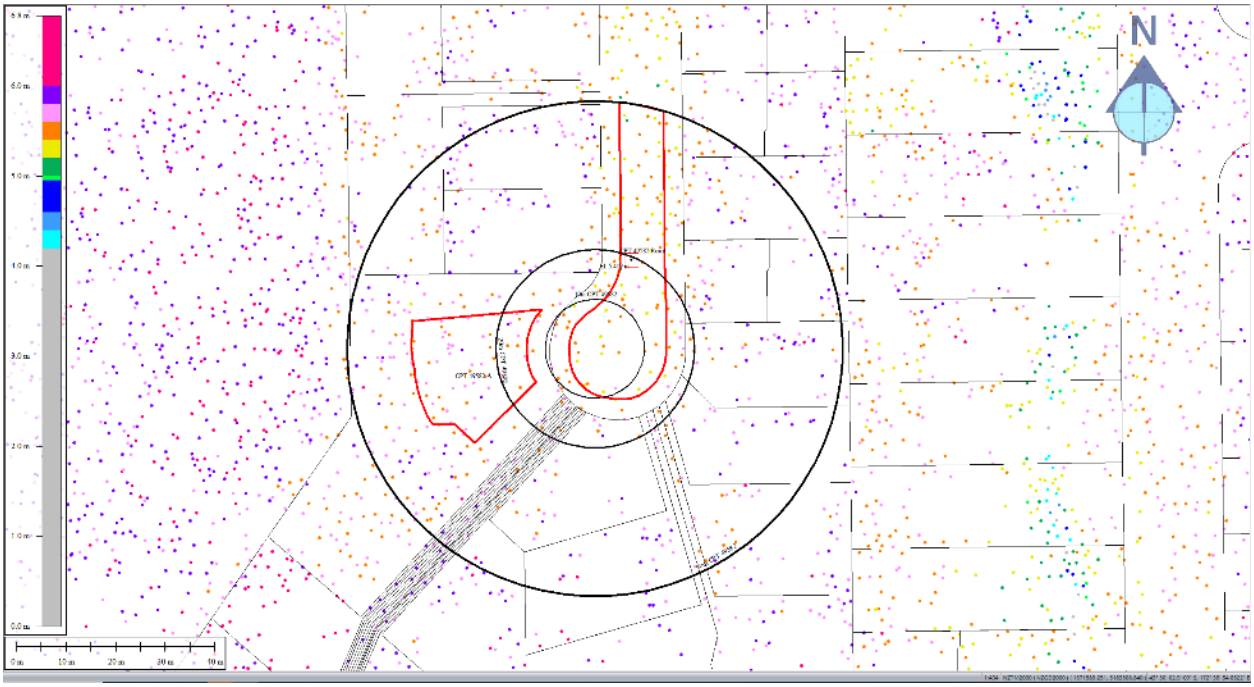

Figure 41: Ground surface elevation averaged over 50-m buffer for Road for Jul 2003 LiDAR survey.

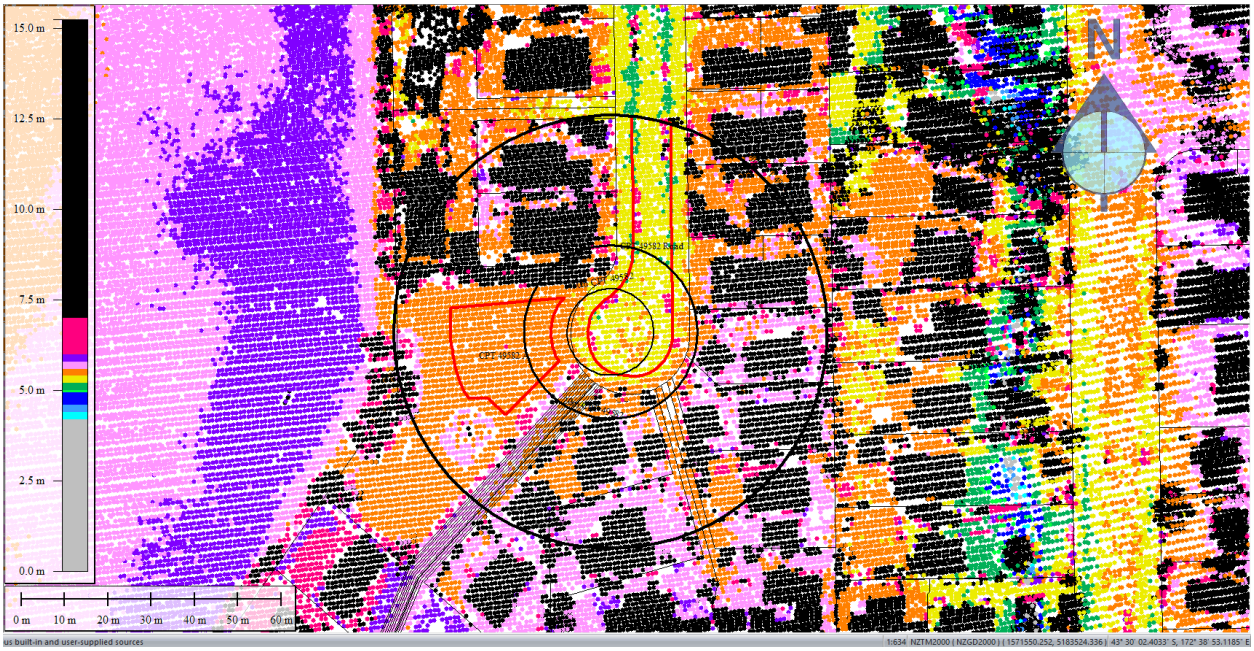

Figure 42: Sep 5, 2010 LiDAR survey.

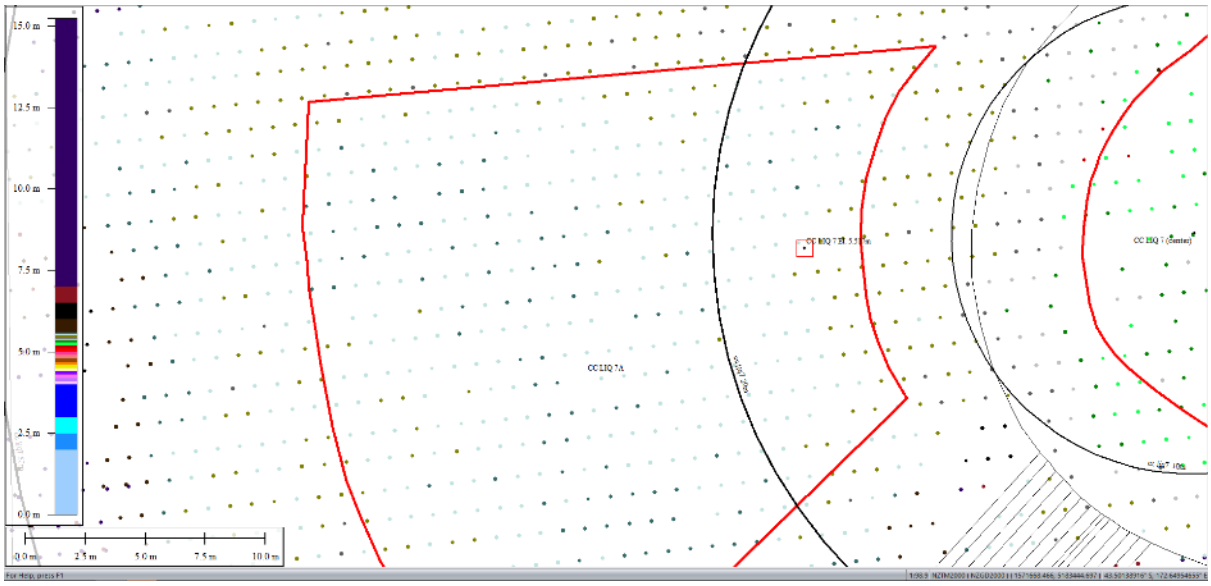

Figure 43: Ground surface elevation averaged over 20-m buffer for Patch A for Sep 5, 2010 LiDAR survey.

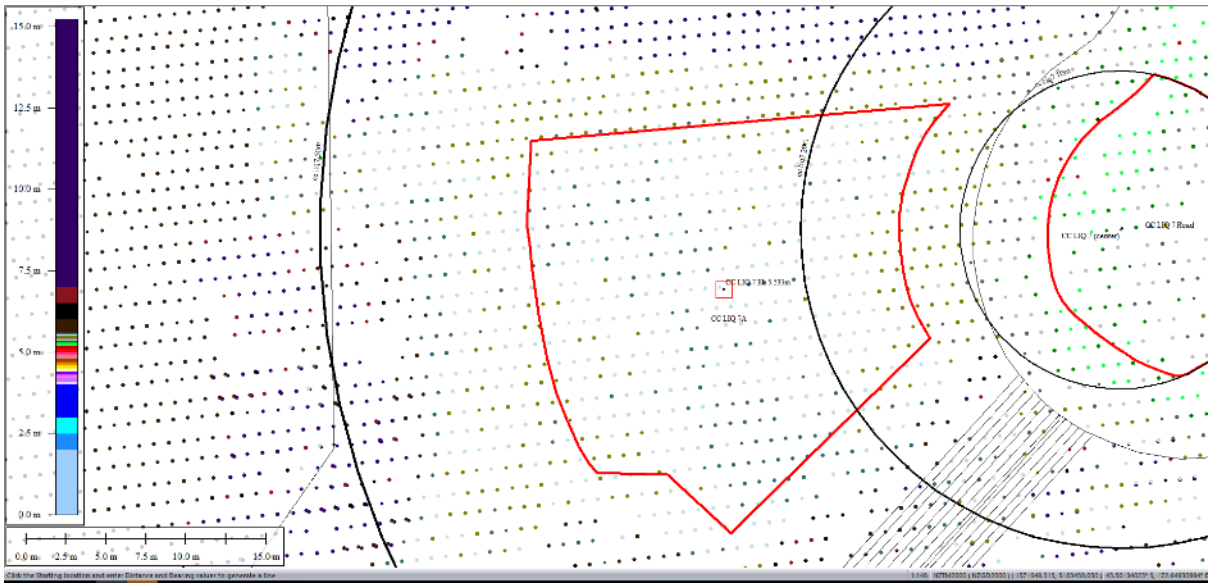

Figure 44: Ground surface elevation averaged over 50-m buffer for Patch A for Sep 5, 2010 LiDAR survey.

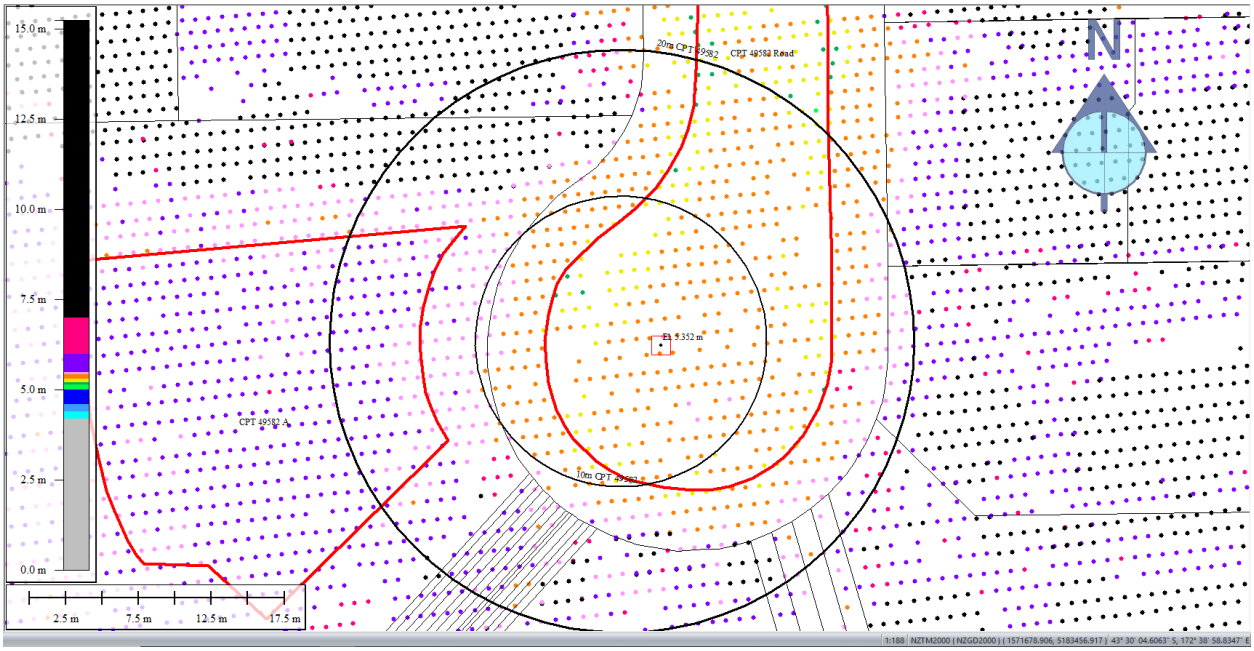

Figure 45: Ground surface elevation averaged over 10-m buffer for Road for Sep 5, 2010 LiDAR survey.

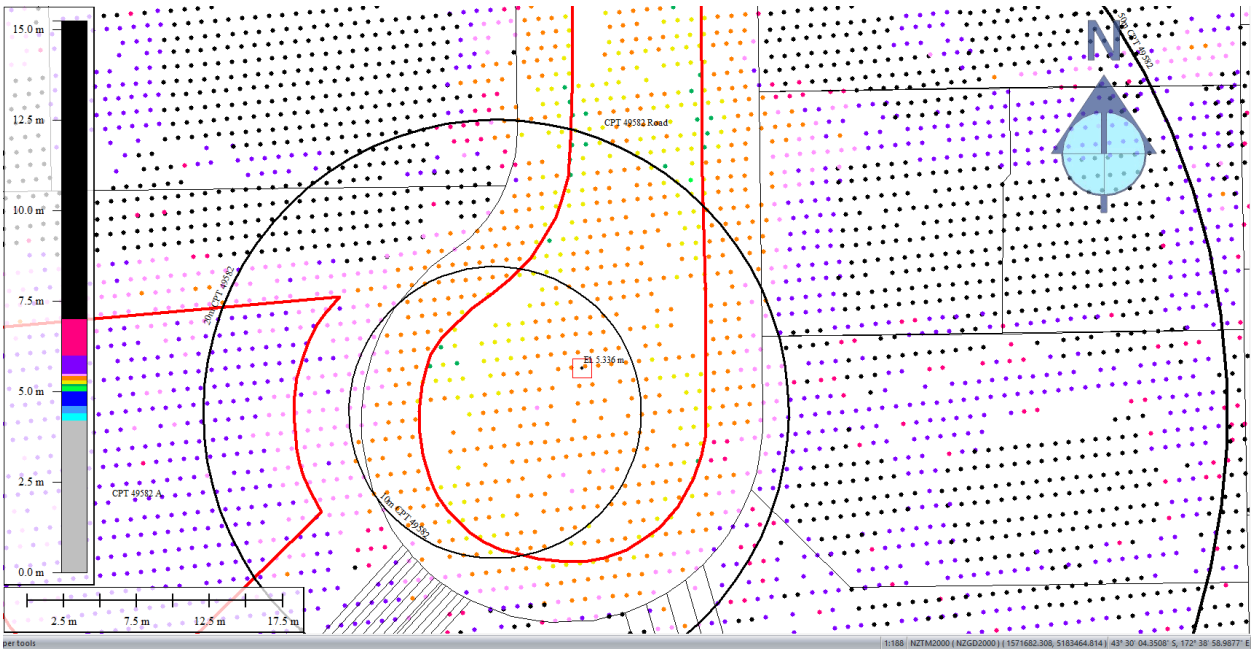

Figure 46: Ground surface elevation averaged over 20-m buffer for Road for Sep 5, 2010 LiDAR survey.

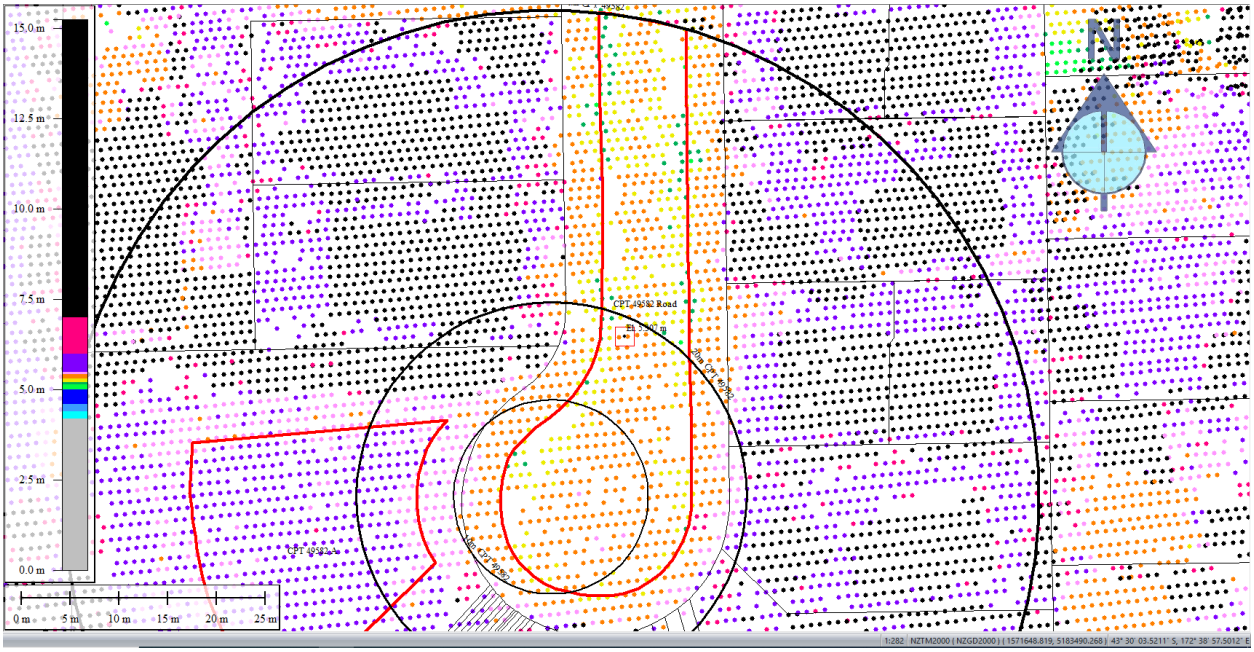

Figure 47: Ground surface elevation averaged over 50-m buffer for Road for Sep 5, 2010 LiDAR survey.

Figure 48: Mar 2011 LiDAR survey.

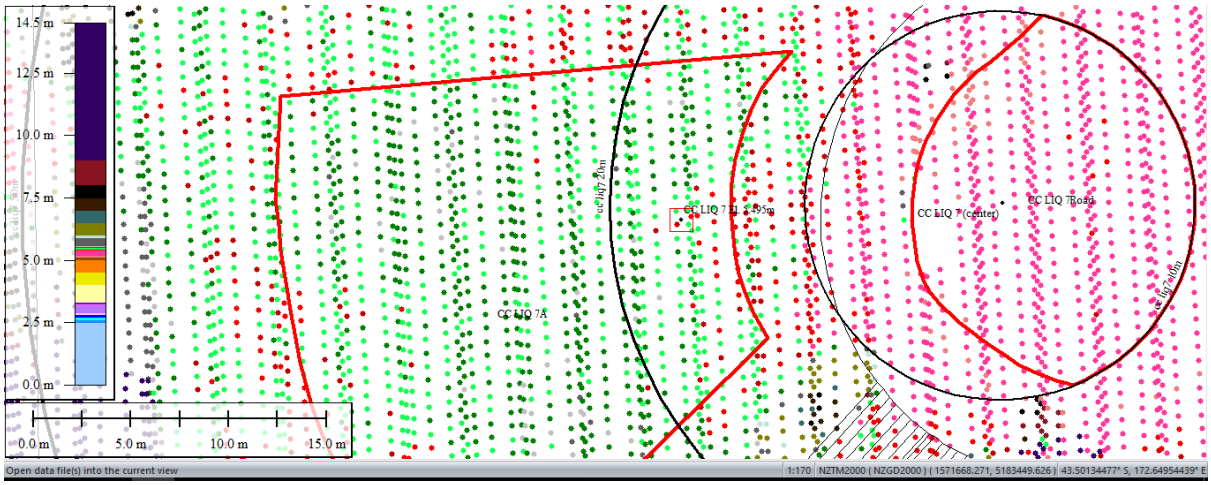

Figure 49: Ground surface elevation averaged over 20-m buffer for Patch A for Mar 2011 LiDAR survey.

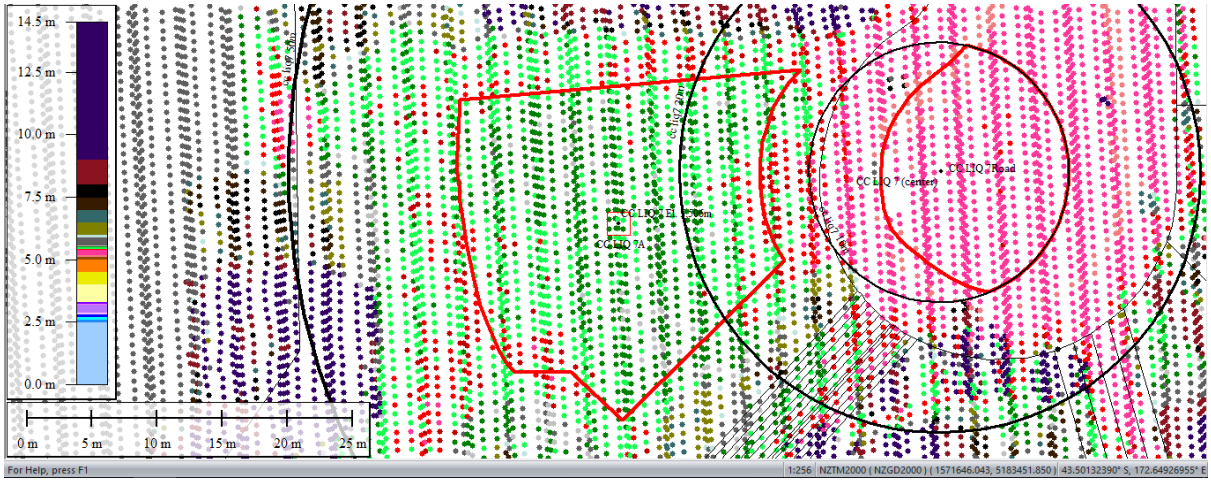

Figure 50: Ground surface elevation averaged over 50-m buffer for Patch A for Mar 2011 LiDAR survey.

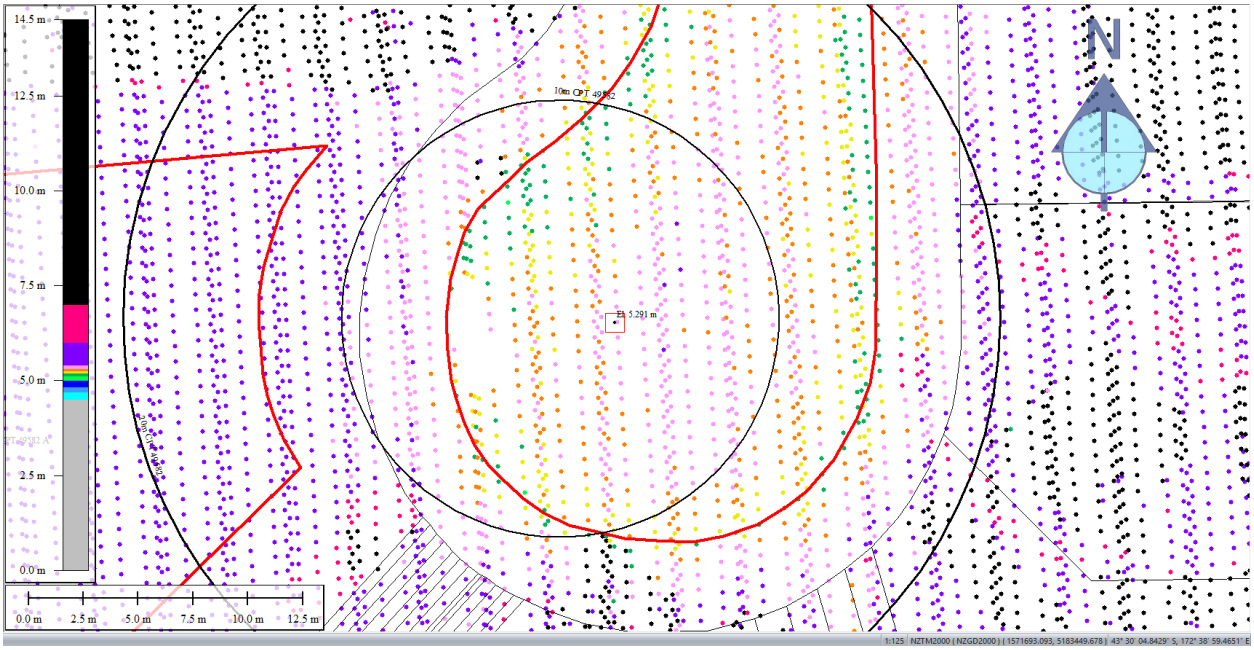

Figure 51: Ground surface elevation averaged over 10-m buffer for Road for Mar 2011 LiDAR survey.

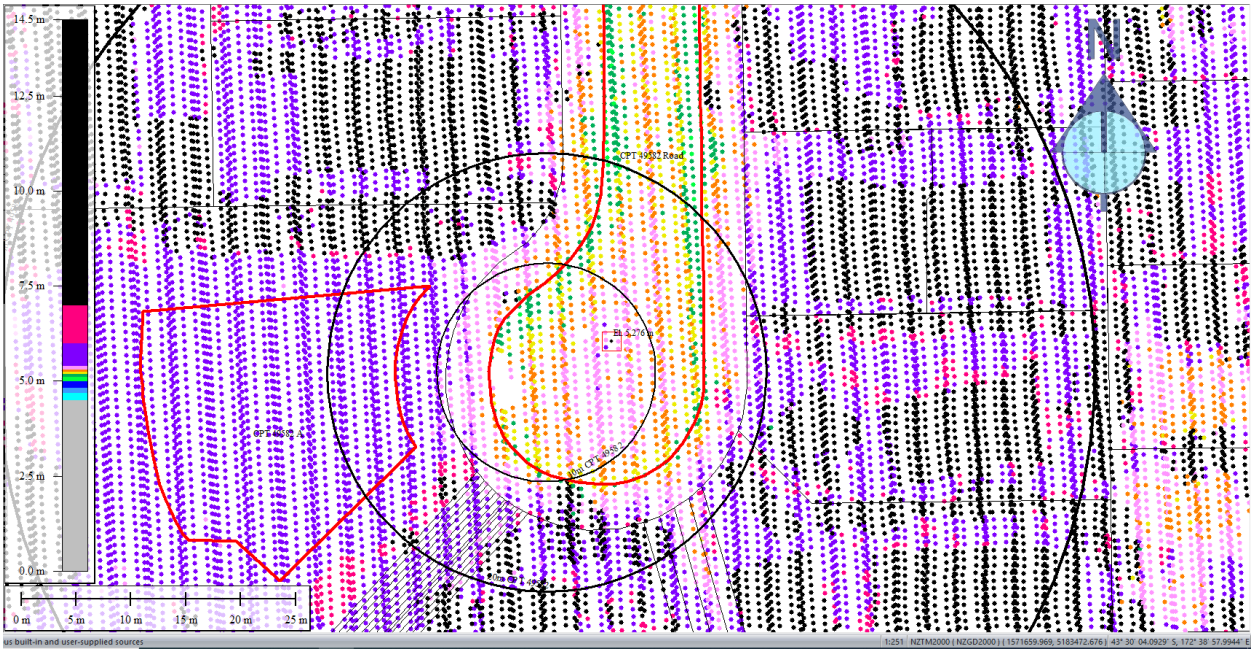

Figure 52: Ground surface elevation averaged over 20-m buffer for Road for Mar 2011 LiDAR survey.

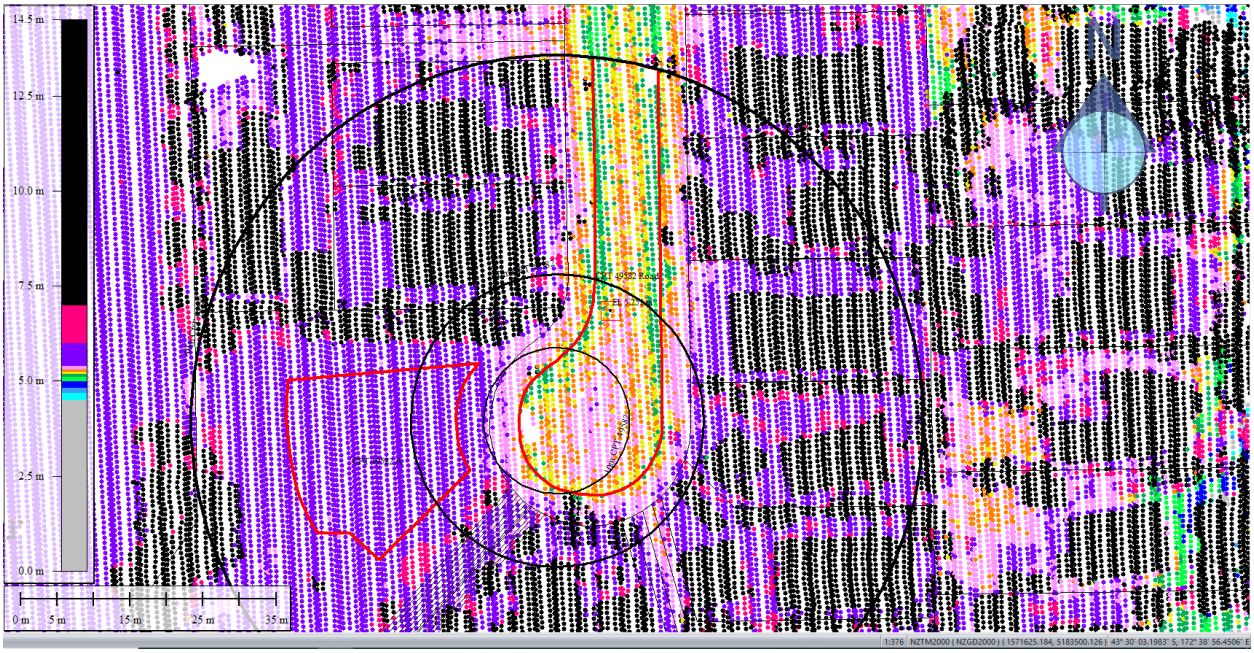

Figure 53: Ground surface elevation averaged over 50-m buffer for Road for Mar 2011 LiDAR survey.

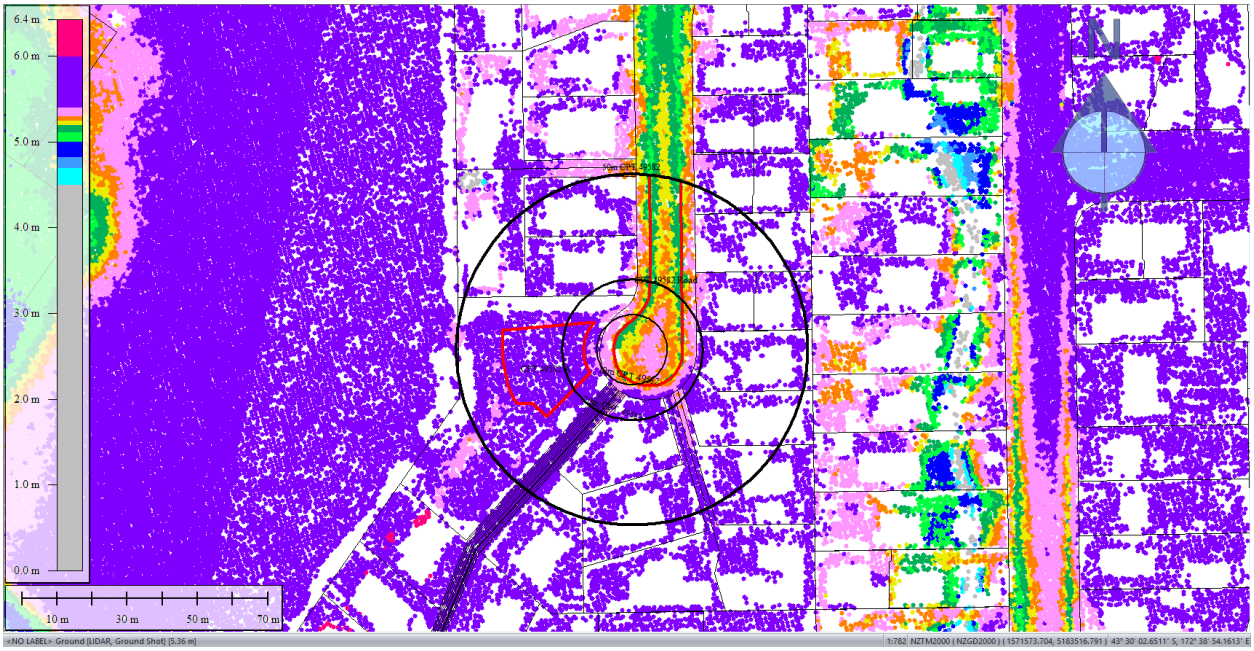

Figure 54: May 2011 LiDAR survey.

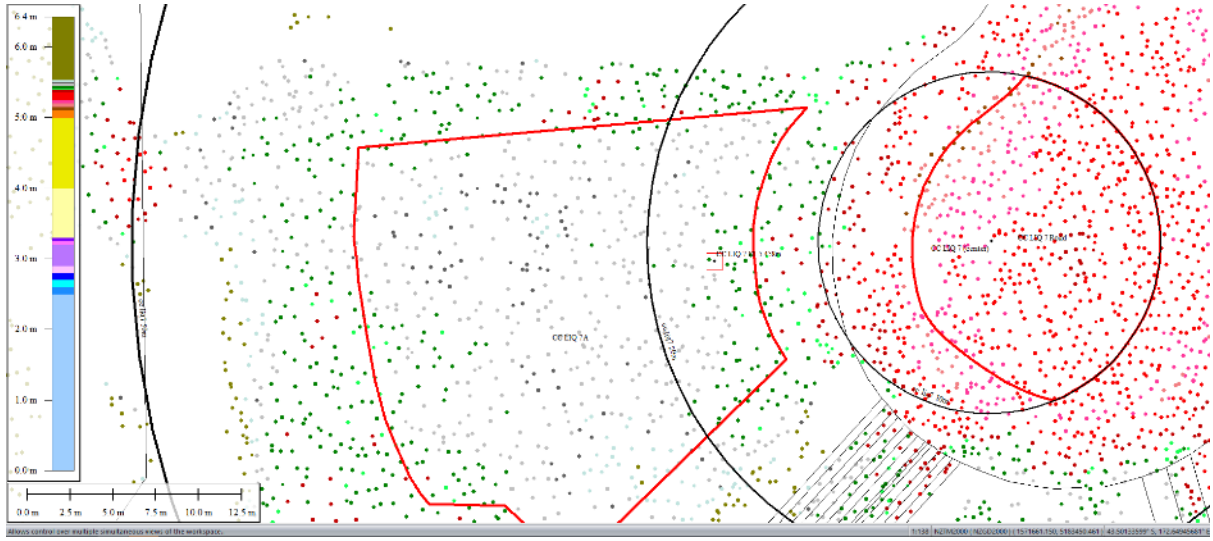

Figure 55: Ground surface elevation averaged over 20-m buffer for Patch A for May 2011 LiDAR survey.

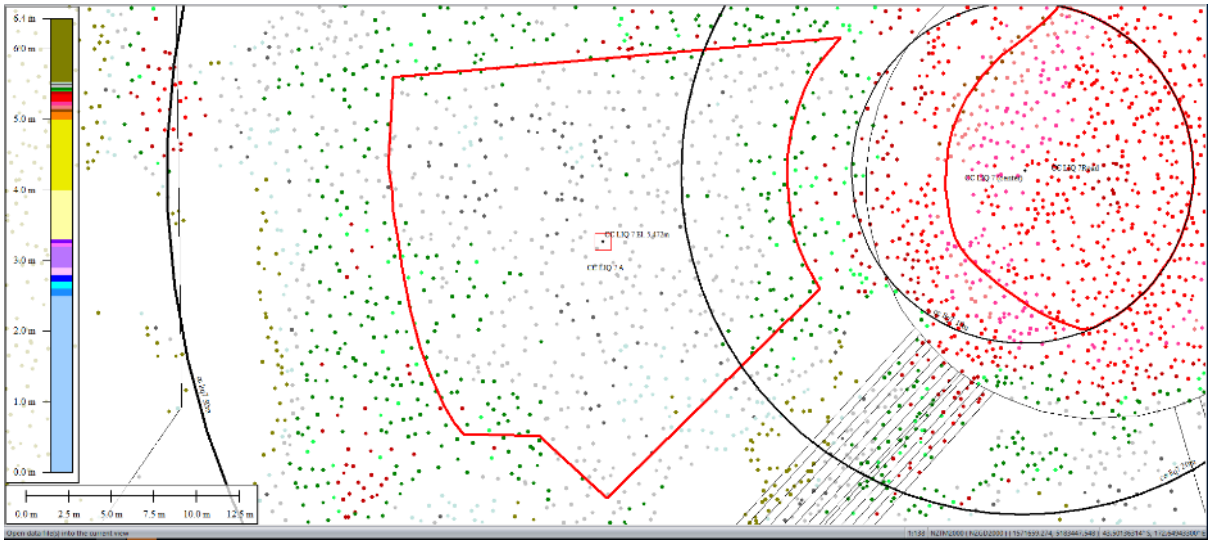

Figure 56: Ground surface elevation averaged over 50-m buffer for Patch A for May 2011 LiDAR survey.

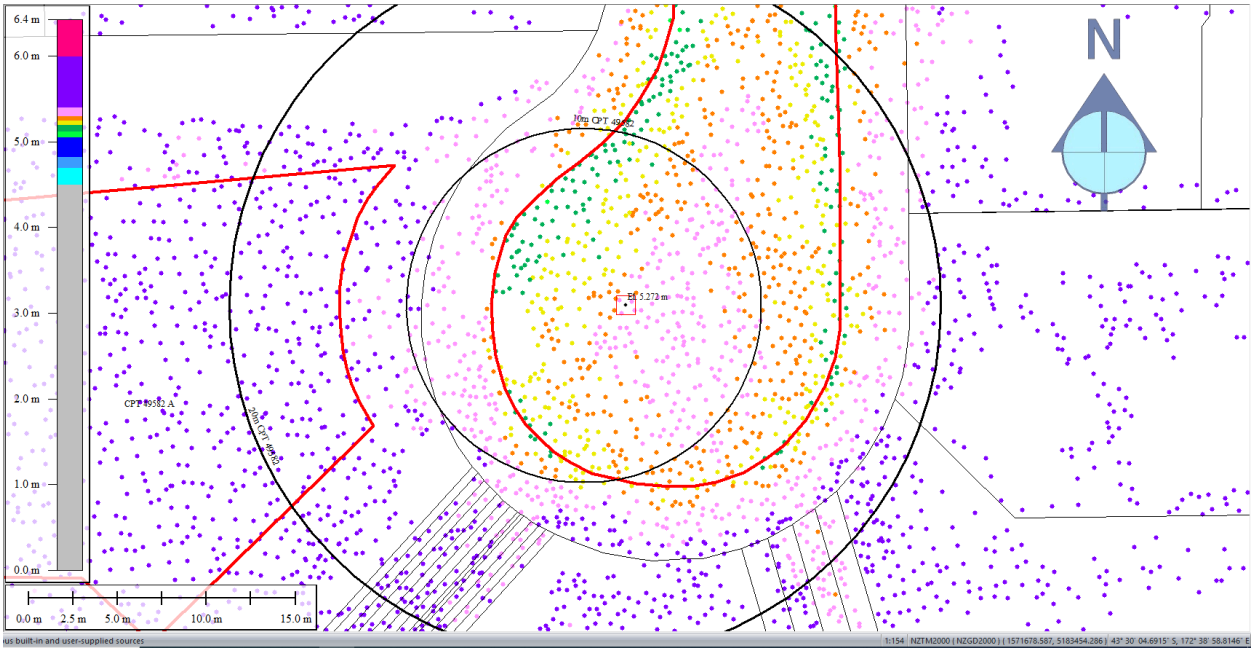

Figure 57: Ground surface elevation averaged over 10-m buffer for Road for May 2011 LiDAR survey.

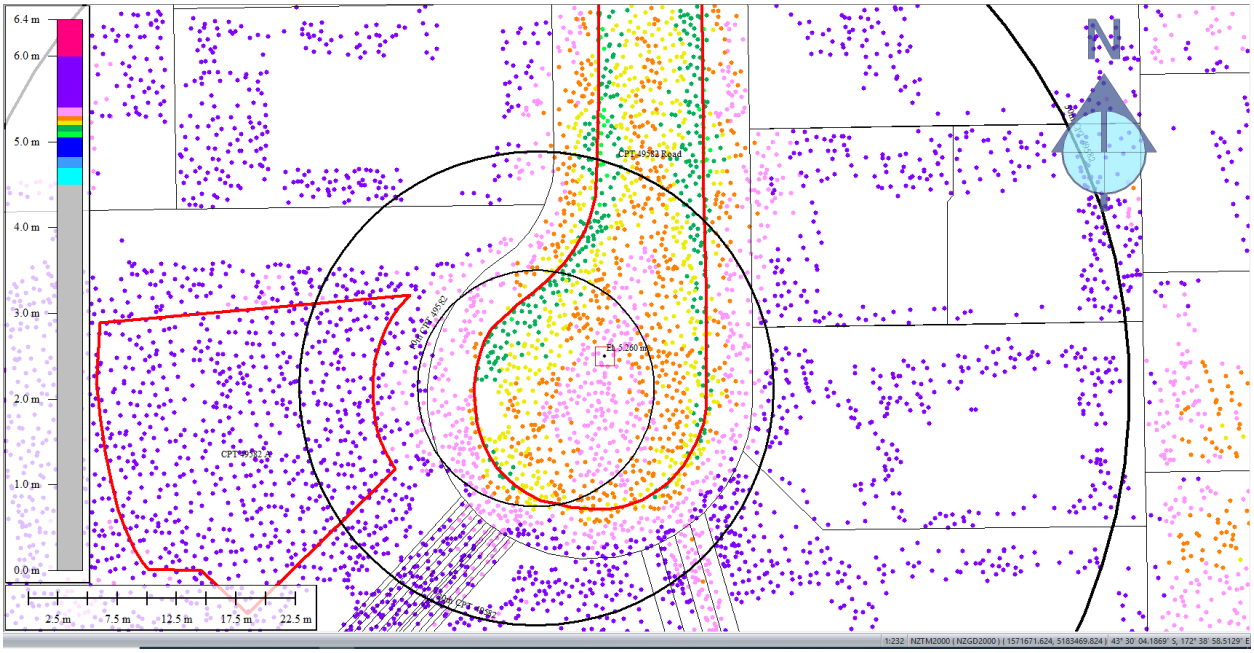

Figure 58: Ground surface elevation averaged over 20-m buffer for Road for May 2011 LiDAR survey.

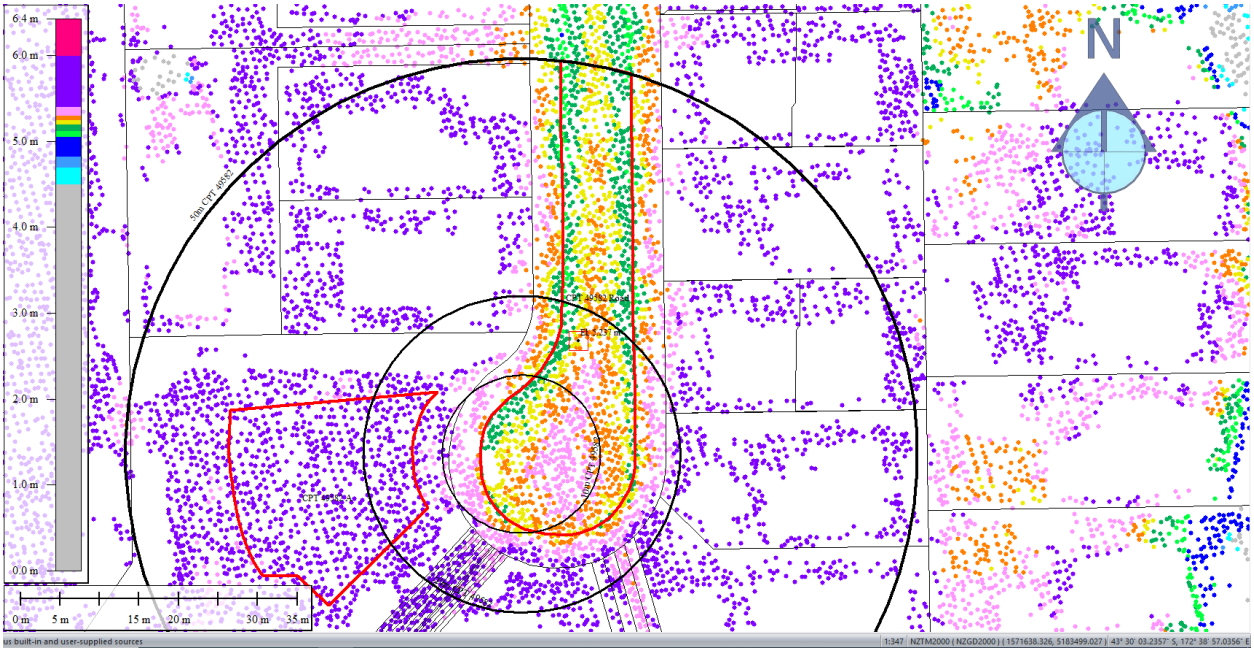

Figure 59: Ground surface elevation averaged over 50-m buffer for Road for May 2011 LiDAR survey.

Figure 60: Sep 2011 LiDAR survey.

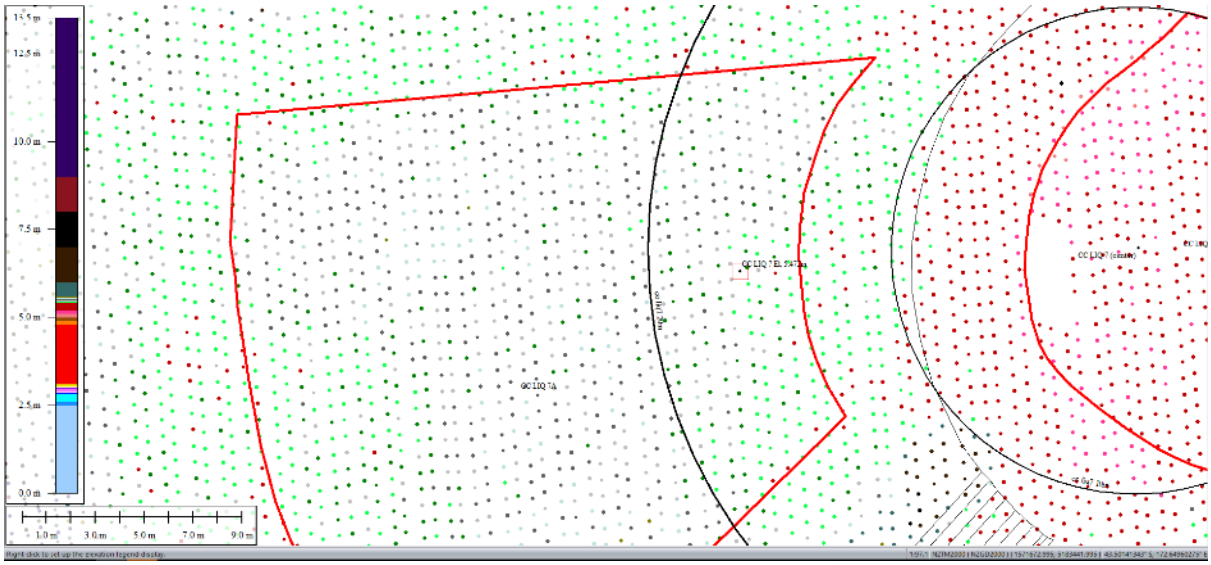

Figure 61: Ground surface elevation averaged over 20-m buffer for Patch A for Sep 2011 LiDAR survey.

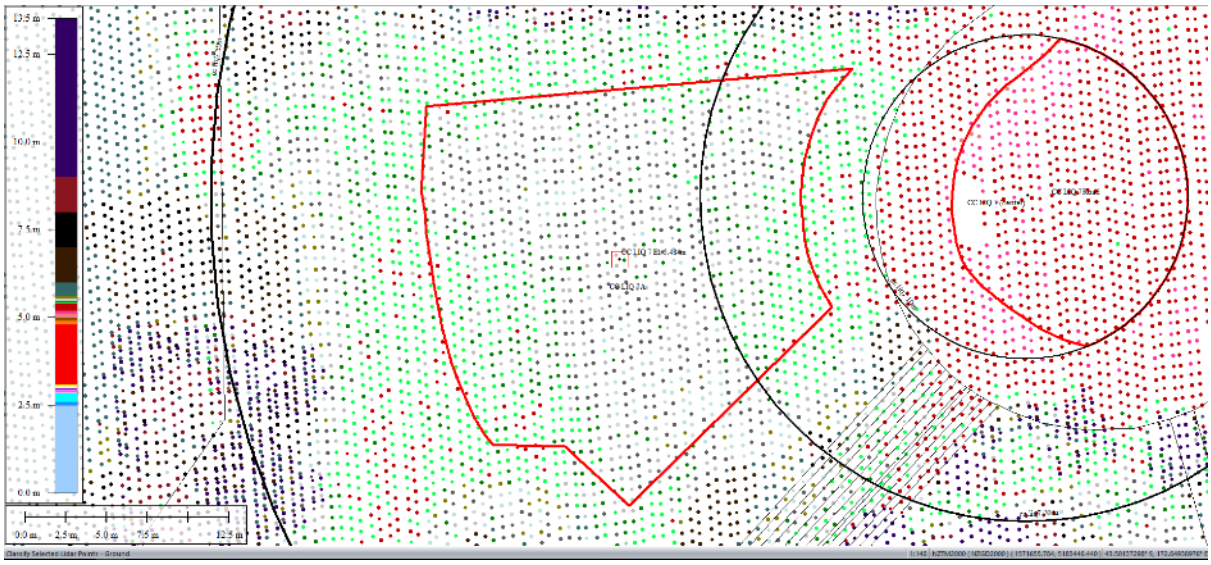

Figure 62: Ground surface elevation averaged over 50-m buffer for Patch A for Sep 2011 LiDAR survey.

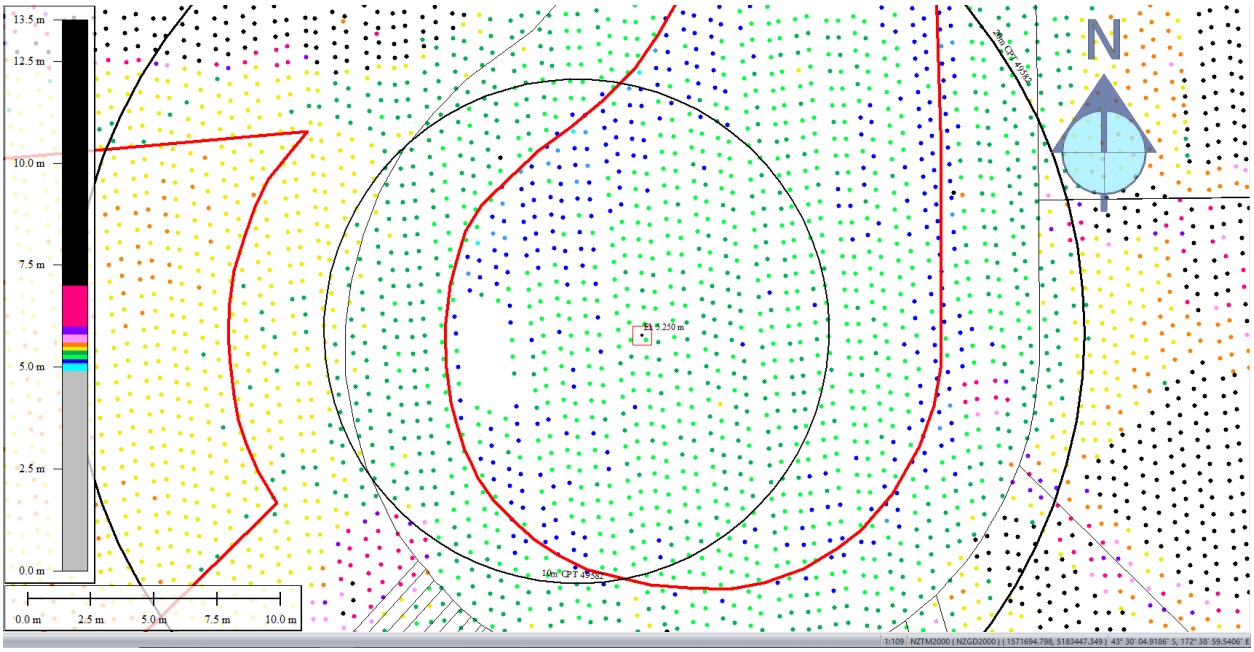

Figure 63: Ground surface elevation averaged over 10-m buffer for Road for Sep 2011 LiDAR survey.

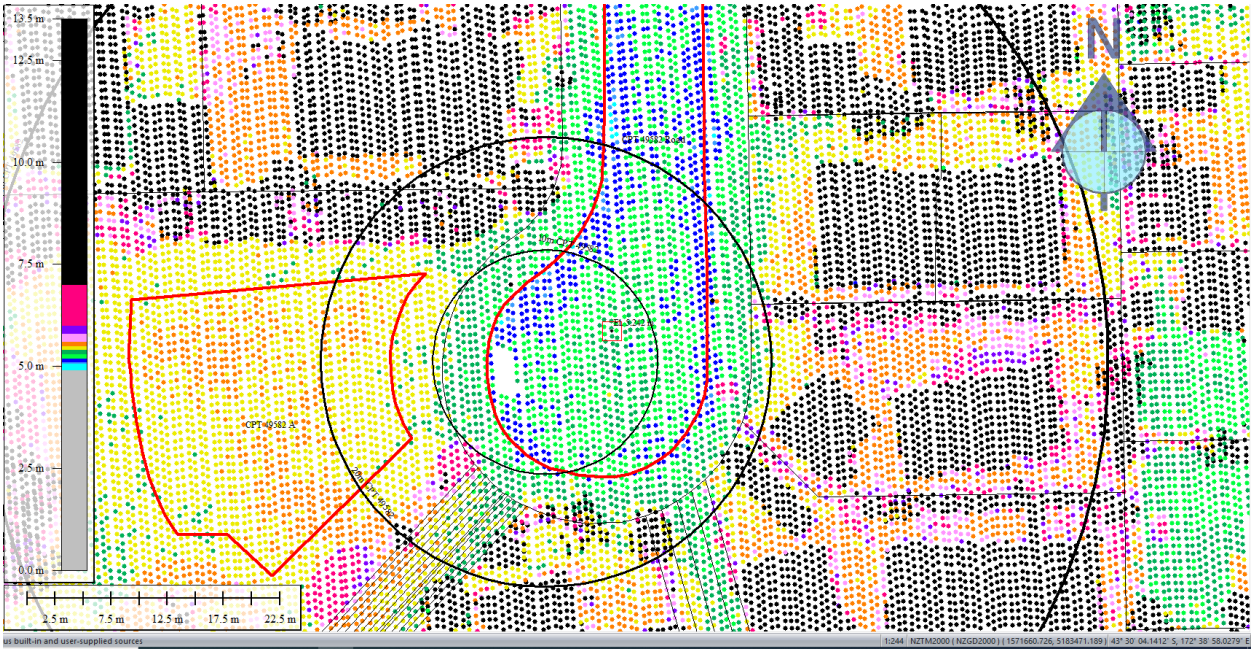

Figure 64: Ground surface elevation averaged over 20-m buffer for Road for Sep 2011 LiDAR survey.

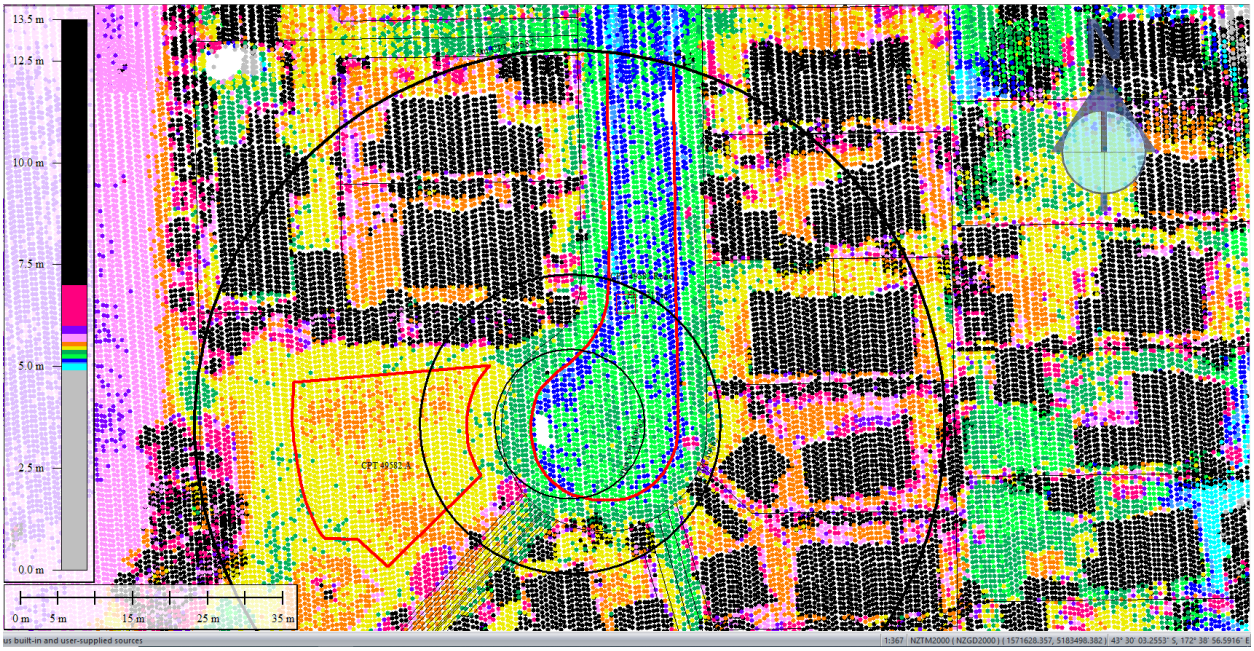

Figure 65: Ground surface elevation averaged over 50-m buffer for Road for Sep 2011 LiDAR survey.

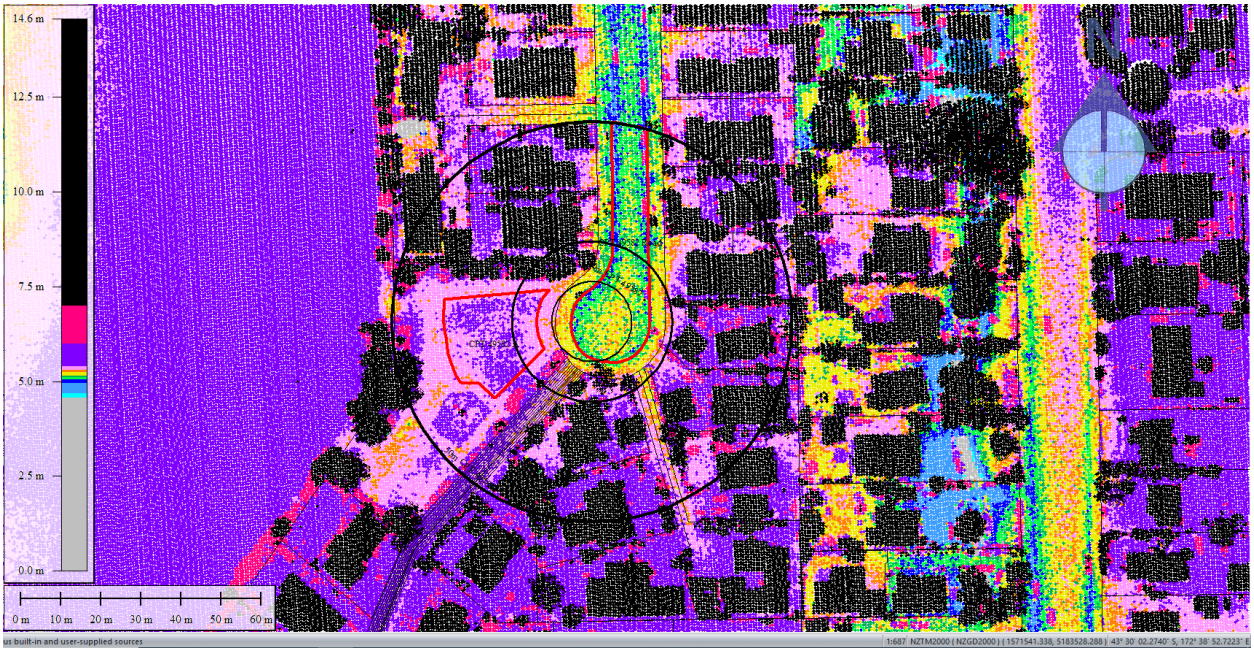

Figure 66: Feb 2012 LiDAR survey.

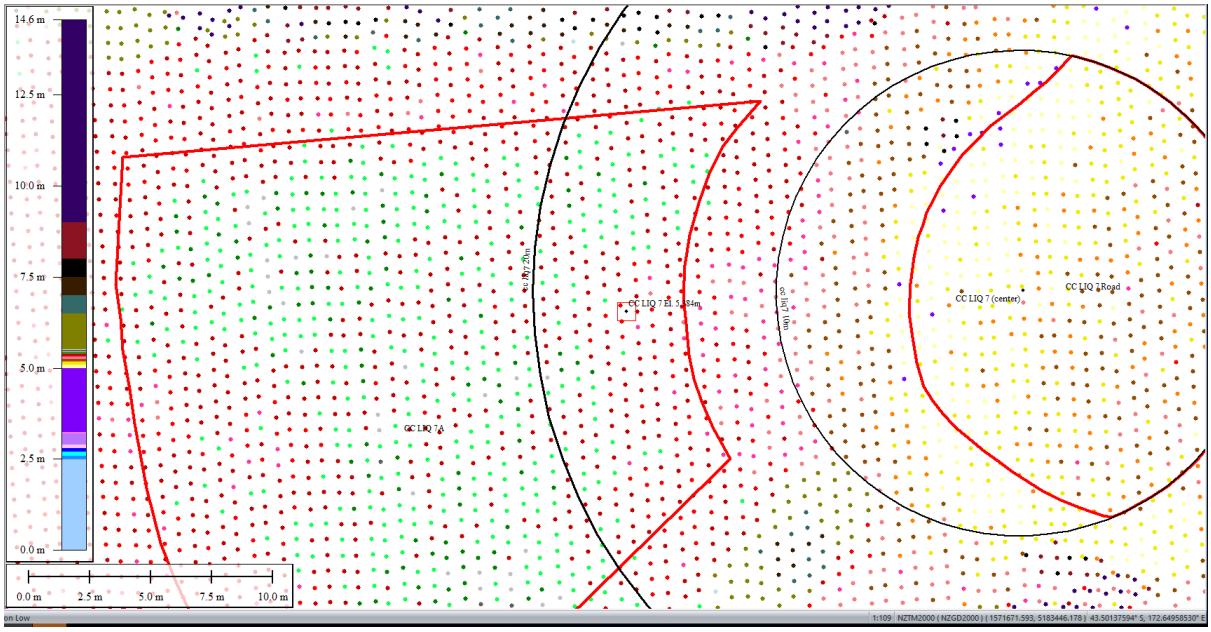

Figure 67: Ground surface elevation averaged over 20-m buffer for Patch A for Feb 2012 LiDAR survey.

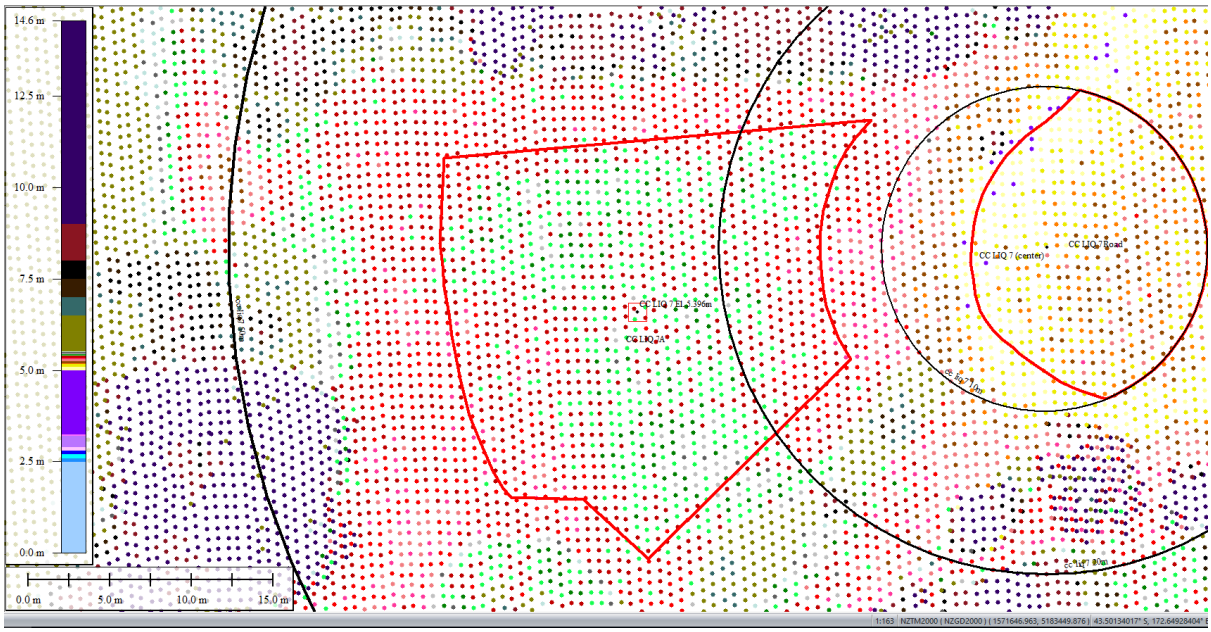

Figure 68: Ground surface elevation averaged over 50-m buffer for Patch A for Feb 2012 LiDAR survey.

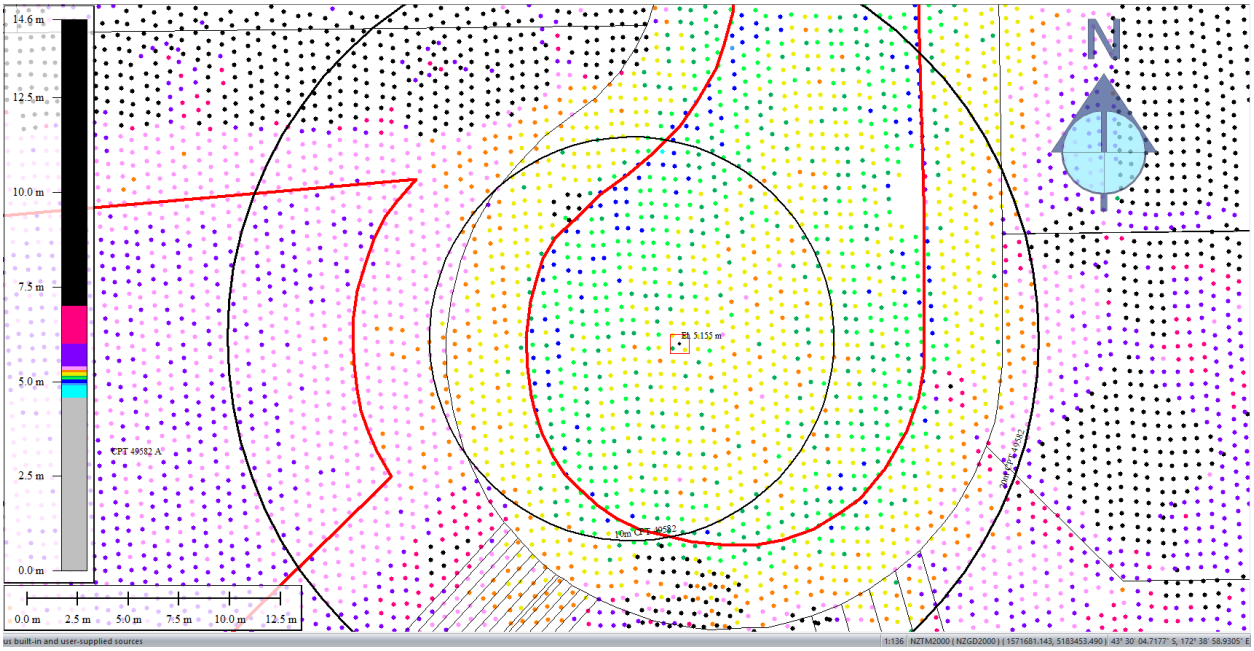

Figure 69: Ground surface elevation averaged over 10-m buffer for Road for Feb 2012 LiDAR survey.

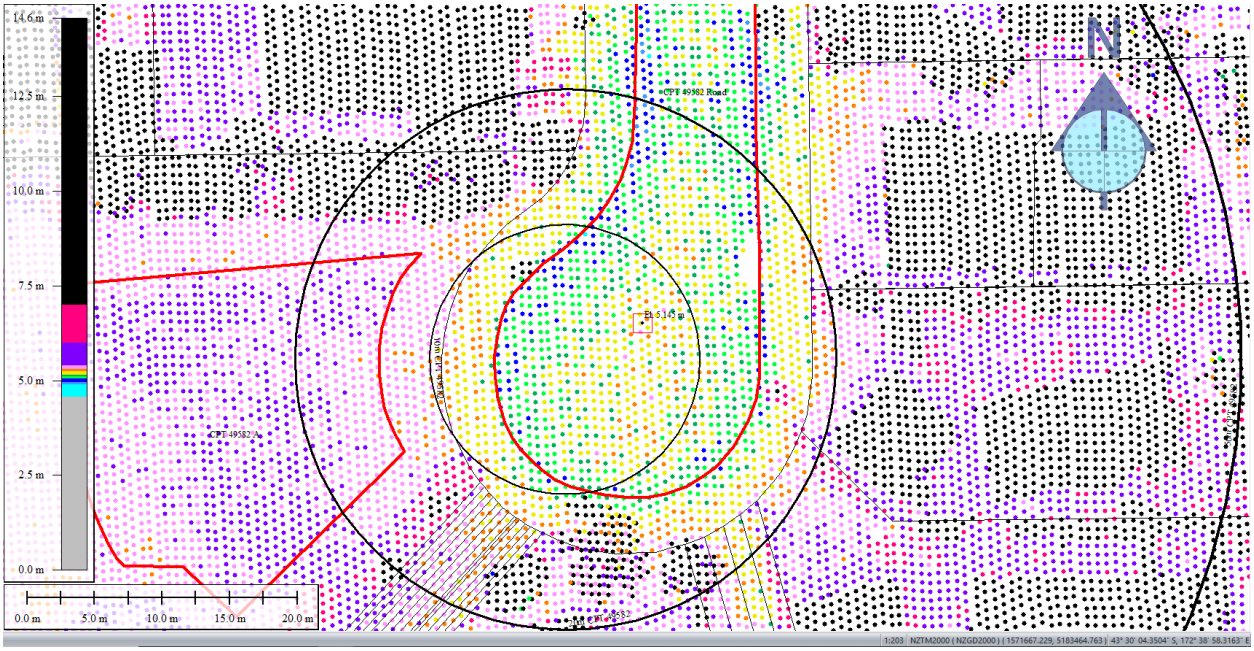

Figure 70: Ground surface elevation averaged over 20-m buffer for Road for Feb 2012 LiDAR survey.

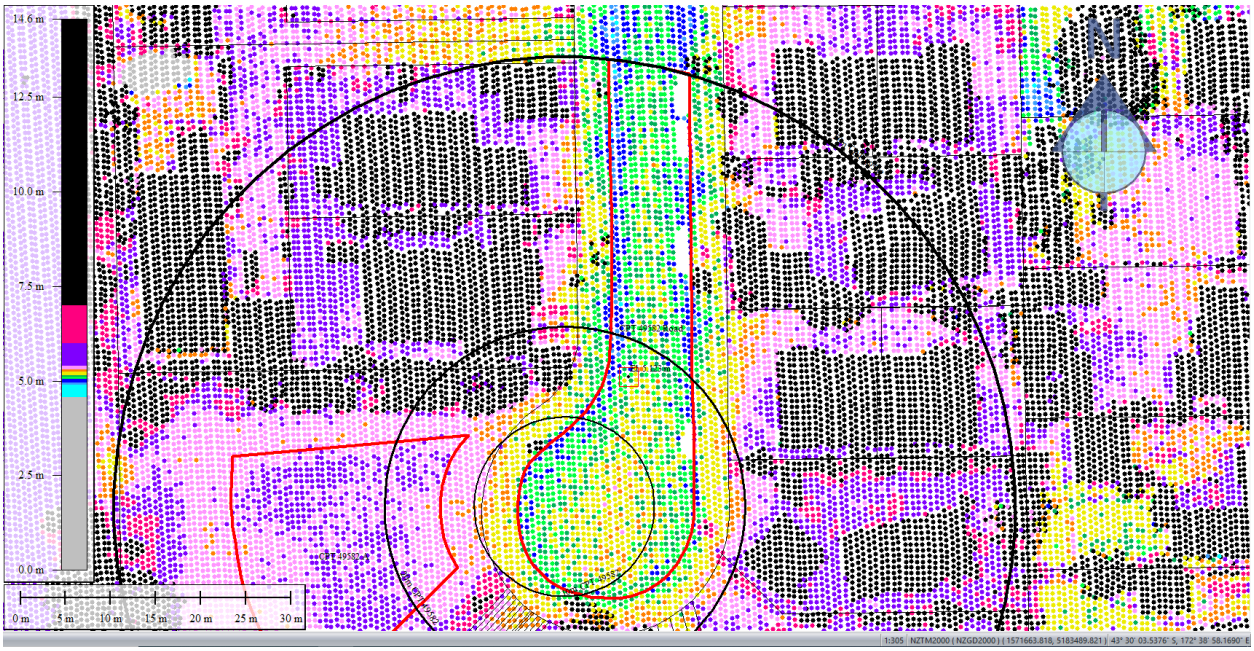

Figure 71: Ground surface elevation averaged over 50-m buffer for Road for Feb 2012 LiDAR survey.

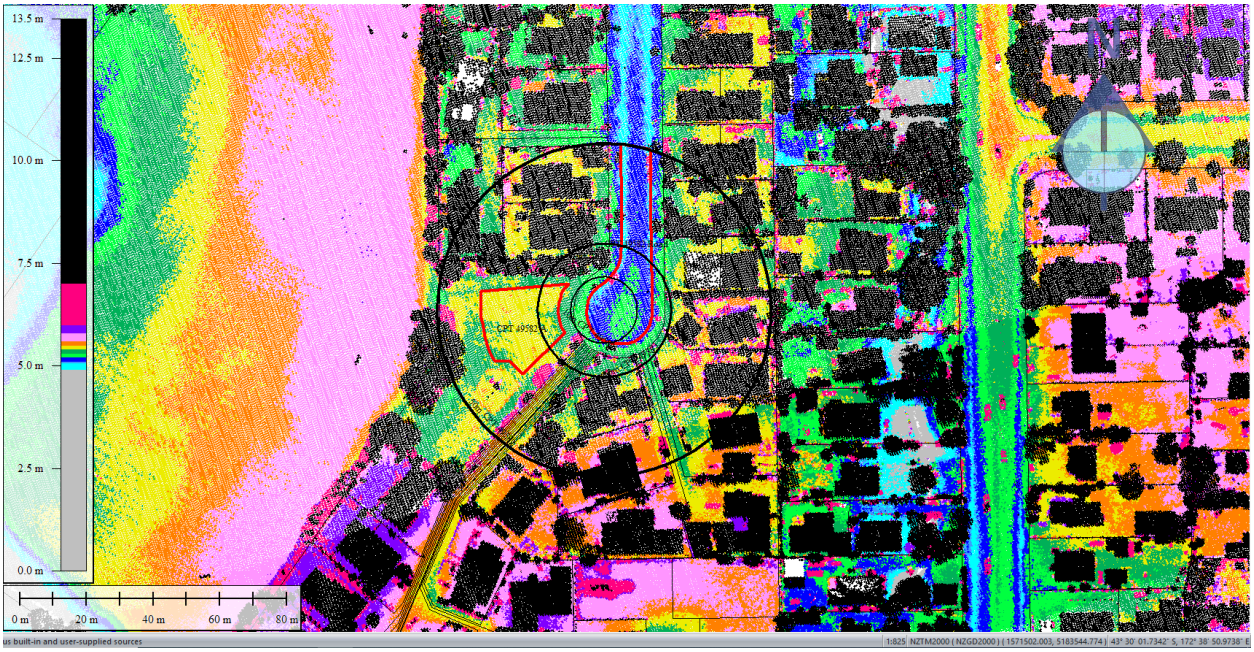

Figure 72: Oct 2015 LiDAR survey.

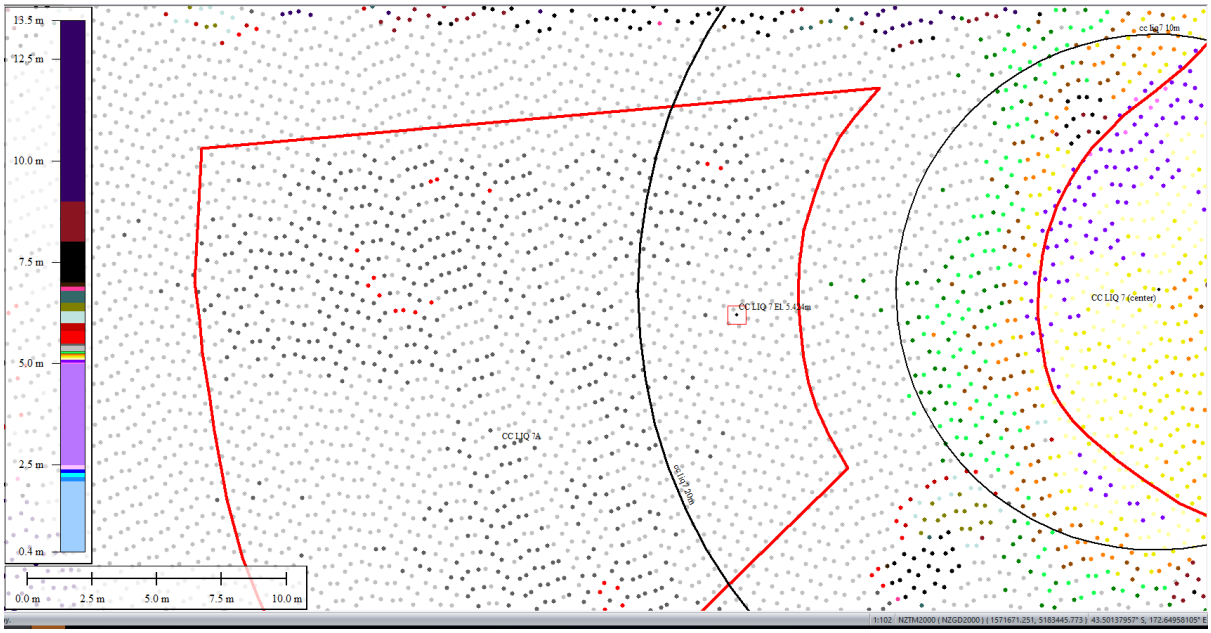

Figure 73: Ground surface elevation averaged over 20-m buffer for Patch A for Oct 2015 LiDAR survey.

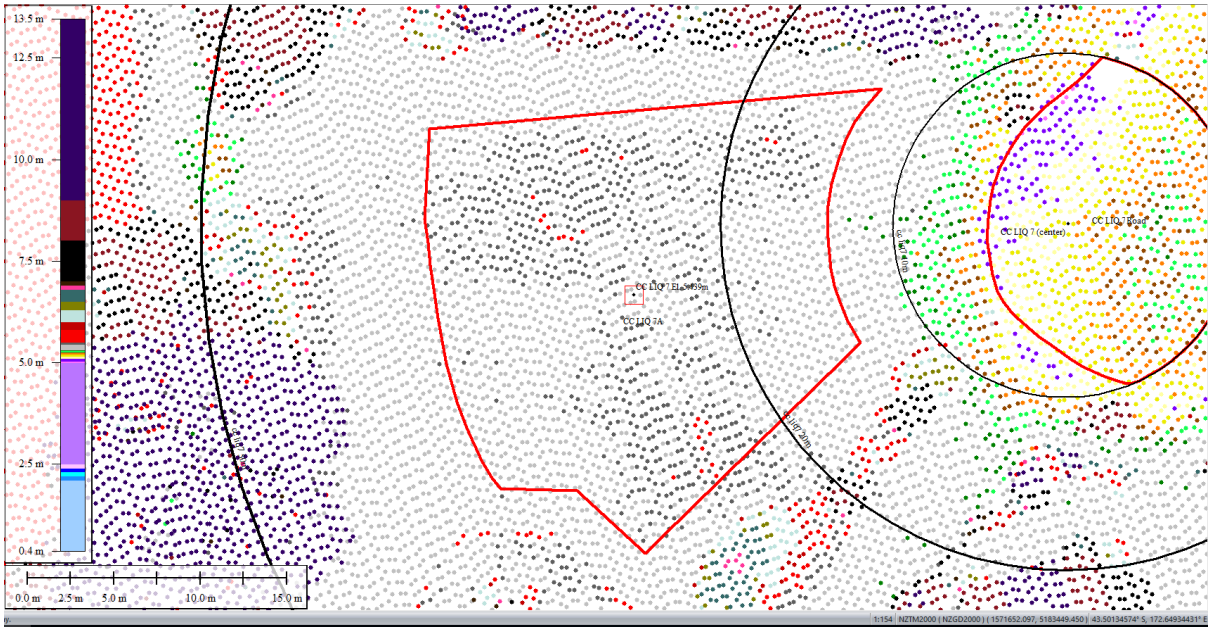

Figure 74: Ground surface elevation averaged over 50-m buffer for Patch A for Oct 2015 LiDAR survey.

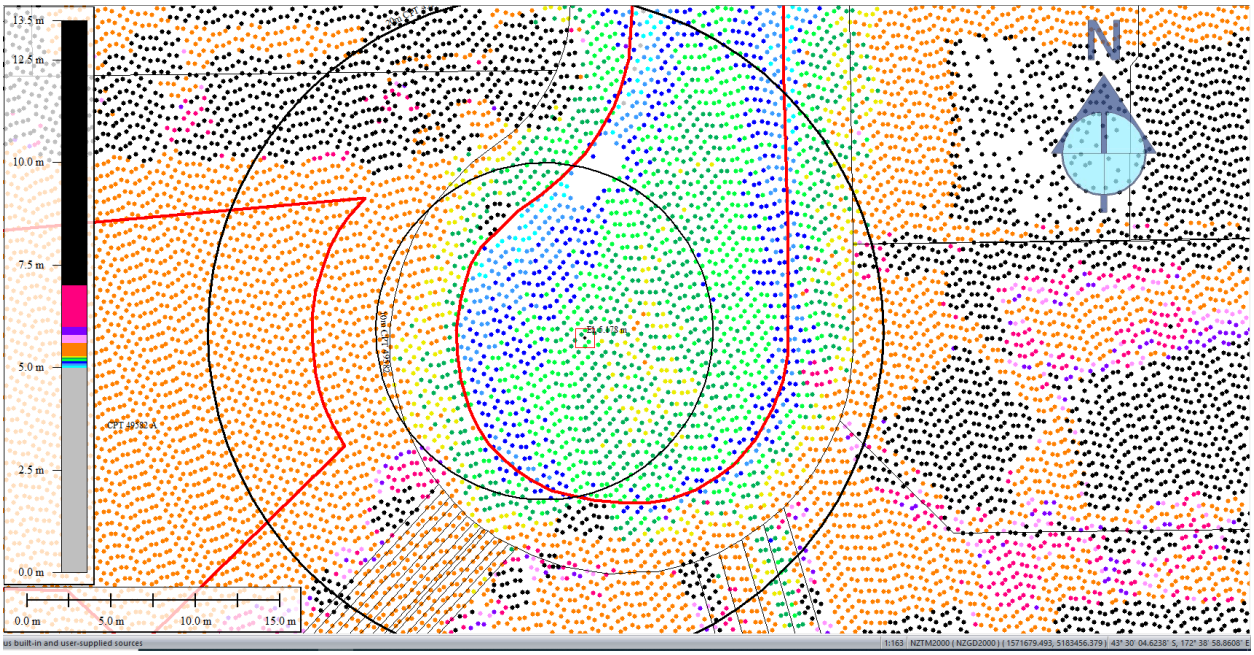

Figure 75: Ground surface elevation averaged over 10-m buffer for Road for Oct 2015 LiDAR survey.

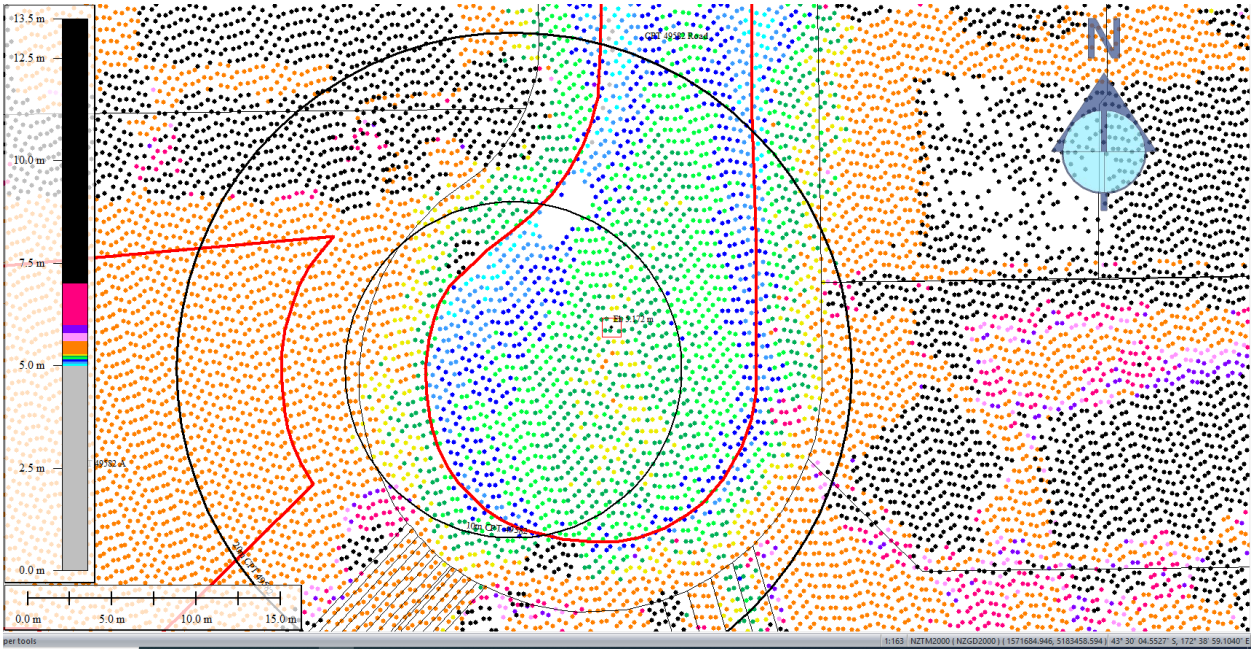

Figure 76: Ground surface elevation averaged over 20-m buffer for Road for Oct 2015 LiDAR survey.

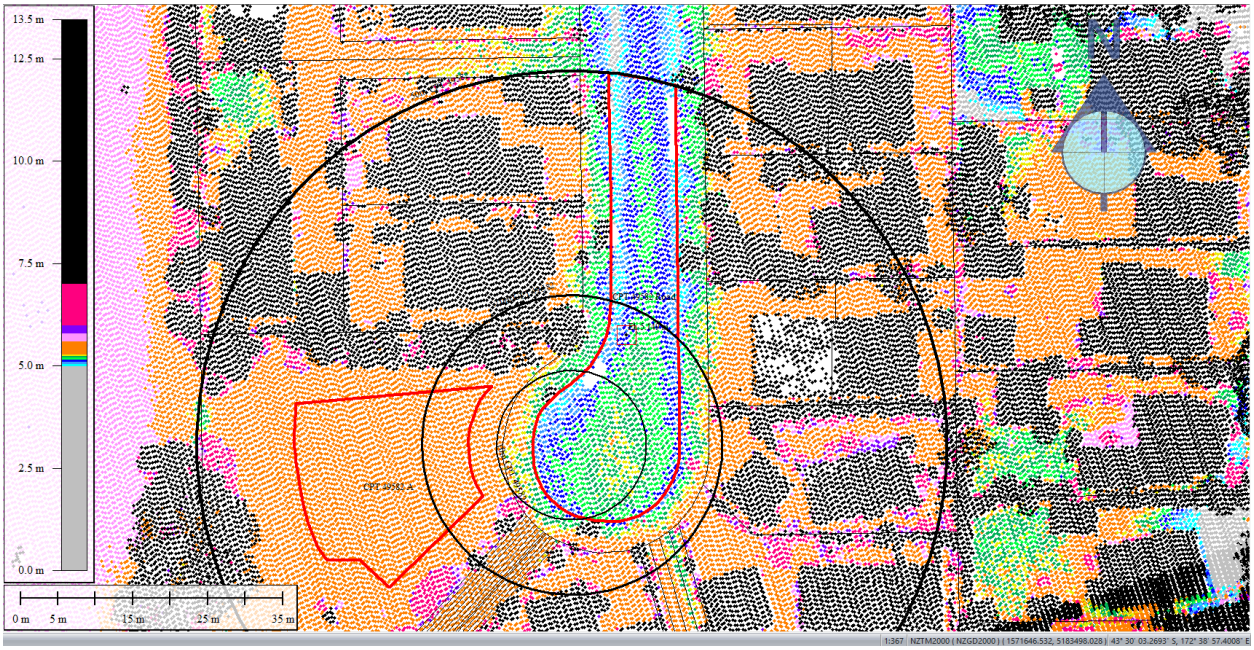

Figure 77: Ground surface elevation averaged over 50-m buffer for Road for Oct 2015 LiDAR survey.

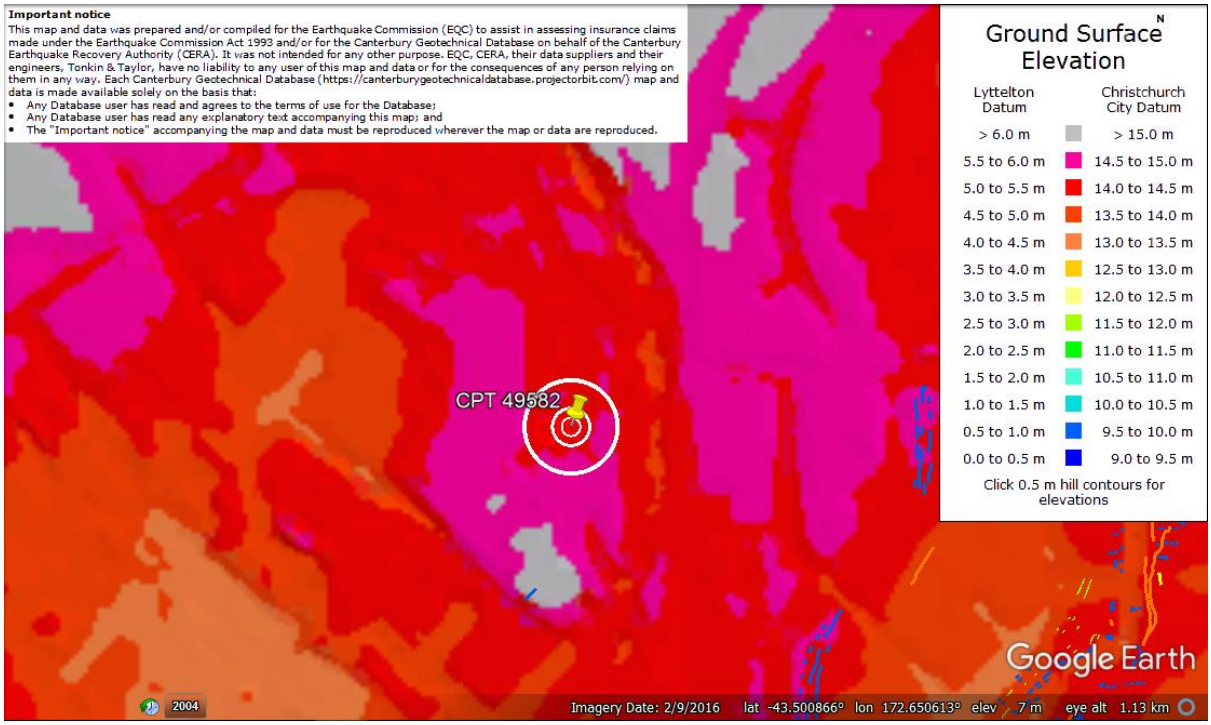

Figure 78: Ground surface elevation difference between the road and properties (LiDAR DEM for Sept 2010).

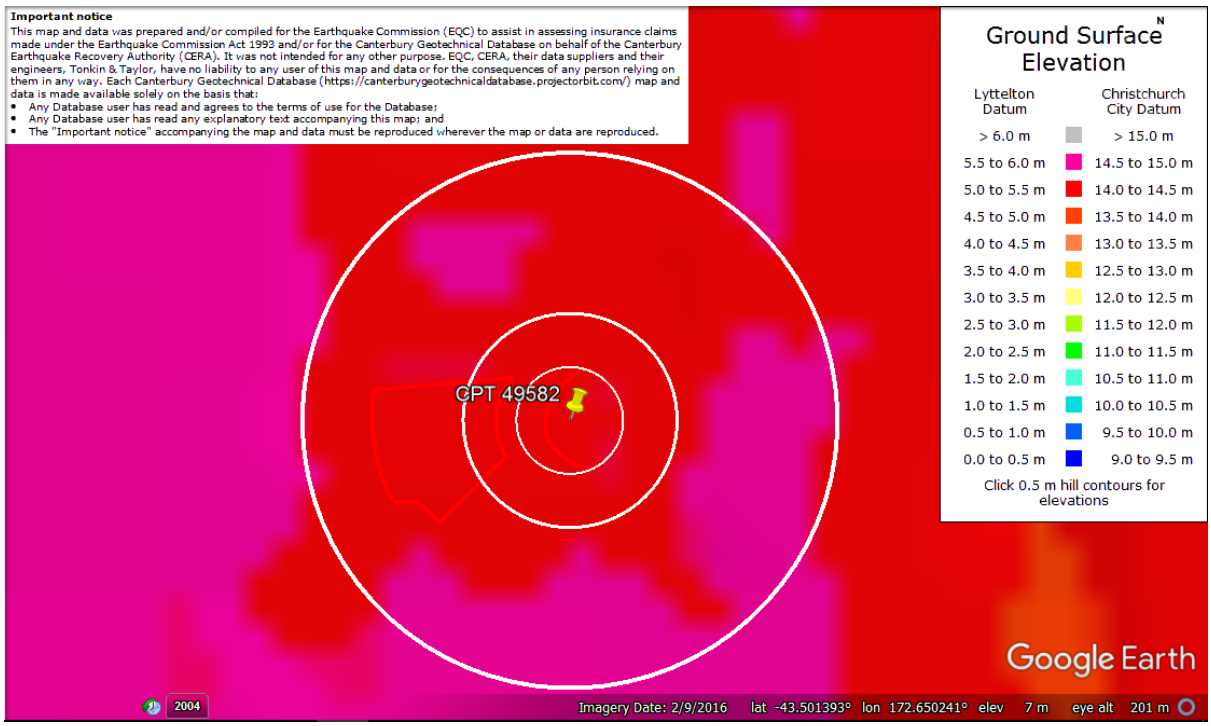

Figure 79: Enlarged view of ground surface elevation difference between the road and properties (LiDAR DEM for Sept 2010).

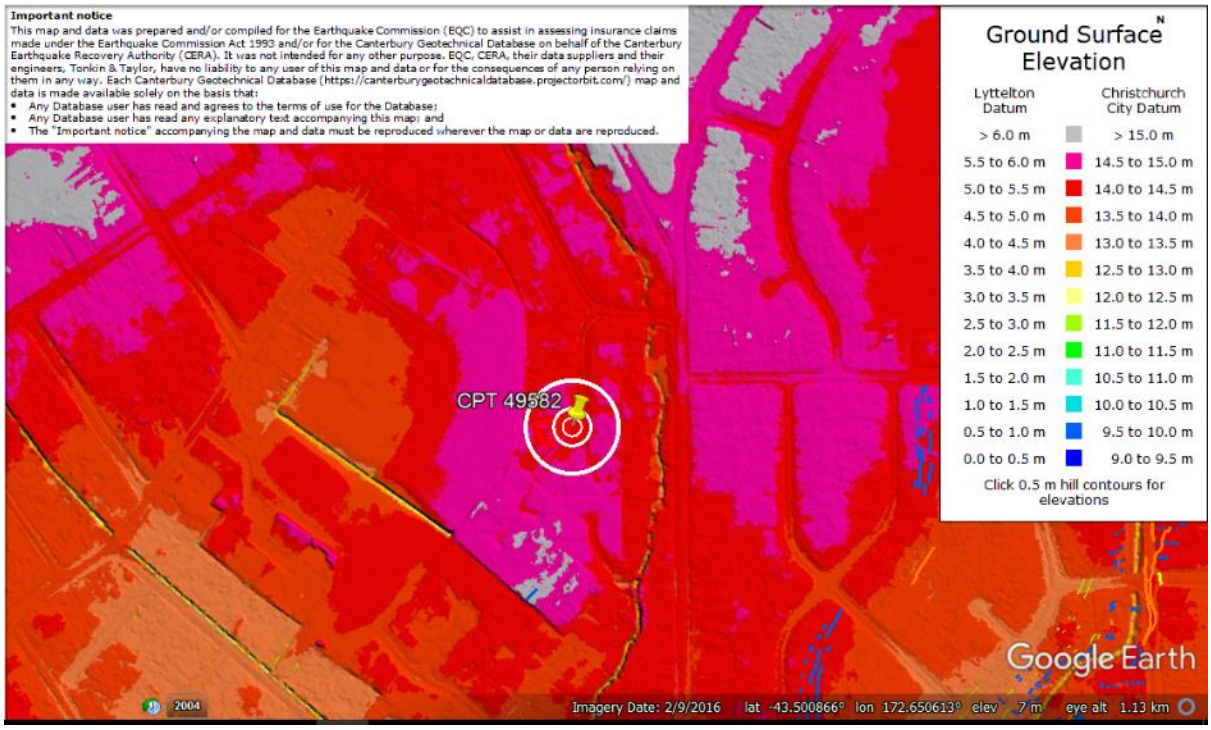

Figure 80: Ground surface elevation difference between the road and properties (LiDAR DEM for Sept 2011).

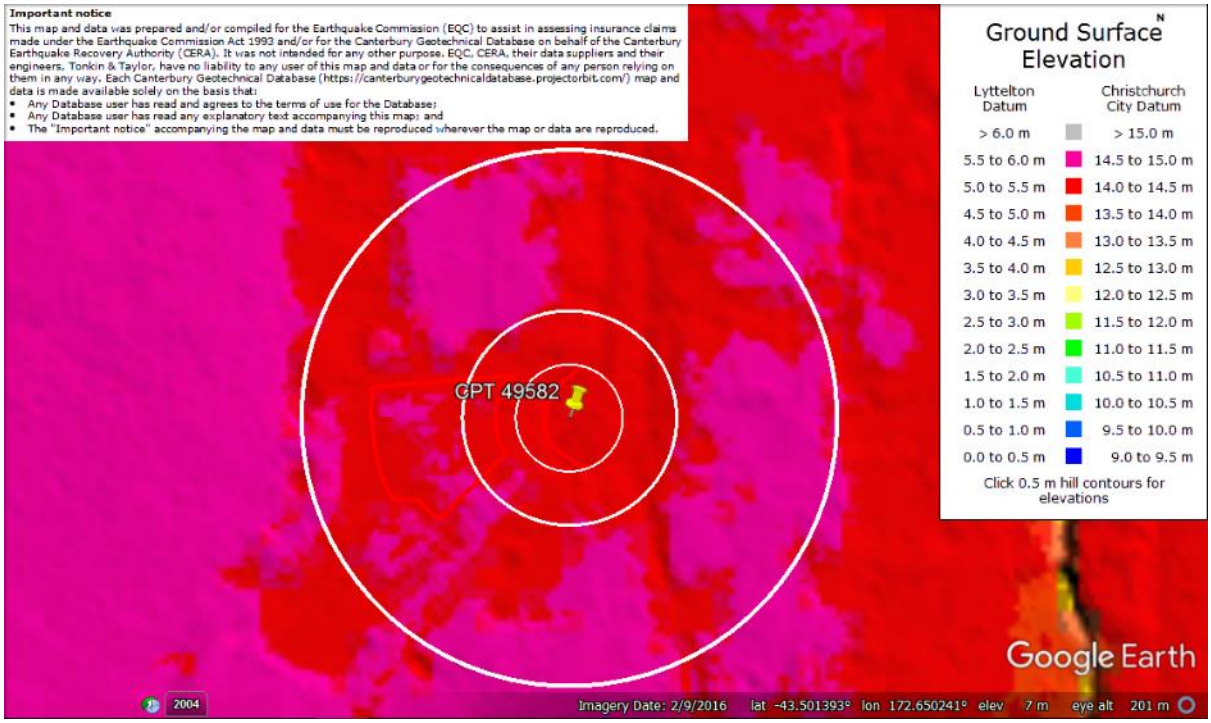

Figure 81: Enlarged view of ground surface elevation difference between the road and properties (LiDAR DEM for Sept 2011).

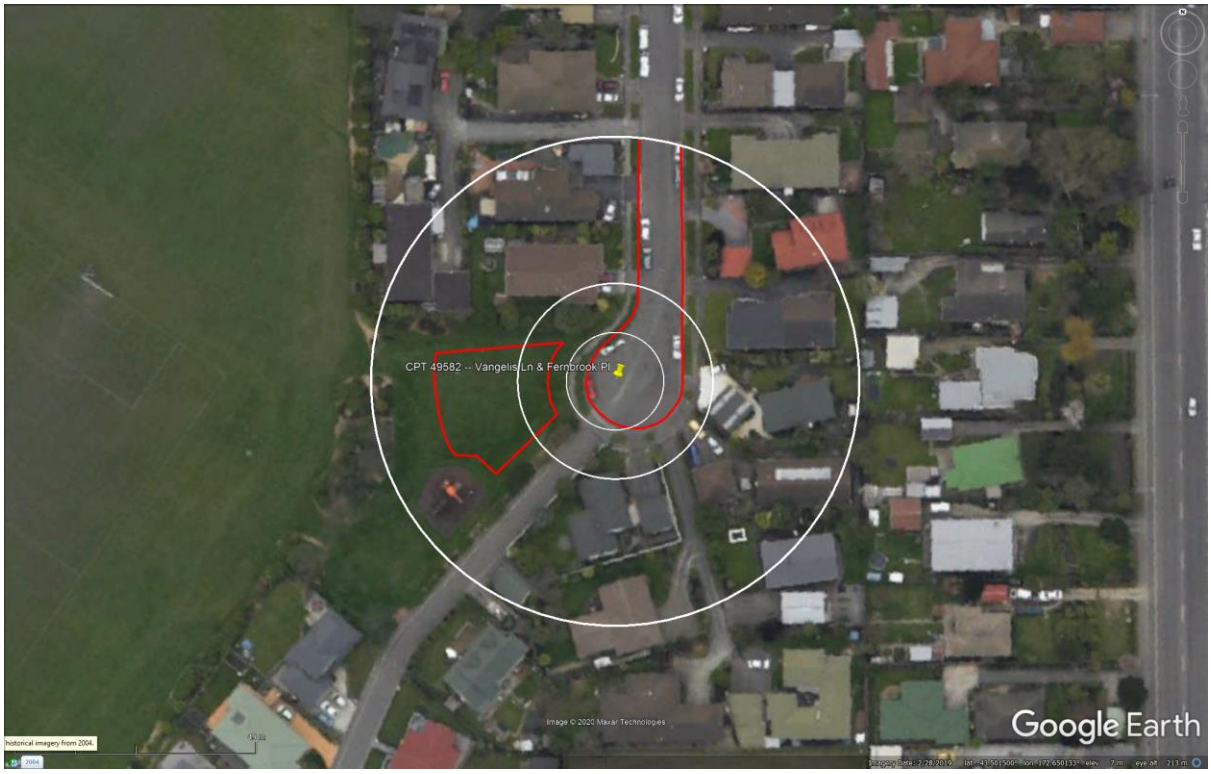

Figure 82: Absence of ejecta at the site for Sep-10 EQ.

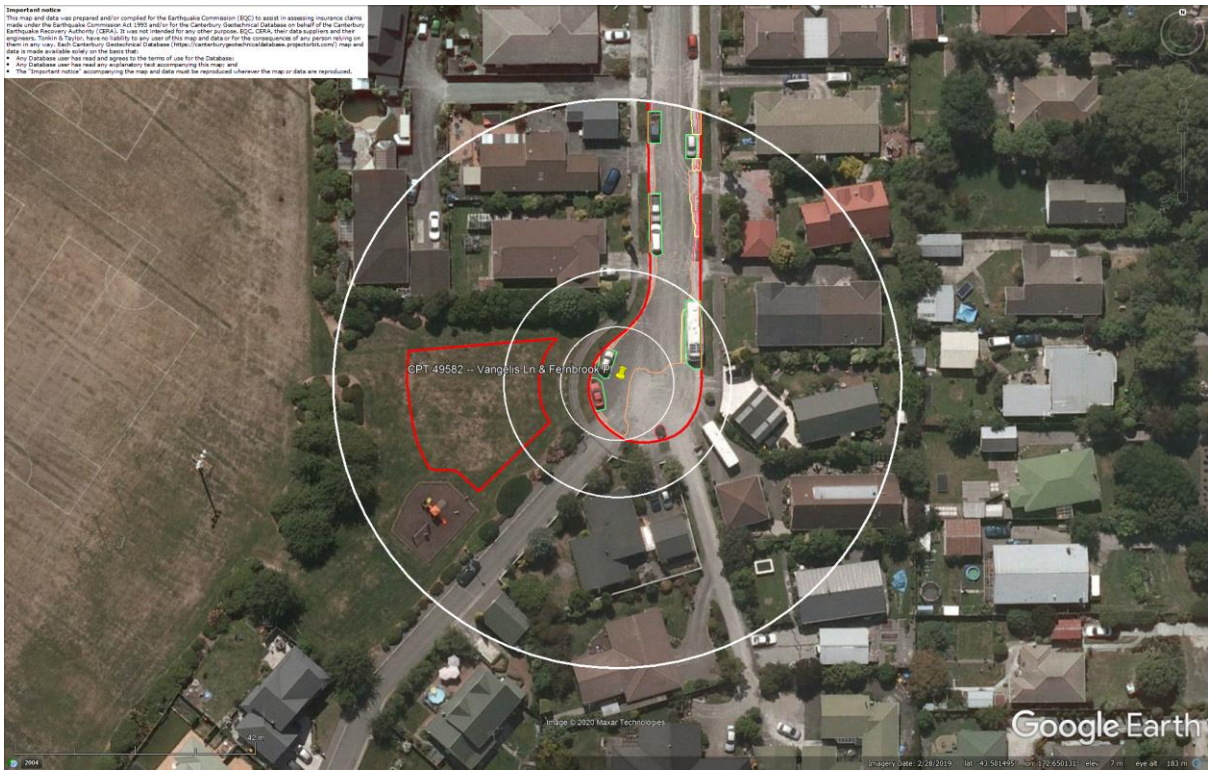

Figure 83: Ejecta outline for Feb-11 EQ.

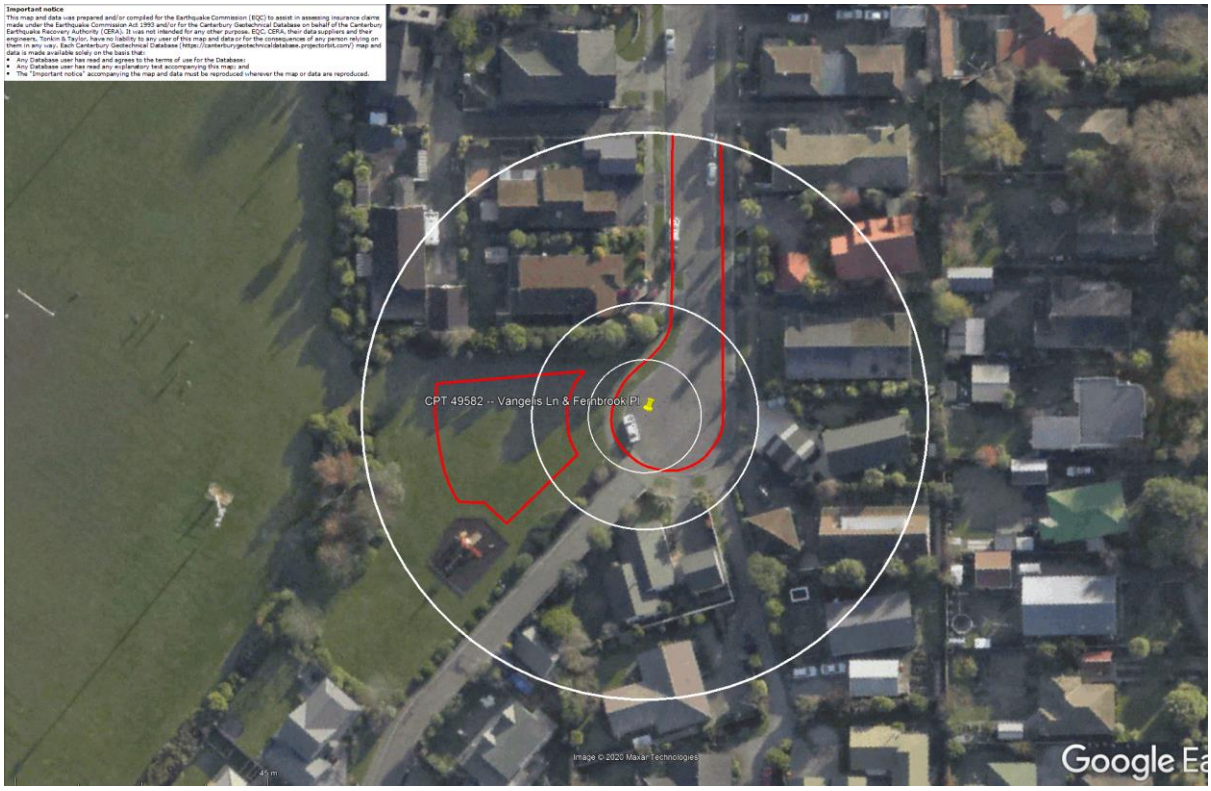

Figure 84: Absence of ejecta at the site for Jun-11 EQ (June 14-15, 2011 aerial photograph).

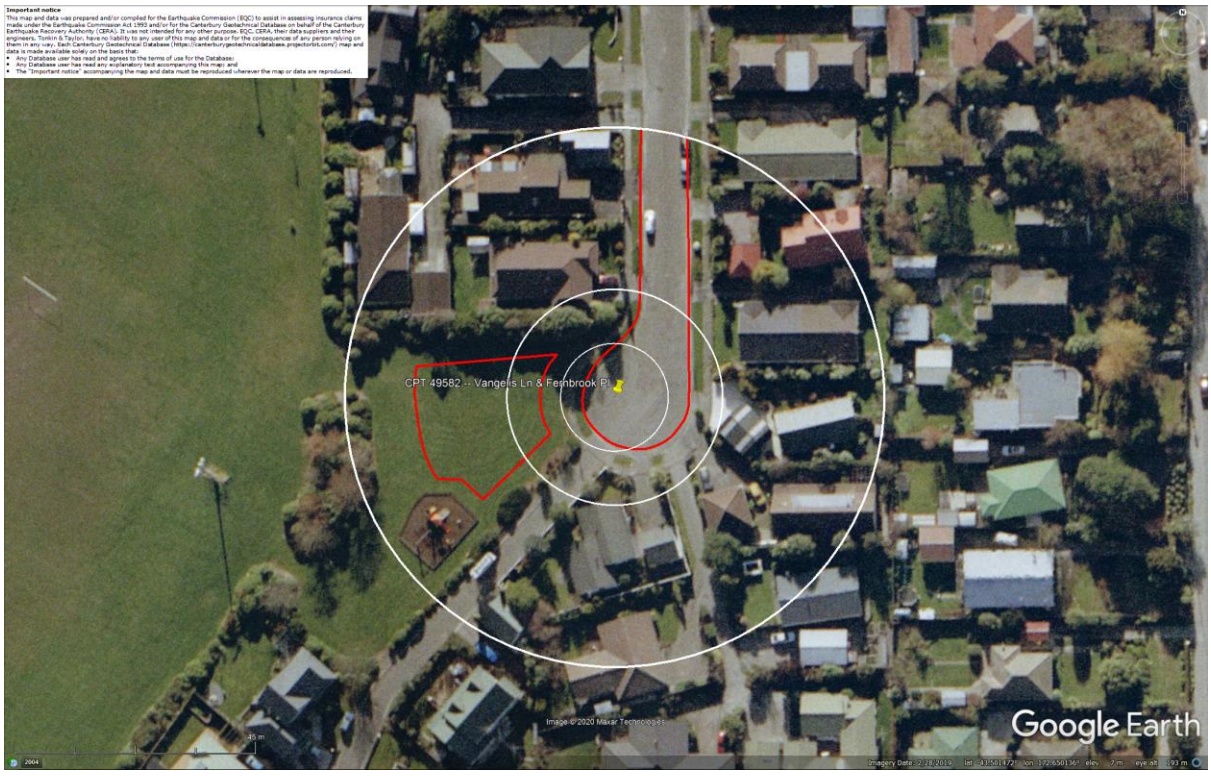

Figure 85: Absence of ejecta at the site for Jun-11 EQ (June 16, 2011 aerial photograph).

Figure 86: Ejecta outline for Dec-11 EQ.

Figure 87: Ground photographs acquired at the site (within the 50-m buffer).

Figure 88: CPT locations.

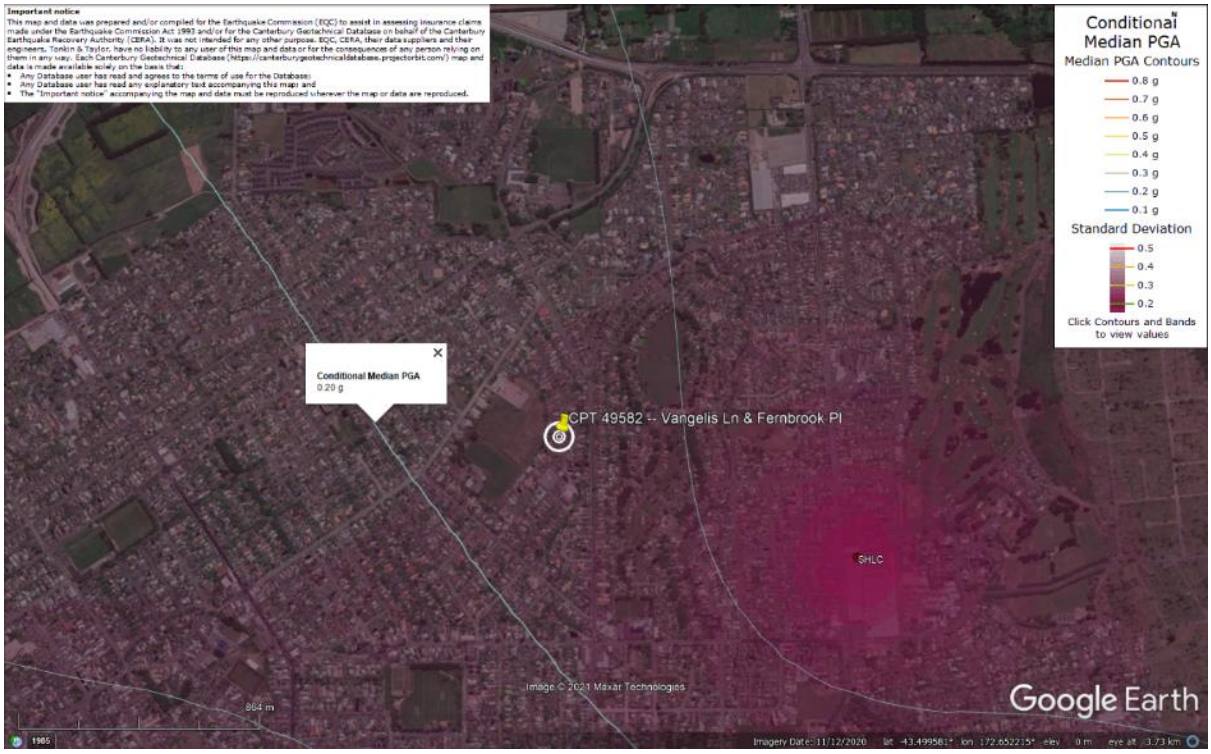

Figure 89: PGA for Sep-10 EQ (st. dev. = 0.300-0.325 ln units).

Figure 90: PGA for Feb-11 EQ (st. dev. = 0.325-0.350 ln units).

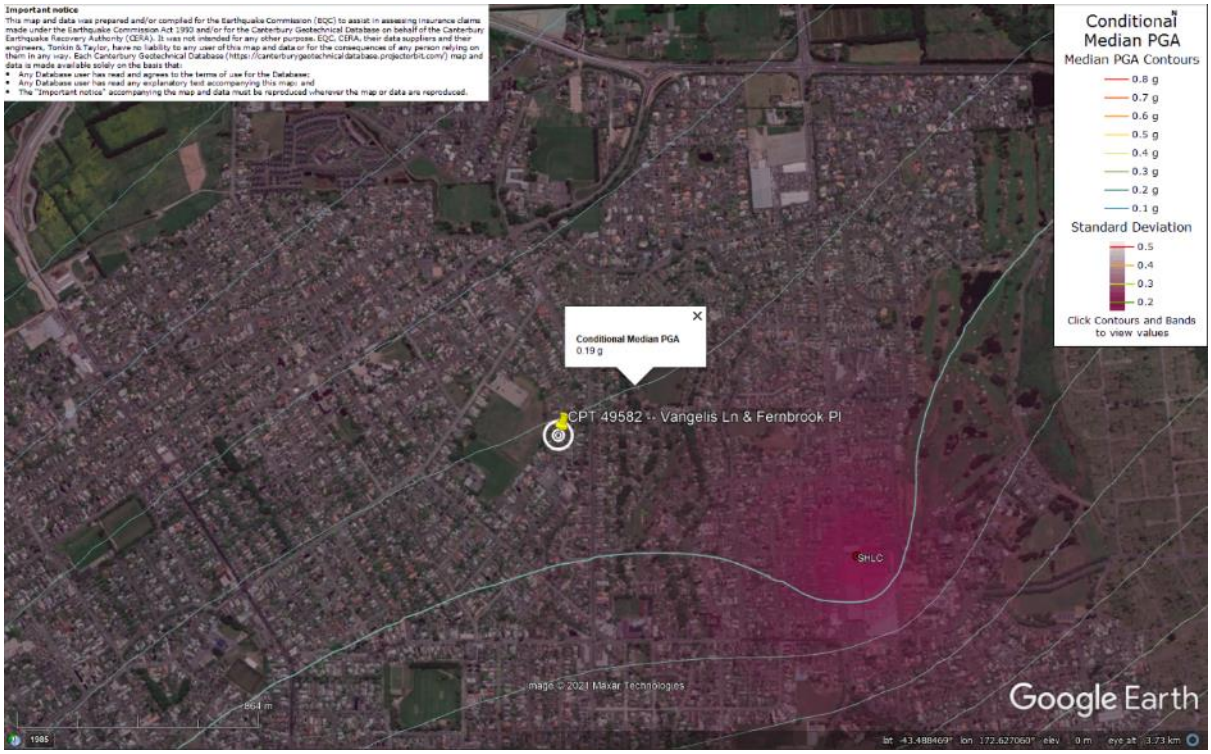

Figure 91: PGA for Jun-11 EQ (st. dev. = 0.350-0.375 ln units).

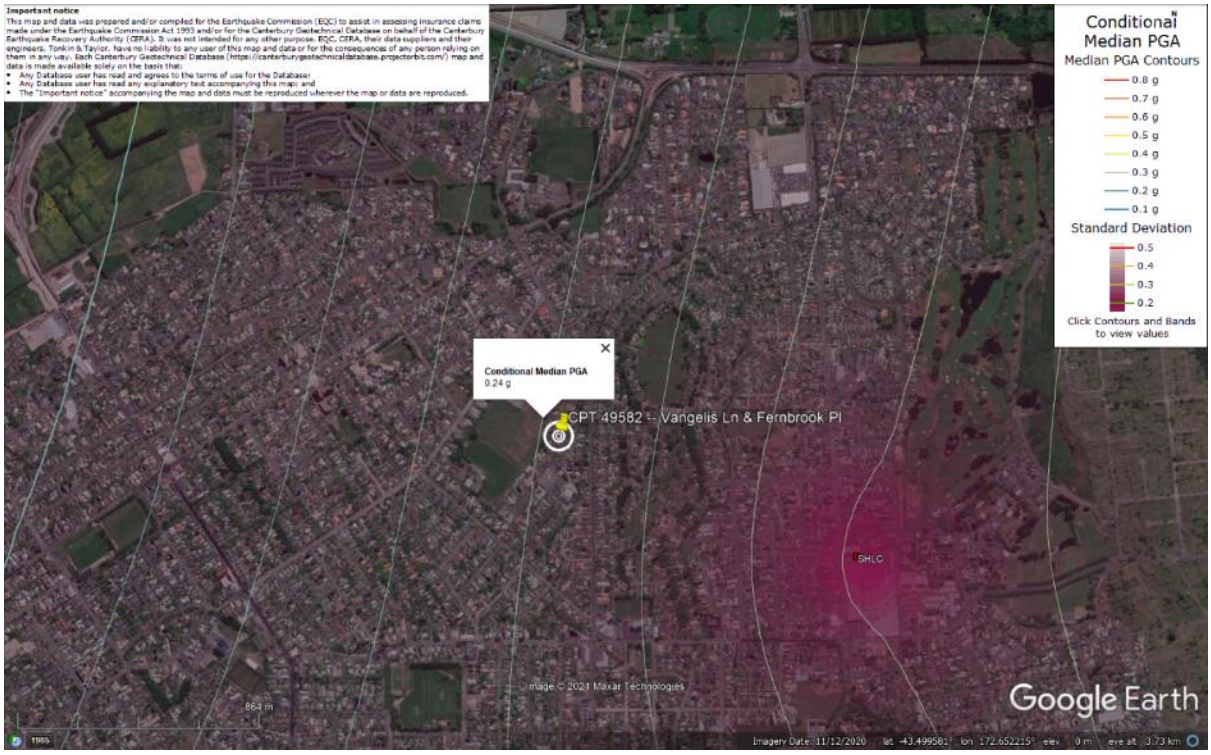

Figure 92: PGA for Dec-11 EQ (st. dev. = 0.350-0.375 ln units).

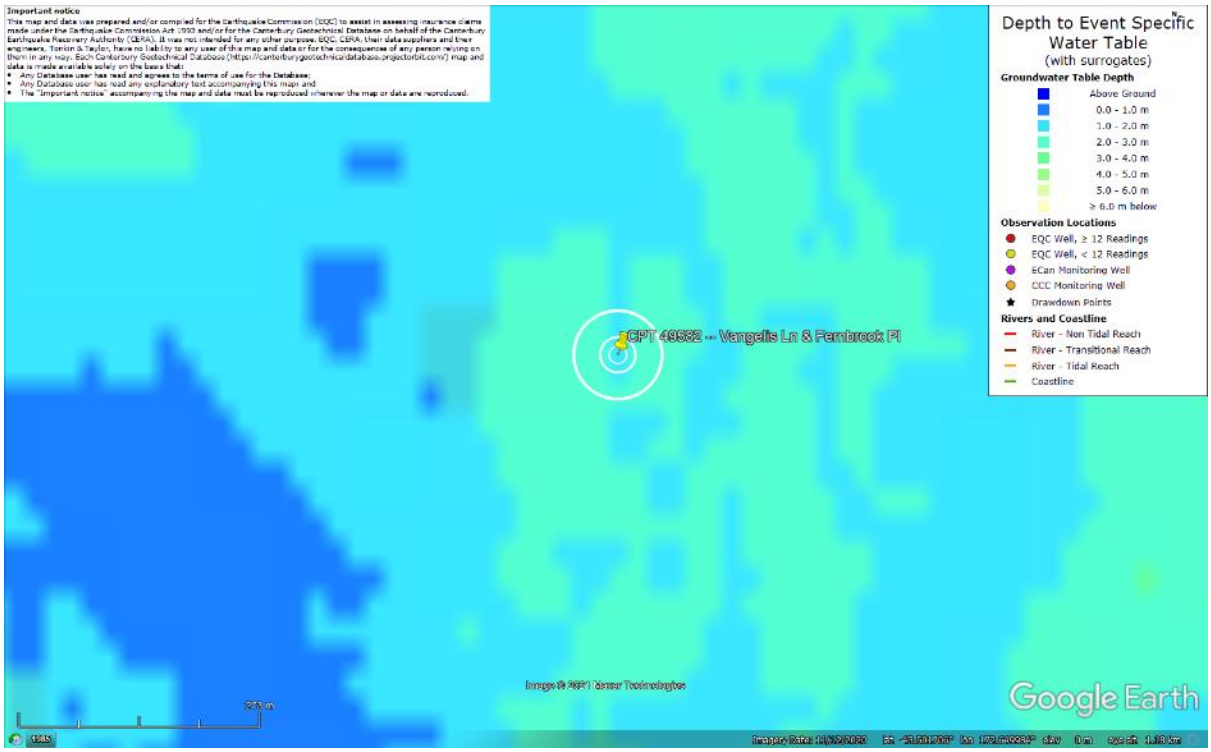

Figure 93: Depth to groundwater table for Sep-10 EQ.

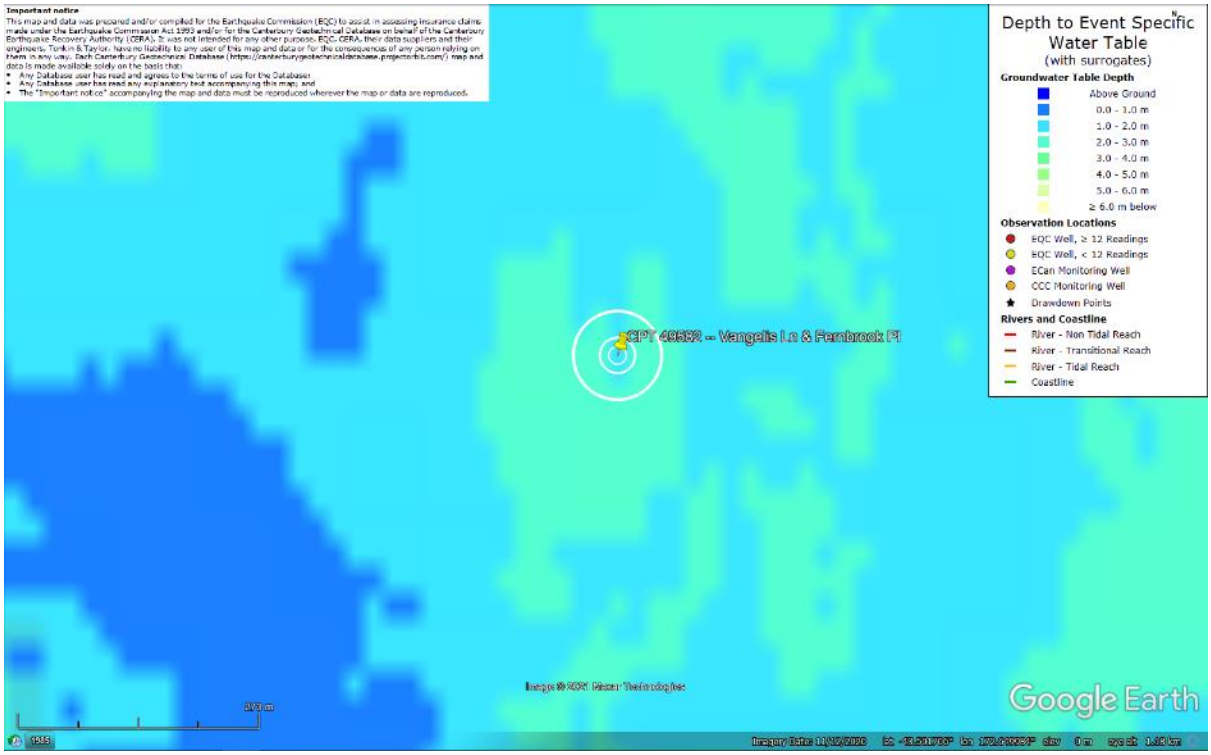

Figure 94: Depth to groundwater table for Feb-11 EQ.

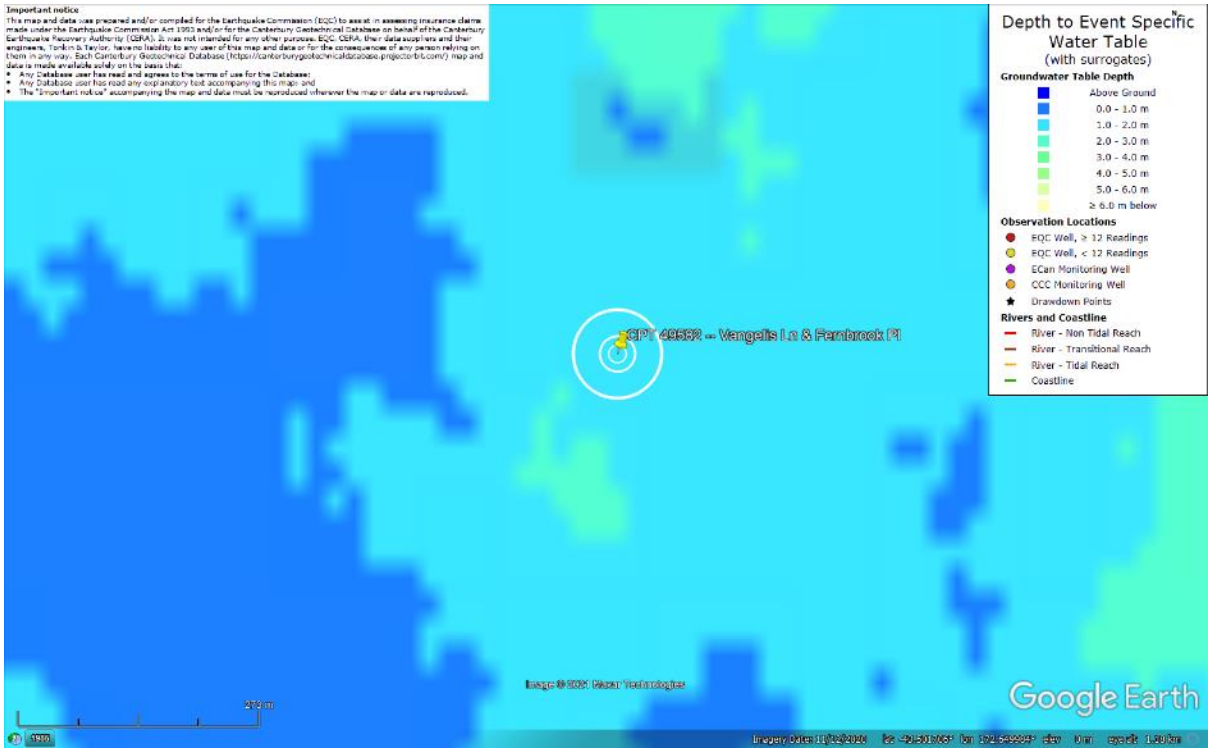

Figure 95: Depth to groundwater table for Jun-11 EQ.

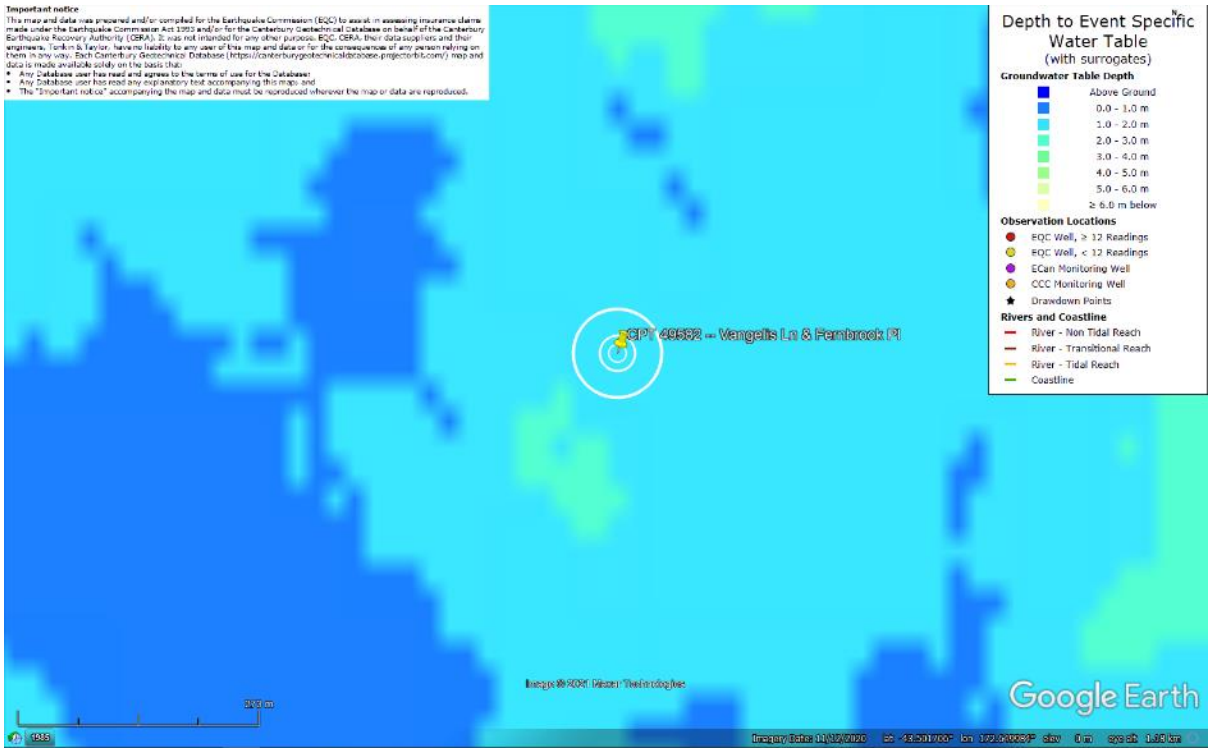

Figure 96: Depth to groundwater table for Dec-11 EQ.

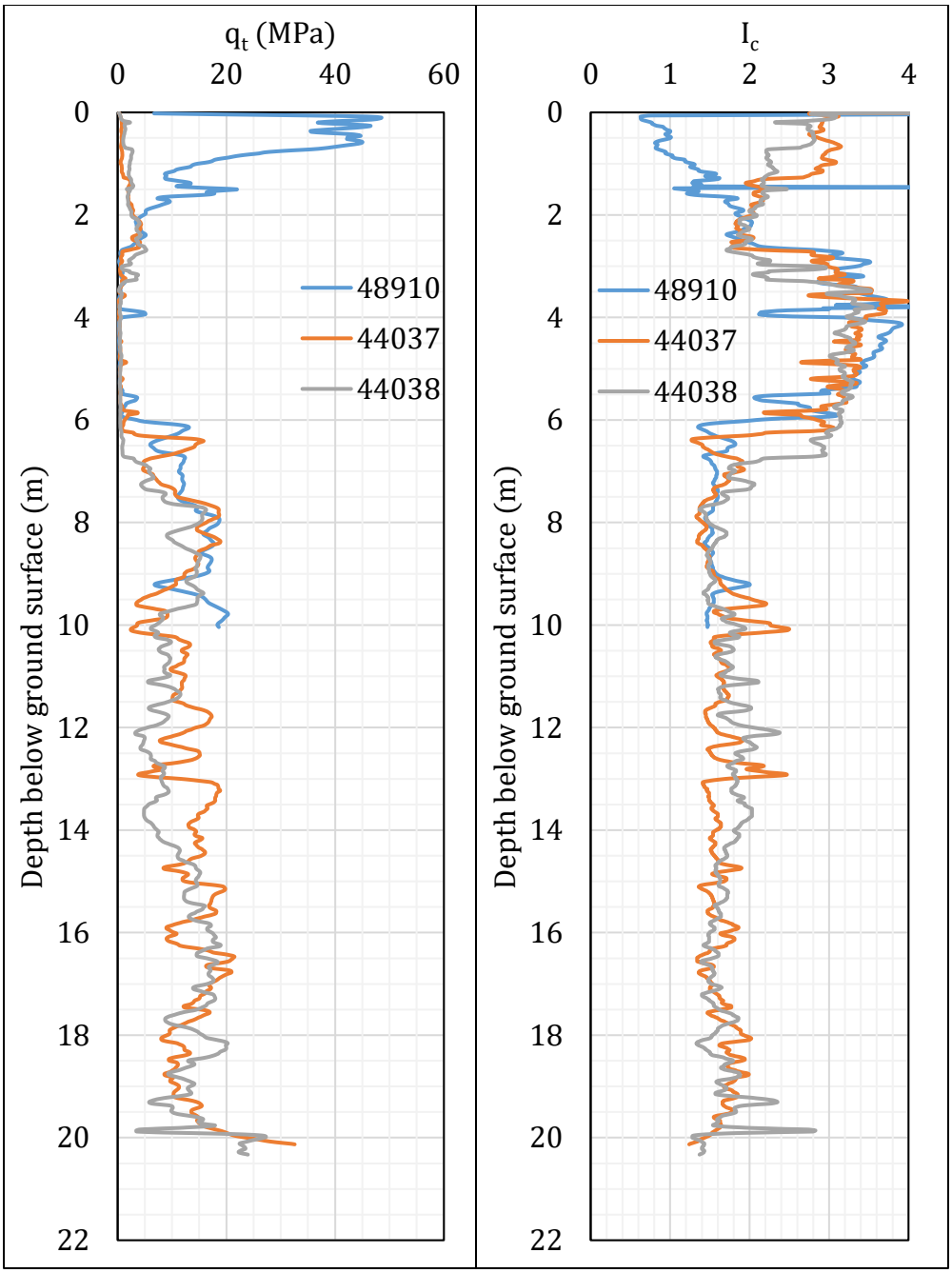

Figure 97: q_t and I_c profiles.

Note 7: The selection of CPTs for the area considered for settlement assessment (Figure 1) is based on the proximity of the CPTs to the considered areas. In accordance with that, the following table shows CPTs that were used for the volumetric settlement analysis in *Cliq v.3.0.3.2*, a CPT soil liquefaction software developed by GeoLogismiki. (The average volumetric settlements were reported in Table 8.)

Table 12: CPT profiles used in volumetric settlement analysis for areas selected for settlement assessment.

CPT ID No.	Patch A	Road
49582 (48910)	✓	✓
44037		
44038		
48318 (48657)		
48317 (48656)		

Note: CPTs 44037 and 44038 were used to calculate the average volumetric settlement for a depth range from 10 m to 20 m.

Table 13: CPT-based results.

		CPT ID			
EQ Event	Parameter	49582	44038	44037	$\Delta_{10m-20m}$*
Sep-10	S_{V1D} (mm)	9	106	68	57
	LSN	2	9	6	5
	LPI	0	2	1	1
	LPI_{ish}	0	0	0	--
	$D_{FS<1}$ (m)	undet.	6.73	6.79	--
Feb-11	S_{V1D} (mm)	25	189	141	116
	LSN	5	19	14	9
	LPI	2	10	6	4
	LPI_{ish}	1	5	3	--
	$D_{FS<1}$ (m)	6.32	2.76	2.39	--
Jun-11	S_{V1D} (mm)	7	52	28	25
	LSN	1	5	3	2
	LPI	0	1	0	0
	LPI_{ish}	0	0	0	--
	$D_{FS<1}$ (m)	undet.	6.73	undet.	--
Dec-11	S_{V1D} (mm)	15	120	76	58
	LSN	3	14	10	5
	LPI	1	4	2	0
	LPI_{ish}	1	0	0	--
	$D_{FS<1}$ (m)	6.36	6.73	6.7	--

Notes: $D_{FS<1}$ = Depth to the first liquefiable layer ($FS_L<1$) that is at least 200-mm thick, as determined by the Boulanger and Idriss (2016) liquefaction-triggering procedure (P_L=50%, C_{FC}=0.13, and $I_{c,cutoff}$ =2.6), and exported from *Cliq v.3.0.3.2*; undet. = the specified soil layer was not detected; * indicates the amount of S_{V1D} and LPI to be added for CPT 48910 due to its penetration depth being shallower than 20 m.

Note 8: Based on the borehole log (BH_TT65290, Figure 88), the groundwater table is at a depth of 0.75 m below the ground surface. The soil profile consists of (1) topsoil (organic silt) to a depth of 0.3 m, (2) non-plastic to low-plasticity silt, ML, the Yaldhurst member of the Springston formation, to a depth of 3.0 m, (4) peat, Pt, the Yaldhurst member of the Springston formation, to a depth of 3.8 m, (5) non-plastic silt, ML, the Yaldhurst member of the Springston formation, to a depth of 6.1 m (the end of the borehole). Trace organics are found occasionally within the silty layers. The nearby borehole (BH 18320, ≈120 m away from the centre of the site, Figure 72) suggests that the ML layer of the Springston formation is followed by an SP layer of the Christchurch formation that extends to a depth of 20 m (the end of the borehole).

Note 9: The ejecta-induced free-field settlement provided in Table 11 is an areal average settlement due to ejecta, which is based on the total settlement assessment area, A_T (provided in Table 9 and repeated in Table 14). However, the considered area was not always covered completely with ejecta; thus, it is important to provide the localized ejecta-induced settlement, too. The localized settlement due to ejecta is estimated using photographic evidence only as

$$S_{E,P\_localized} = \frac{V_E}{A_E}$$

where V_E is the total volume of ejecta within A_T and A_E is the total coverage area of ejecta within A_T. Please note that the areal ejecta-induced settlement provided in Table 14 as S_{E,P_areal} is the same as $S_{E,P}$ in Table 11, which was estimated as

$$S_{E,P\_areal} = S_{E,P} = \frac{V_E}{A_T}$$

where V_E is the total volume of ejecta within A_T and A_T is the total settlement assessment area.

Table 14a: Areal and localized ejecta-induced settlement estimates for Road (10-m buffer) based on photographic evidence.

Earthquake Event	A_T (m^2)	A_E (m^2)	V_E (m^3)	S_{E,P_areal} (mm)	$S_{E,P\_localized}$ (mm)
Sep-10	227	0	0	0	0
Feb-11	191	86.0	0.9-2.6	10±5	20±10
Jun-11	227	0	0	0	0
Dec-11	225	7.3	0.04-0.0.7	<5	10±5

Notes: S_{E,P_areal} = $S_{E,P}$ reported in Table 11 = areal ejecta-induced settlement; $S_{E,P\_localized}$ = localized ejecta-induced settlement; A_T = total settlement assessment area; V_E = total volume of ejecta within A_T; A_E = total area of ejecta within A_T; The estimates of both areal and localized ejecta-induced settlement are rounded to the nearest 5; Final plus/minus values are also rounded to the nearest 5; NA = Not available.

Table 14b: Areal and localized ejecta-induced settlement estimates for Road (20-m buffer) based on photographic evidence.

Earthquake Event	A_T (m^2)	A_E (m^2)	V_E (m^3)	S_{E,P_areal} (mm)	$S_{E,P\_localized}$ (mm)
Sep-10	401	0	0	0	0
Feb-11	353	173	1.8-5.2	10±5	20±10
Jun-11	401	0	0	0	0
Dec-11	375	7.3	0.04-0.0.7	<5	10±5

Notes: S_{E,P_areal} = $S_{E,P}$ reported in Table 11 = areal ejecta-induced settlement; $S_{E,P\_localized}$ = localized ejecta-induced settlement; A_T = total settlement assessment area; V_E = total volume of ejecta within A_T; A_E = total area of ejecta within A_T; The estimates of both areal and localized ejecta-induced settlement are rounded to the nearest 5; Final plus/minus values are also rounded to the nearest 5; NA = Not available.

Table 14c: Areal and localized ejecta-induced settlement estimates for Road (50-m buffer) based on photographic evidence.

Earthquake Event	A_T (m^2)	A_E (m^2)	V_E (m^3)	S_{E,P_areal} (mm)	$S_{E,P\_localized}$ (mm)
Sep-10	679	0	0	0	0
Feb-11	595	241	2.4-6.7	10±5	20±10
Jun-11	679	0	0	0	0
Dec-11	632	7.3	0.04-0.0.7	<5	10±5

Notes: S_{E,P_areal} = $S_{E,P}$ reported in Table 11 = areal ejecta-induced settlement; $S_{E,P\_localized}$ = localized ejecta-induced settlement; A_T = total settlement assessment area; V_E = total volume of ejecta within A_T; A_E = total area of ejecta within A_T; The estimates of both areal and localized ejecta-induced settlement are rounded to the nearest 5; Final plus/minus values are also rounded to the nearest 5; NA = Not available.

Summary 2:

The best estimate of the localized ejecta-induced settlement of the road at the Vangelis Ln and Fernbrook Pl site for the SEP 2010, FEB 2011, JUN 2011, and DEC 2011 earthquake is 0 mm, 20±10 mm, 0 mm, and 10±5 mm, respectively.